COPPE
Instituto Alberto Luiz Coimbra de Pós-Graduação e Pesquisa de Engenharia
UFRJ

SYNCHRONVERTER APPLIED TO POWER SYSTEMS

Emanuel Leonardus van Emmerik

Tese de Doutorado apresentada ao Programa de Pós-graduação em Engenharia Elétrica, COPPE, da Universidade Federal do Rio de Janeiro, como parte dos requisitos necessários à obtenção do título de Doutor em Engenharia Elétrica.

Orientador: Maurício Aredes

Rio de Janeiro
Março de 2018

SYNCHRONVERTER APPLIED TO POWER SYSTEMS

Emanuel Leonardus van Emmerik

TESE SUBMETIDA AO CORPO DOCENTE DO INSTITUTO ALBERTO LUIZ COIMBRA DE PÓS-GRADUAÇÃO E PESQUISA DE ENGENHARIA (COPPE) DA UNIVERSIDADE FEDERAL DO RIO DE JANEIRO COMO PARTE DOS REQUISITOS NECESSÁRIOS PARA A OBTENÇÃO DO GRAU DE DOUTOR EM CIÊNCIAS EM ENGENHARIA ELÉTRICA.

Examinada por:

_____
Prof. Maurício Aredes, Dr.-Ing.

_____
Prof. Antônio Carlos Ferreira, Ph.D.

_____
Prof. Luís Guilherme Barbosa Rolim, Dr.-Ing.

_____
Prof. Vitor Hugo Ferreira, D.Sc.

_____
Prof. Denizar Cruz Martins, Dr. Ing.

RIO DE JANEIRO, RJ - BRASIL
MARÇO DE 2018

Emmerik, Emanuel Leonardus van

Synchronverter applied to Power Systems/ Emanuel Leonardus van Emmerik. – Rio de Janeiro: UFRJ/COPPE, 2018.

XIV, 97 p.: il.; 29,7 cm.

Orientador: Maurício Aredes

Tese (doutorado) – UFRJ/ COPPE/ Programa de Engenharia Elétrica, 2018.

Referências Bibliográficas: p. 94-97.

1. Static Synchronous Generator. 2. Damping. 3. Electromechanical Oscillation Modes. I. Aredes, Maurício. II. Universidade Federal do Rio de Janeiro, COPPE, Programa de Engenharia Elétrica. III. Título.

Dedico este trabalho ao meu pai,
Leonardus Theodorus Aloysius van
Emmerik (15/7/1936 – 4/7/2017)

“The hardest thing to understand is income taxes” Albert Einstein.

AGRADECIMENTOS

Graças a Deus, Fonte de tudo. Ofereço humildemente esta obra a Ti, procurando em primeiro lugar a Sua aceitação.

Aos meus pais, Leonardus Theodorus Aloysius van Emmerik, que ele descanse em Paz, e Christina Petronella Margaretha van Emmerik Rooijakkers, dois grandes exemplos complementares na minha vida toda. *Bedankt voor alles, Ma*.

À minha irmã, Maria Cristina Monteiro de Carvalho van Emmerik, por todo apoio e diversão durante tantos anos. Sempre disponível para achar soluções e informações, especialmente nos momentos mais difíceis.

À minha esposa, Dilma dos Santos Reis, o apoio absoluto na minha vida. Obrigado pela convivência, força, e, ter aceitado percorrer a vida junto comigo. A vida é muita mais rica com você.

Aos meus filhos, Phoebe Silva van Emmerik, Zowie Silva van Emmerik e Victoria Reis. Por serem maravilhosos e pelos estímulos. Aprendo muito com vocês.

Ao meu orientador, Prof. Maurício Aredes, por ser uma fonte inspiradora inesgotável durante um período significativo da minha vida. Espero que fique assim por mais tempo. Agradeço por todas as oportunidades dadas e criadas, e por achar e acreditar nos potenciais da gente.

Aos amigos Prof. Bruno Wanderley França, Leonardo Francisco da Silva e Bruno de Mello Laurindo, primeiramente pela amizade. Por dar moral e apoio quando mais precisa. Especialmente, Prof. Bruno pelas orientações, e pela luta junto no artigo do *sliding droop*. Quanta emoção. Leonardo pelos anos de conversas. Literalmente. Este homem, com coração de ouro, tem muito empenho para o LEMT. E especialmente por ter ido ao LEMT na quinta-feira depois do Carnaval, ter secado e ter dado acesso ao meu pc.

Aos amigos/colegas:

Gustavo Figueiredo Gontijo e Thiago Cardoso Tricarico, por ter estado do meu lado no momento mais apertado discutindo sobre como fechar os loops. Agradeço o primeiro especialmente pelas muitas conversas sobre tudo e o último pela ajuda no árduo desenvolvimento das funções de transferência, programação no Matlab e a figura linear de tudo.

Juliano Caldeira por estar no mesmo barco como eu. É suavizante dividir momentos difíceis idênticos. André Ramos Castro pela cooperação muito agradável no

artigo do *multiple electromechanical oscillations damping* em especial e pelo interesse dele de ajudar a todos. Diego de Souza de Oliveira pelo apoio com algumas matérias ligadas aos sistemas de potência. Foi bom ter passado por tudo isso contigo. Os irmãos, Milena e Rodrigo Villarino por sempre estar atenciosos com as necessidades e bem estar do LEMT e a sua Família. Especialmente, Rodrigo, por ter ido ao LEMT na quarta-feira de Cinzas, descobrindo a causa da falha no acesso ao meu pc e as tentativas para resolver. E Leandro de Oliveira Abreo pelo apoio administrativo no último dia da entrega da tese à banca e ao registro.

Agradeço aos demais da Família LEMT por ter dado a sua contribuição a criar e manter esta Família, inclusive aqueles que já voaram para mundo afora (e também muitas vezes voltam). Cada um tem enriquecido a minha vida de uma forma ou outra. Vocês todos estão no meu coração. Sem exceção.

Termino aqui com os meus agradecimentos para a banca pelas sugestões em relação da minha tese e pelo apoio financeiro do CNPq, CAPES e FAPERJ.

Resumo da Tese apresentada à COPPE/UFRJ como parte dos requisitos necessários para a obtenção do grau de Doutor em Ciências (D.Sc.)

SYNCHRONVERTER APLICADO NOS SISTEMAS DE POTÊNCIA

Emanuel Leonardus van Emmerik

Março/2018

Orientador: Maurício Aredes

Programa: Engenharia Elétrica

Este trabalho desenvolve uma adaptação do modelo do synchronverter para ser adequado para operação sem fonte de energia elétrica conectada ao elo CC, como por exemplo, um STATCOM ou um filtro ativo. Além disso, desenvolve também um modelo dinâmico teórico para o projeto deste controlador caso o conversor seja aplicado em sistemas de potência, baseado na investigação para a origem das oscilações na frequência do sistema, concluindo sua aplicabilidade. Parte do sistema de potência do Brasil foi modelada no simulador PSCAD e o modelo adaptado do synchronverter foi inserido para operar como um STATCOM para testar a eficácia do modelo. Os resultados observados corroboram os resultados previstos analiticamente.

Abstract of Thesis presented to COPPE/UFRJ as a partial fulfillment of the requirements for the degree of Doctor of Science (D.Sc.)

SYNCHRONVERTER APPLIED TO POWER SYSTEMS

Emanuel Leonardus van Emmerik

March/2018

Advisor: Maurício Aredes

Department: Electrical Engineering

This work presents an adapted model for the synchronverter to become suitable for operation without an electric energy source connected to the dc-link, like for example, a STATCOM or an active filter. In addition, a theoretical dynamic model for the project of the controller is presented, if the converter is applied to power systems, based on an investigation on the origins of the system-frequency oscillations. To verify the theories, part of the Brazilian National Grid (SIN) was modeled in the PSCAD simulator and the adapted synchronverter model was inserted to operate as a STATCOM. The results agree with those predicted analytically.

CONTENTS

1 Background and motivation 1
1.1 Motivation 2
1.2 Objectives 3
1.3 Document structure 4
1.4 Published and submitted contributions 4
2 Static Synchronous Generator 6
2.1 Synchronverter 7
2.2 Virtual Synchronous Generator/Machine 12
2.3 Differences between synchronverter and VSG/VSM. 14
3 The non-generating synchronverter 16
3.1 Power System 18
3.2 Classic solution 24
3.3 Proposed solution 24
4 Results and analysis 31
4.1 Frequency domain 32
4.2 Time domain 36
Comparison between [24] and thesis proposal 40
Simple system simulations 49
THE BRAZILIAN POWER SYSTEM 76
5 Conclusions and suggestions 92
References 94

LIST OF FIGURES

Fig. 1 Basic two-level voltage source inverter with 6 IGBTs in 3 legs and a LCL-filter [21] for illustrative purposes only. 8
Fig. 2 Synchronverter with active and reactive power control [21]. 8
Fig. 3 Redrawn diagram as in Fig. 2 to emphasize the main active and reactive power channels (without technical interface blocks). 9
Fig. 4 Diagram of original synchronverter controller for STATCOM without frequency droop controller as in [22]. 11
Fig. 5 Control diagram for active power synchronization with virtual admittance as presented in [12]. 12
Fig. 6 Control diagram for active power synchronization with virtual admittance. As presented in [28]. 14
Fig. 7 Passive network with a controlled voltage source at one extremity controlling the voltage amplitude at the voltage controlled bus and an infinite bus, representing the grid, at the other extremity. 18
Fig. 8 Diagram of original synchronverter controller [21] with a derivative droop in red. 25
Fig. 9 Diagram of original synchronverter controller for STATCOM in black as in [22] with proposed proportional gain in red for stability purposes and speeding up transients. 26
Fig. 10 The proposed synchronverter controller with signal for virtual mechanical torque, T_m, to compensate for physical losses in the VSC. 27
Fig. 11 The proposed synchronverter controller adapted to motor convention and parameter name adaptations, with input for dc-voltage control to compensate for physical losses in the VSC, and reactive power control. 28
Fig. 12 Active power control block diagram with linearized plant $H_{\delta P}$ for controller project for STATCOM with proposed controller. 29
Fig. 13 Reactive power control block diagram with newly developed linearized plant H_{EQ} for controller project for STATCOM. 29
Fig. 14 Active- and reactive-power control block diagram connected with the disturbance transfer functions between the active- and reactive-loops as modeled in Simulink. 30
Fig. 15 P_{ref} to P. System frequency resonance pole pair starts (black cross) stable and goes with higher gain $k_{p\omega}$ towards (red cross) instability. Pole pair of synchronverter starts instable and goes with higher gain towards stability. R = 0.00686 Ω. L = 0.00091 H. J = 2H = 1 s. $K_{p\omega}$ from 0 to 0.1. 33
Fig. 16 P_{ref} to P. Phase and Gain Margin as a function of $K_{p\omega}$. R = 0.00686 Ω, L = 0.00091 H, J = 2H = 1 s. Stable for $0.00107 < K_{p\omega} < 0.0122$. 34
Fig. 17 Q_{ref} to Q. System frequency resonance pole pair starts (black cross) stable and goes with higher gain Ki_f towards (red cross) instability. Pole of synchronverter starts in zero. R = 0.00686 Ω, L = 0.00091 H. Ki_f from 0 to 10. 35
Fig. 18 Q_{ref} to Q. Phase and Gain Margin as a function of Ki_f. R = 0.00686 Ω, L = 0.00091 H. Stable for $Ki_f < 4.37$. 36
Fig. 19 Test bed based on [24]. Values of series elements were not given. Loads were scaled with S_{nom}. 37
Fig. 20 Inside of the module SVC_BJL of Fig. 19. Transformer data based on transformer in operation at Bom Jesus de Lapa (BH), connecting SVC to the 500 kV

transmission grid. Signal V_rms, RMS value of the voltage at the high-voltage side, #1, of the transformer, measured at the AV-meter is sent to the module “Ideal Statgen”. .. 38
Fig. 21 Inside of the module Ideal Statgen of Fig. 20. Motor convention is adopted. Synchronverter current is measured at breaker BRK. 39
Fig. 22 Mathematical model to calculate the voltage difference, in p.u., on the dc-capacitor, DV_{dc}, based on the integrated active power entering the converter, E_{inv}, and the integrated power consumption in a resistor parallel to the capacitor, E_{rdc}, representing energy losses due to switching and thermal losses in all the components behind the converter terminal (motor convention). 40
Fig. 23 Results to compare with the first simulation set concerning the voltage regulation of Nguyen et al in paper [24]. Generator convention. 41
Fig. 24 Variables of the synchronverter during the simulation as in Fig. 23. Generator convention. 42
Fig. 25 The active control loop of [24] modeled in PSCAD for comparison with the thesis proposal. 43
Fig. 26 Results from the controller of [24] applied to a system with high X/R values for the voltage control simulation. 44
Fig. 27 Frequency variation on the infinite bus source. 45
Fig. 28 Proposed controller of this thesis for the frequency track simulation in a system with high X/R. 46
Fig. 29 Results with the controller of [24] for the frequency track simulation in a system with high X/R. 47
Fig. 30 Results with the controller of [24] for the frequency track simulation in a system with lower X/R. 48
Fig. 31 Simplified model of Fig. 19. 49
Fig. 32 Result of the first simulation case with only 10% of the load on the bus. To compare with Fig. 23 and Fig. 35. Generator convention. 50
Fig. 33 Synchronverter variables with only 10% of the load on the bus. To compare with Fig. 24. Generator Convention. 51
Fig. 34 Result of the first simulation case with J= 2H = 10 μs. To compare with Fig. 23. Generator convention. 52
Fig. 35 Results of the simple model base case. To compare with Fig. 23..... 54
Fig. 36 Synchronverter variables of the simple model base case. To compare with Fig. 24 55
Fig. 37 K_{if} increased from 1 to 2. To compare with Fig. 35. Resonance frequency oscillation has increased twice as well. 56
Fig. 38 K_{if} increased from 1 to 2. To compare with Fig. 36. Resonance frequency oscillation has increased twice as well. 57
Fig. 39 K_{if} increased to 5 s^{-1}. System becomes unstable. 58
Fig. 40 Kif increased to 5 s^{-1}. System becomes unstable. 59
Fig. 41 $K_{p\omega}$ from 100 to 2. $K_{i\omega}$ = 1/(2H)= 20. Compare with Fig. 35. 60
Fig. 42 $K_{p\omega}$ from 100 to 2. $K_{i\omega}$ =1/(2H)= 20. Compare with Fig. 36. 61
Fig. 43 K_{pdc} from 100 to 10. To compare with Fig. 41. $K_{p\omega\delta}$ was removed and resulted in elimination of oscillation at connection. 62
Fig. 44 K_{pdc} from 100 to 10. To compare with Fig. 42. $K_{p\omega\delta}$ was removed and resulted in elimination of oscillation at connection. 63
Fig. 45 K_{pdc} from 100 to 10. ΔV_{dc} increased 10 times (from 0.3% to 3%). The liquid total energy, Etotpu = Einv –Erdc, energy that entered the inverter minus dissipated energy, is still practically double of the voltage loss on the dc-link, as predicted by the

linear model. $K_{p\omega\delta}$ was removed and resulted in elimination of oscillation at connection. 64
Fig. 46 K_{pdc} from 10 to 1. $K_{p\omega\delta}$ was removed and resulted in elimination of oscillation at connection..... 65
Fig. 47 K_{pdc} from 10 to 1. $K_{p\omega\delta}$ was removed and resulted in elimination of oscillation at connection..... 66
Fig. 48 K_{pdc} from 10 to 1. $K_{p\omega\delta}$ was removed and resulted in elimination of oscillation at connection..... 66
Fig. 49 K_{pdc} = 10. $K_{p\omega}$ = 2. $K_{i\omega}$ = 20 (2H = 0.05 s)..... 68
Fig. 50 K_{pdc} = 10. $K_{p\omega}$ = 2. $K_{i\omega}$ = 20 (2H = 0.05 s)..... 69
Fig. 51 The frequency of the resonance oscillation, 62.4 Hz is equal to the system frequency (see Fig. 27), 1.04 p.u. times 60 Hz..... 70
Fig. 52 The frequency of the resonance oscillation, 57.6 Hz is equal to the system frequency (see Fig. 27), 0.96 p.u. times 60 Hz..... 70
Fig. 53 K_{pdc} = 10. $K_{p\omega}$ = 1. $K_{i\omega}$ = 20 (2H = 0.05 s)..... 71
Fig. 54 K_{pdc} = 10. $K_{p\omega}$ = 1. $K_{i\omega}$ = 20 (2H = 0.05 s)..... 72
Fig. 55 K_{pdc} = 10. $K_{p\omega}$ = 0. $K_{i\omega}$ = 20 (2H = 0.05 s). Unstable right after connection with grid..... 73
Fig. 56 K_{pdc} = 10. $K_{p\omega}$ = 0. $K_{i\omega}$ = 20 (2H = 0.05 s). Unstable right after connection with grid..... 74
Fig. 57 K_{pdc} = 10. $K_{P\omega}$ = 2. $K_{I\omega}$ = 10 (2H = 0.1 s). 75
Fig. 58 K_{pdc} = 10. $K_{P\omega}$ = 2. $K_{I\omega}$ = 10 (2H = 0.1 s). 76
Fig. 59 Part of the National Interconnected System, configuration of January 2009, modeled in PSCAD – source: website of ONS (National System Operator)..... 77
Fig. 60 Overview of the simulated system with modular construction based on data of Fig. 59 [22]. 78
Fig. 61 Block diagram for the signal treatment of the active power flow in the transmission line S. Mesa – Gurupi..... 78
Fig. 62 Block diagram to delay the signal Pmesawashed and output the additional control signal Pref (see Fig. 11)..... 79
Fig. 63 Electrical torque, T_e, reactive power (+), Q, of the synchronverter (motor convention), controlled bus voltage, V_{col}, in droop mode with Vref = 1.04 p.u., synchronverter terminal-voltage, V_{lv}, virtual flux, M_fi_f, synchronverter angular velocity, w_{eag}, angular velocity calculated by a PLL at the synchronverter terminals, w_{grid}, and the angular velocity, omega_{sm}, of the dynamic equivalent representing the generation of region South/South-east/Center-West. $K_{p\omega}$=0. 80
Fig. 64 Results when dc-capacitor is considered, in contrast with [22] and [23], which utilized T_m = 0. $K_{p\omega}$=0. 81
Fig. 65 At t=5s occurs a short-circuit in the grid. Etot = Einv – Erdc. $K_{p\omega}$=0. 82
Fig. 66 J = 2H = 50 ms and $K_{p\omega}$=0.009, system stable in contrast with Fig. 63..... 83
Fig. 67 J = 2H = 50 ms and $K_{p\omega}$=0.009, system stable in contrast with Fig. 64..... 83
Fig. 68 Total active power flowing North (negative), P_{smesa}, measured at Serra de Mesa, the filtered active power, P_{smesator} (see Fig. 61), POD-signal, V_{Pref} (see Fig. 62), angular velocities, omega, of the 4 dynamic equivalents at Lajeado, {la}, Paulo Afonso, {pa}, Marabá, {mb} and Serra de Mesa,{sm}. $K_{p\omega}$=0.009. 84
Fig. 69 $K_{p\omega}$=0.009, system stable in contrast with Fig. 65. Small energy contribution at short-circuit occurrence with 2H = 50 ms. 85
Fig. 70 J = 2H = 1 s and $K_{p\omega}$=0. Capacitor voltage remains above half the reference value even with a virtual inertia 20 times bigger than the electric energy contained on the dc-capacitor. 86

Fig. 71 The instability of the virtual inertia with a natural frequency of a little less than 5 Hz starts even to impact the dynamic equivalent of Lajeado with natural frequency of around 2 Hz. 87
Fig. 72 J = 2H = 1 s and $K_{p\omega}$=0. More energy contribution at short-circuit occurrence than for 2H = 50 ms as shown in Fig. 69..... 88
Fig. 73 J = 1 s and $K_{p\omega}$ = 0.012. To compare with Fig. 66..... 89
Fig. 74 J = 1 s and $K_{p\omega}$ = 0.012. To compare with Fig. 67..... 89
Fig. 75 J = 1 s and $K_{p\omega}$ = 0.012. No interference with the dynamic equivalent of Lajeado. 90
Fig. 76 J = 1 s and $K_{p\omega}$ = 0.012. At the instant of the short-circuit, the synchronverter contributes more to the frequency than in the case with inertia 20 times smaller, as can be seen in Fig. 69..... 91

ABBREVIATIONS AND ACRONYMS

ac	Alternating Current
dc	Direct Current
EMF	back Electromotive Force
FACTS	Flexible AC Transmission System
HVDC	High Voltage Direct Current
IGBT	Insulated Gate Bipolar Transistor
MMC	Modular Multilevel Converter
PLC	Power Loop Controller
PLL	Phase Locked Loop
POD	Power Oscillation Damper
PSS	Power System Stabilizer
PWRLL	Power-Locked Loop
p.u.	per unit
SIN	Brazilian National Interconnected Grid
SSG	Static Synchronous Generator
STATCOM	Static Synchronous Compensator
SVC	Static VAR Compensator
VISMA	Virtual Synchronous Machine
VSC	Voltage Source Converter
VSG	Virtual Synchronous Generator
VSI	Voltage Source Inverter
VSM	Virtual Synchronous Machine

1 Background and motivation

This chapter contains the motivation and objectives of the thesis “Synchronverter applied to power systems”. At the end of the section a description is given of the document structure.

1.1 Motivation

An exponential increase of installed renewable technologies and connection of Microgrids to the Power System [1][2][3][4][5] in the last two decades [6] has led to a decrease of Power System stability. The instability is related to voltage stability [7], frequency stability [8], and rotor angle stability [9]. Although the object of analysis, a Static Synchronous Compensator (STATCOM), is equipped with voltage control, the research is related to frequency stability.

In the last decade the Virtual Synchronous Machine concept (VSM) [10][11][12][13] has been developed to overcome problems with Phase Locked Loops (PLLs) for grid-connected inverters, load sharing [14][15][16][17][18] and the diminishing participation of rotational energy. Imitating a synchronous generator leads to the possibility of utilizing all the benefits of decades of experience with droop controllers, the natural behavior of the generator to maintain itself synchronized and creation of virtual inertia to stabilize the Power System. Besides, mimicking a synchronous generator makes it possible to utilize all available Power Stability Programs when parameters are kept constant as for a rotating synchronous generator.

In [19] it is even shown with a 3-order model that no limit exists in the complexity of emulating a synchronous generator. Although, one may ask if this leads to more benefits, it shows that it is possible to replace all inverters by a synchronous generator model that facilitates the analysis of the system with a growing number of inverters.

[20] has demonstrated that a frequency droop controller, which is part of a VSM or synchronverter [21], is intrinsically a PLL. The paper states further that the droop controller has a slow response in relation to an explicit PLL, which normally locks in two cycles with the input signal. It suggests recovering the integral effects hidden in the frequency and voltage paths to design a dynamic droop controller by replacing the integrator.

A synchronverter operating as a Static VAR Compensator (SVC) or STATCOM is presented in [22][23]. Here, the synchronverter was tested to show its capability to mitigate electromechanical oscillations without focusing on the dc-capacitor voltage of the STATCOM. In other words, the voltages calculated by the control system of the

synchronverter were used as inputs of ideal voltage sources. Since the STATCOM is not supposed to deliver active power, the frequency droop loop was eliminated. Even without this loop the synchronverter has been shown to be stable within a simulation model with dynamic equivalents, in other words, without a fixed frequency.

Nevertheless, the synchronverter without a frequency droop controller has been shown to be poorly damped. In a simplified power transmission model, the synchronverter in STATCOM operation has been shown to be unstable even for small virtual inertia values. Besides, oscillations of the synchronous frequency became apparent and in some cases even unstable.

In [24], with participation of the author of [21], the idea of torque loop is abandoned for a STATCOM and the calculated frequency is based on the dc-capacitor voltage without any explanation for having discarded the original idea of mimicking a synchronous generator. As a consequence, the virtual mechanical inertia, the swing equation, has been directly replaced by electric energy contained on the dc-capacitor, distancing this way the direct utilization of already available stability calculation programs. Besides this alteration, a PD-controller was placed in series with the integrator to obtain the calculated phase, which results in a PI-controller, with the objective to speed up the dynamic response of the original integrator. As a rule of thumb, a relative value for the derivative time constant has been given.

1.2 Objectives

The objective of this thesis is the analysis of the viability of the application of Power Electronic Converters emulating Virtual Synchronous Generators (VSG), Static Synchronous Generator (SSG) with virtual mechanical swing equation, in the Brazilian National Interconnected Grid (SIN) with focus on the Dynamic Electromechanical behavior of the Static Synchronous Generator, operating as a STATCOM, in the SIN. The SIN was modeled in the Electro Mechanical Transient Program PSCAD for the simulations in the time-domain.

This analysis contains virtual-generator parameter-variation, something impossible to do with real synchronous generators, to obtain better damping for electromechanical oscillations and transient response, hence, to obtain a more stable configuration. These studies were performed in the frequency domain with the program MATLAB/Simulink. Based on frequency domain analysis, besides determining

adequate parameter values, adaptations on the original controller [21] were proposed, were a proportional gain is added parallel to the virtual inertia. A comparison is made with a proposal for STATCOM operation without a virtual mechanical swing equation [24].

1.3 Document structure

Chapter 2 describes the current state-of-the art in developing synchronverter controllers, alternative configurations, and the differences between them.

Chapter 3 contains the proposals for controller adaptations with references to PSCAD simulation results of the Synchronverter in the appendix. Firstly a brief description of the classic controller for a non-generating synchronverter is presented. Then after, controller adaptations are proposed for non-generating synchronverters.

Chapter 4 presents the results of both classic and proposed non-generating synchronverter controllers. These results are represented in both the frequency- and time-domain.

Chapter 5 contains the conclusions and suggestions for future works, based on the presented analysis and results.

1.4 Published and submitted contributions

Non generating synchronverter:

[22] E. L. van Emmerik, B. W. França and M. Aredes, "A synchronverter to damp electromechanical oscillations in the Brazilian transmission grid," in *Industrial Electronics (ISIE), 2015 IEEE 24th International Symposium on*, 3-5 June 2015.

[23] E. L. van Emmerik, B. W. França, A. R. Castro, G. F. Gontijo, D. S. Oliveira and M. Aredes, "Synchronverter to damp multiple electromechanical oscillations," *Proceedings of the 8th Asia-Pacific Power and Energy Engineering Conference, Suzhou, China, April 15-17, 2016,* pp. 617-622, Mar 2016.

To be submitted:

"Shunt Active Filter Operation as Synchronverter to Provide Frequency Support Functionality".

Generation:

[25] B.W. França, E.L. van Emmerik, J. Caldeira and M. Aredes, "Sliding Droop Control For Distributed Generation In Microgrids" , *Eletrônica de Potência,* vol. 22, pp. 429-439, 12 2017.

Other related paper by author (in reviewing process):

Gustavo Gontijo, Thiago Tricarico, Bruno França, Leonardo da Silva, Emanuel van Emmerik and Maurício Aredes, "Robust Model Predictive Rotor Current Control of a DFIG Connected to a Distorted and Unbalanced Grid Driven by a Direct Matrix Converter", in IEEE Transactions on Sustainable Energy.

2 Static Synchronous Generator

This chapter describes the current state-of-the art in developing synchronverter controllers, alternative configurations, and the differences between them.

In 1997 proposed terms and definitions were given for the Flexible Alternating Current (ac) Transmission System (FACTS) by the FACTS Working Group [26]. The term Static Synchronous Generator is one of the 13 defined Shunt Connected Controllers by this group. It states: “A static, self-commutated switching power converter supplied from an appropriate electric energy source and operated to produce a set of adjustable multi-phase output voltages, which may be coupled to an ac power system for the purpose of exchanging independently controllable real and reactive power.”.

A quick searching made on 18/3/2016 in the IEEE database gave 20 results for Synchronverter [10][19][21][22][27], 169 for VSG [6][8][9][12][13][28][29][30][31] [32][33][34], and 3 for Virtual Synchronous Machine with acronym VISMA [35] and acronym VSM [11][36]. Furthermore, the control concept of emulated inertia can be found in Voltage Source Converters (VSC) applied to High Voltage Direct Current (HVDC) [37][38]. To show the development of interest on the subject, the IEEE database was searched again on 12/1/2018 giving 53 results for Synchronverter, 412 for Virtual Synchronous Generator, 512 for Virtual Synchronous Machine, 4 with acronym VISMA. In other words, in less than two years, publications related to SSG with virtual inertia have more than doubled.

Basically, VISMA and VSM have the same control configuration, as well is VSG which is a machine operating as a generator. All types use a similar kind of emulation of inertia through the swing equation [39]. The synchronverter has some particular differences in relation to the VSM and so a rough division between synchronverter and VSM is made in this chapter. The first section is dedicated to the synchronverter and the second to VSG- or VSM-like solutions.

2.1 Synchronverter

The synchronverter is one of the configurations to mimic a real synchronous generator and was first published in 2009 at the PSCE [40] with only simulation results to show the concept; one year after this idea was internationally filed for patent in [41]. This concept was published in a more didactic way and with experimental results in IEEE Transactions on Industrial Electronics in 2011 [21]. The synchronverter configuration and others [12][13] contain the same hardware, a basic voltage source inverter (VSI) with 6 Insulated Gate Bipolar Transistors (IGBTs) in 3 legs and a LCL-

filter for the switching harmonics. A diagram [21] of this two-level inverter is found in Fig. 1. Although the fundamental behavior of the converter remains similar, for higher powers other hardware configurations are applied as, for example, cascaded multilevel inverters and Modular Multilevel Converter (MMC). Nevertheless, the hardware configuration is not object of study in this thesis.

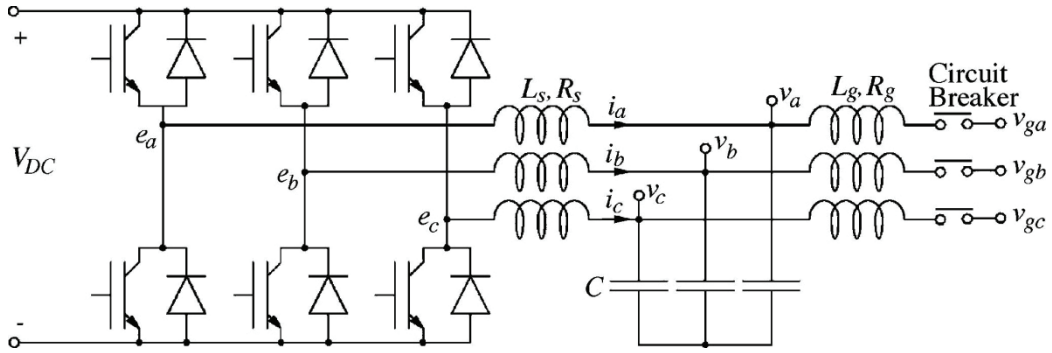

Fig. 1 Basic two-level voltage source inverter with 6 IGBTs in 3 legs and a LCL-filter [21] for illustrative purposes only.

The control part of the synchronverter, as presented in [21], is shown in Fig. 2.

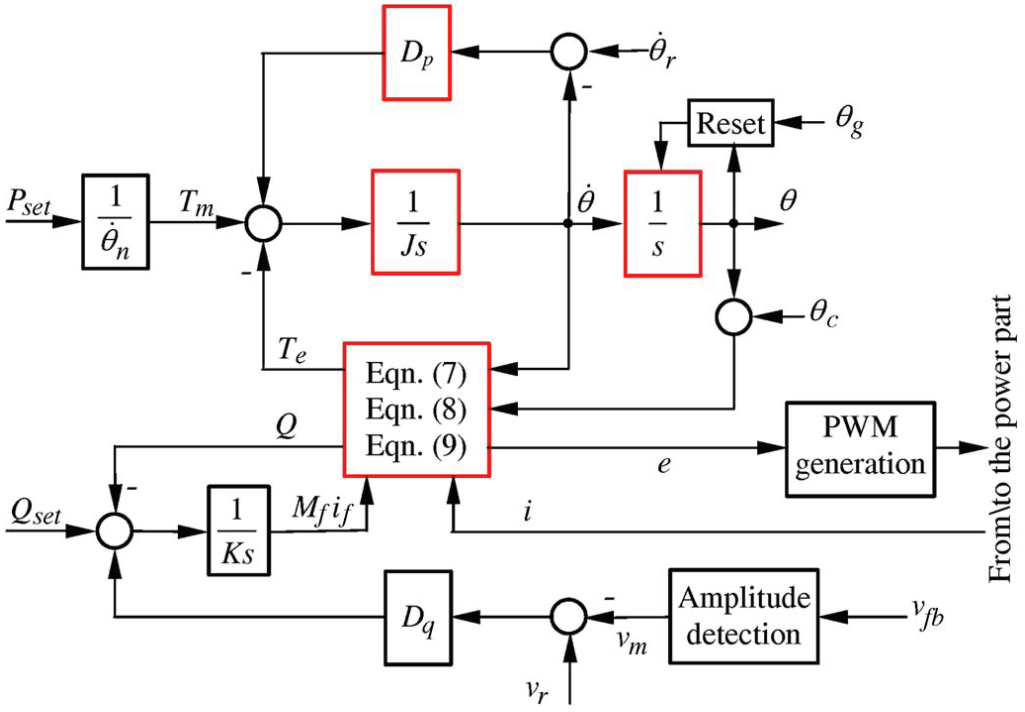

Fig. 2 Synchronverter with active and reactive power control [21].

To emphasize the control structure and to have a base for the proposed adaptation to this control structure, the diagram is redrawn in Fig. 3 without a physical interface or technical implementation.

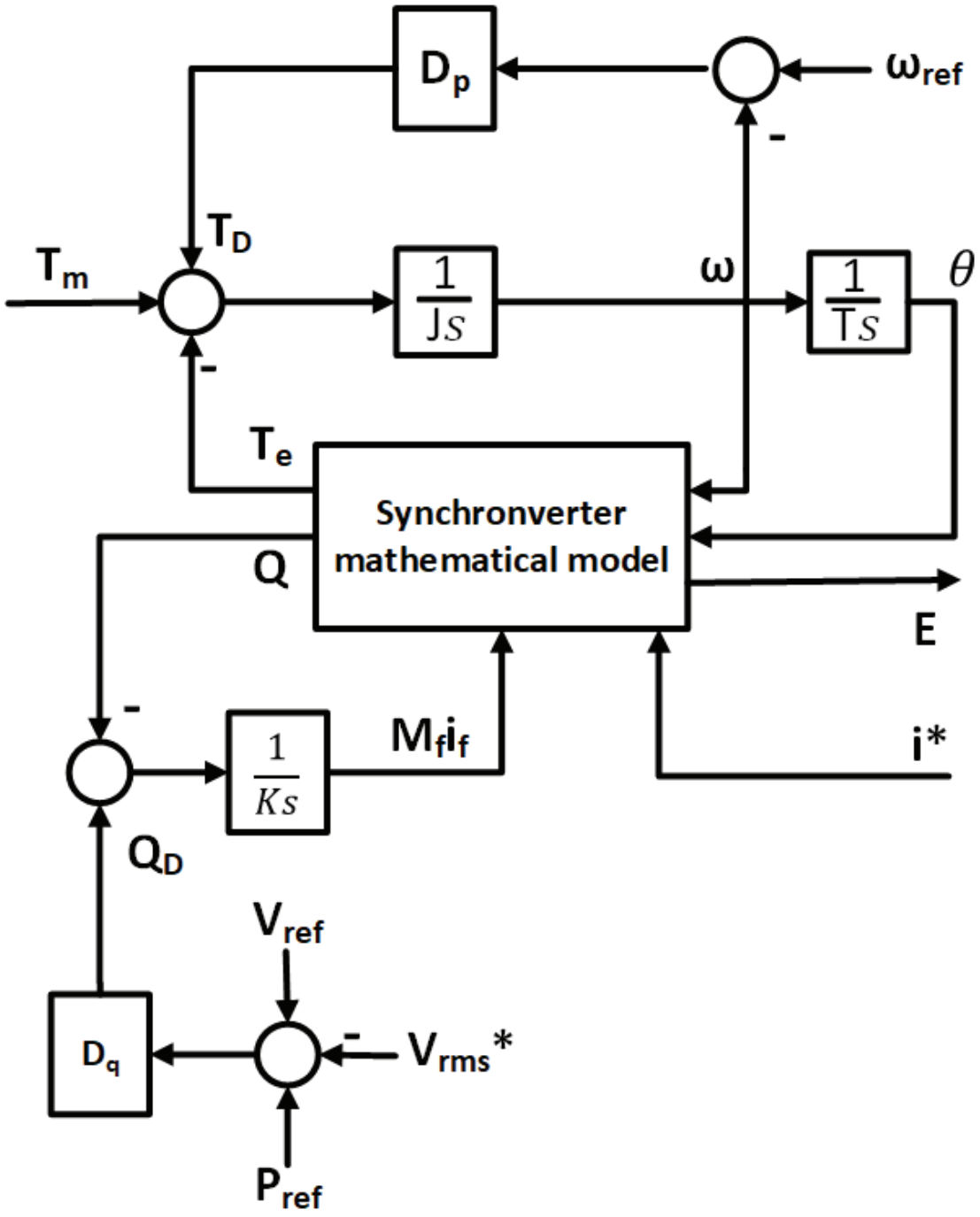

Fig. 3 Redrawn diagram as in Fig. 2 to emphasize the main active and reactive power channels (without technical interface blocks).

In short follows the idea of emulating a synchronous generator with a Voltage Source Converter (VSC), as presented in [21]. The “Synchronverter mathematical

model" box, see Fig. 3, contains the three well known equations [39] of a synchronous generator and are repeated here [42]:

$$T_e = pM_f i_f \begin{bmatrix} sin\theta \\ \sin(\theta - 120°) \\ \sin(\theta - 240°) \end{bmatrix}^T \cdot \begin{bmatrix} i_a \\ i_b \\ i_c \end{bmatrix} , \tag{2.1}$$

$$e_{a,b,c} = \begin{bmatrix} e_a \\ e_b \\ e_c \end{bmatrix} = \omega M_f i_f \begin{bmatrix} sin\theta \\ sin\ (\theta - 120°) \\ sin\ (\theta - 240°) \end{bmatrix} \text{ and} \tag{2.2}$$

$$Q = -\omega M_f i_f \begin{bmatrix} cos\theta \\ \cos(\theta - 120°) \\ \cos(\theta - 240°) \end{bmatrix}^T \cdot \begin{bmatrix} i_a \\ i_b \\ i_c \end{bmatrix} . \tag{2.3}$$

where the electrical torque, T_e, relates with the pole pair, p, which is always considered 1 in this thesis, the maximum mutual inductance between the field coil windings and each one of the stator coil windings, M_f, the excitation current, i_f, and the stator phase-currents, i_a, i_b and i_c. The back electromotive force (EMF), $e_{a,b,c}$ is linearly related to the angular velocity, ω, and the excitation current. Q is the generated reactive power and a result of the inner product of the quadrature of the EMF and the stator currents.

The only directly measured signal that inputs the model box is the generator current i*. The reactive droop to the voltage V_{rms}^* of the voltage-controlled bus, Q_D, is zero, when $D_q=0$ and/or $\Delta V = V_{ref} - V_{rms} = 0$ and the additional signal for Power Oscillation Damper (POD), $P_{ref} = 0$. Hence, in per unit (p.u.), equaling the value of $M_f I_f$ to the value of the bus voltage at the moment of physical connection between the grid and the synchronverter, the synchronverter, through the integrator, will only stabilize when outputting zero reactive power. This means, according to equation (2.2), that the generated voltage amplitude, E, of the EMF only changes with the calculated angular velocity ω and at connection should be equal to the angular velocity of the grid, ω_g.

The last physical interconnection is through T_m, which is related to the capacitor dc-voltage. In case of an infinite dc-capacitor and without voltage control, the synchronverter maintains itself synchronized based only on the measured generator current. This is the basis for the proposal in this thesis, as described in item 3.3, where the similarity between a PLL [43] and the synchronverter is utilized.

The following should be noted from [21]. Since the parameters of the virtual generator at first can be chosen freely, the question is stated if small inertia is good for overall grid stability. In the next chapters this will be partially addressed. Further, [21] states that the energy-storage function of the synchronverter should be decoupled from the inertia (unlike [13]). Obviously this is only possible when the virtual mechanical energy is smaller than the real electric energy contained in the dc-link or that the virtual energy is considered for a limited time, as long as the capacitor voltage doesn't drop below, or slides above, critical values.

In [22][23] the synchronverter is applied as a STATCOM in the SIN to control bus voltage and to damp electromechanical oscillations based on classical POD [44] or Power System Stabilizer (PSS) [39] techniques. The basic structure of Fig. 3 was maintained, though, since a STATCOM doesn´t participate, in steady state, in active power to the grid, the active power droop loop was eliminated as shown in Fig. 4.

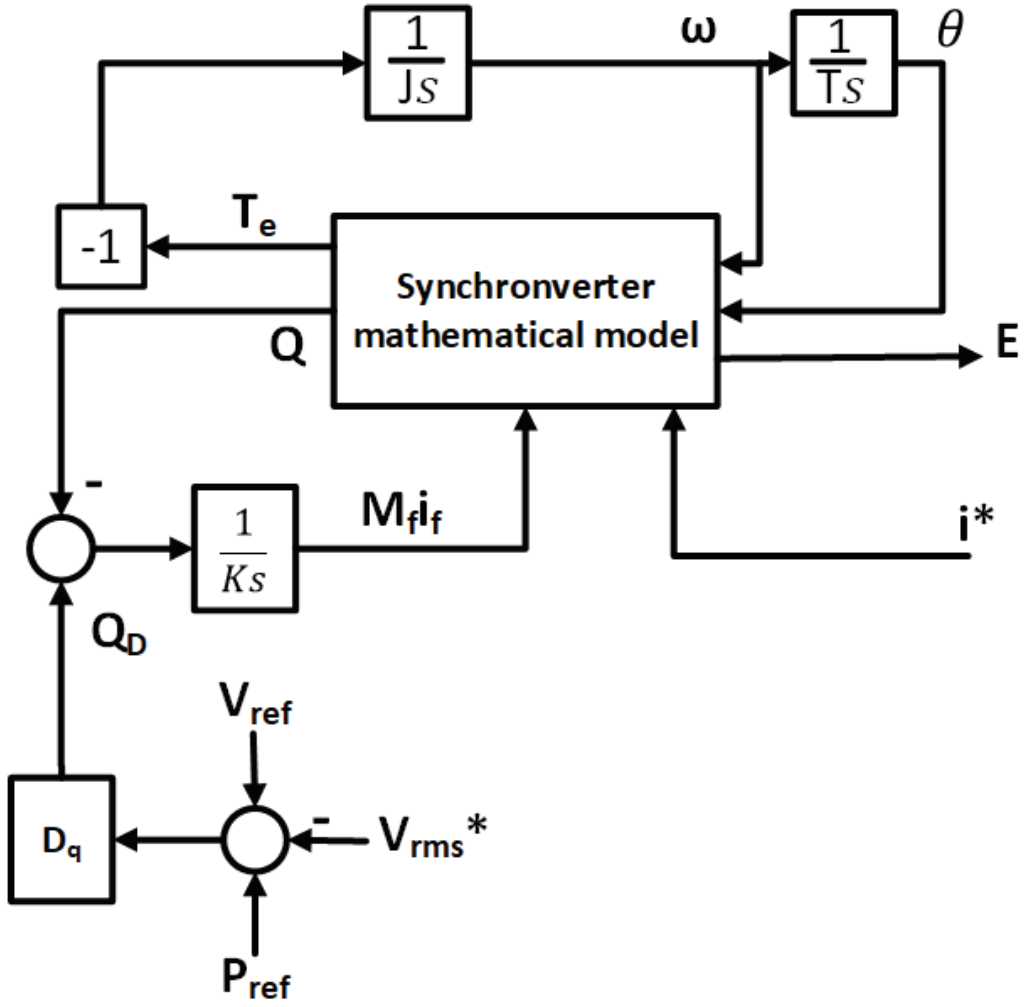

Fig. 4 Diagram of original synchronverter controller for STATCOM without frequency droop controller as in [22].

Beside the removal of the active droop loop, the signal for the virtual torque, T_m, was removed as well for the reported studies in [22][23]. In the next chapter the influence of this signal, representing variations of the dc-link capacitor voltage, is considered again.

2.2 Virtual Synchronous Generator/Machine

Around two and a half months before the international filing date of the synchronverter presented with the title SSG [41], a patent was internationally filed for "Control of a voltage source converter using synchronous machine emulation" [45]. Besides these two patents, three more patents were found. All three filed by the same inventors (for US only), or same company (for the rest of the world). These patents have 7/9/2012 as international filing date and have sequential numbers, as if they have been filed at once. The first of them is titled "Synchronous power controller for a generating system based on static power converters" [46], defining a Power Loop Controller (PLC) with natural frequency and damping as input parameters. With small-signal modeling of the closed-loop transfer function of the power-locked loop (PWRLL), the Power Loop Controller, transfer function between ΔP and $\Delta\omega_{ref}$ is designed as presented in [12] and the control diagram as presented in that paper is shown in Fig. 5.

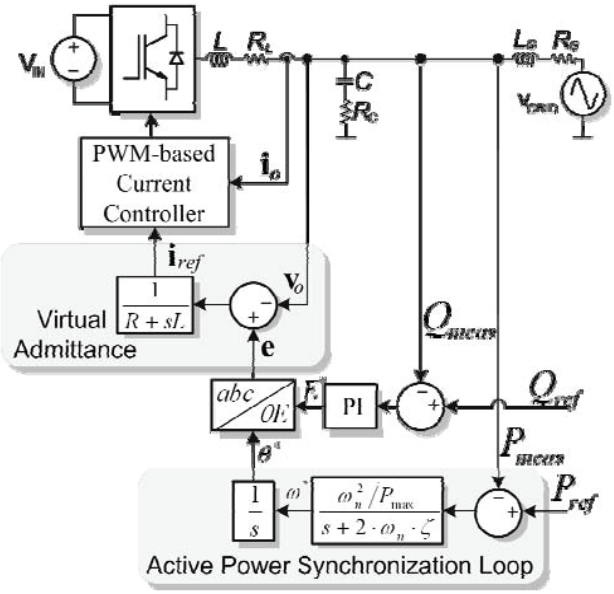

Fig. 5 Control diagram for active power synchronization with virtual admittance as presented in [12].

In fact the first patent refers to the whole system as depicted in Fig. 5. The second patent is titled “Virtual Controller of electromechanical characteristics for static power converters” [47] and refers to the design of the PLC.

The last patent is titled “Virtual admittance controller based on static power converters” [48]. While the current controller was normally based on virtual impedance, the authors made a breakthrough considering admittance, thus, eliminating the differential related to the inductance. Hence, practical problems with applying differentiators to measure currents were eliminated and substituted by applying a lagging pole *{1/(Ls + R)}* to the voltage difference to create the current reference.

Further, in all three patents the idea is stated of a variety of virtual admittances for electrical resonances, and, a variety of virtual inertias and damping factors for electromechanical oscillation resonances. The implementation is based on band-pass filters. Publications were not found on this subject.

In [28] the idea of [12] is repeated with the addition of a relation between the virtual kinetic energy and the electric energy contained in the dc-link. Further it contains a proposal for the decoupling of electric and kinetic energy, in case a storage system is present, e.g. a battery, by creating a variable capacitor through a dc/dc-converter between the storage system and real filter capacitor. The general control diagram, which is a redrawn diagram of [12], is re-presented in Fig. 6 and in this case the virtual inertia, *J*, has been made explicit in the active power synchronization loop.

Qref and Pref are determined by droop controllers with inputs, voltage deviation, Δv, and grid frequency deviation, $\Delta\omega$, respectively. Here, the first differences are found with the synchronverter.

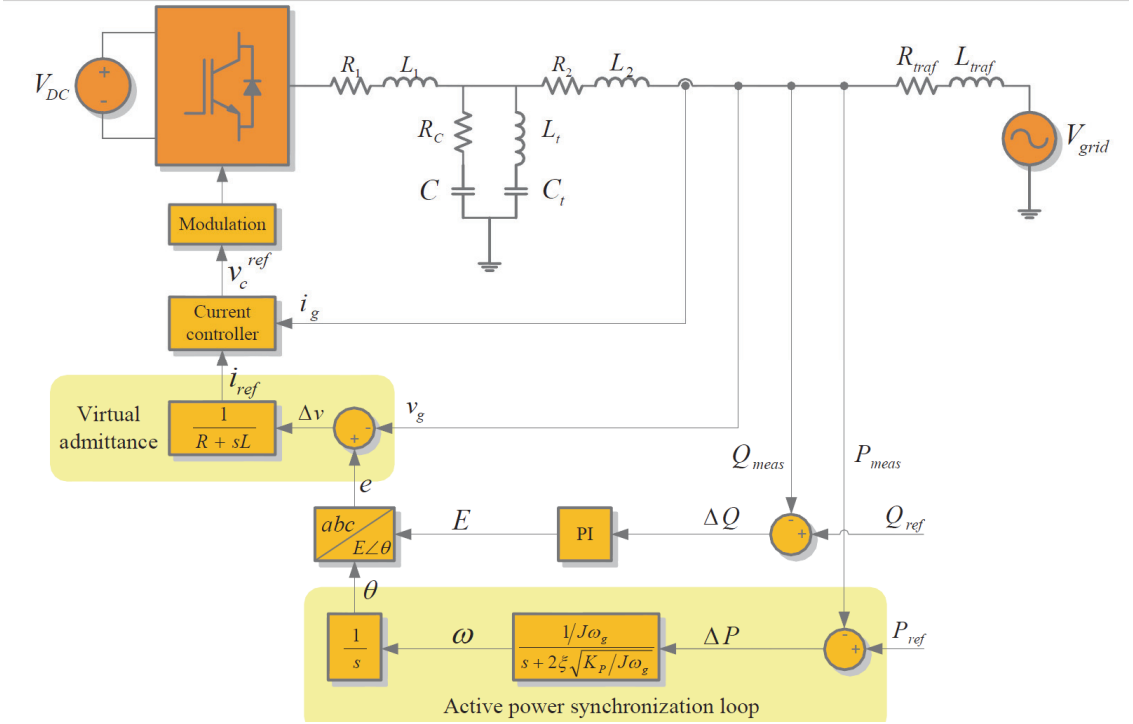

Fig. 6 Control diagram for active power synchronization with virtual admittance. As presented in [28].

2.3 Differences between synchronverter and VSG/VSM.

While the VSG [12][28][29][30][32][33][34] utilizes the measured voltage to determine the reactive and active power deviation, the synchronverter utilizes its own calculated voltage reference. In case of synchronverter based STATCOM in reactive power mode [24], ac-voltage measurement becomes obsolete. Anyway, the voltage measurement utilized to determine the deviation at the controlled bus for the synchronverter is far less critical then the one utilized by the VSG to determine the measured active and reactive powers.

Another main difference between the VSG- or VSM-like SSG, and, synchronverter is that the first is current controlled, although some others omit the current controller [33][34]. The synchronverter does not need virtual impedance or admittance, unless one chooses to omit a PLL for grid connection [10] and in this case the virtual admittance is only utilized before physical connection with the grid. Therefore, in all cases the synchronverter is more naturally seen as a real synchronous generator then the VSG. This is especially seen in the difference of determining the

back electromotive force by the synchronverter and the other VSGs. The synchronverter adjusts the amplitude of the EMF, see Fig. 4, based on the machine equations, see (2.2) and (2.3). While the back electromotive force for the other VSGs is directly determined through a PI-controller with the reactive power difference as input, between an externally measured reactive power and a reference signal, without considering the internal virtual rotation ω. Anyway, the proposed synchronverter controller for STATCOM application operates also well with instantaneous reactive power calculation for the controlled bus as can been seen in the next chapters.

3 The non-generating synchronverter

This chapter describes the particularities of the synchronverter that doesn´t have an electric energy source to maintain its capacitor voltage regulated. Firstly, transfer functions are developed, with the aim to take into account system frequency resonance. Secondly, a classic solution is shortly presented. After that an adaption is proposed to the classic synchronverter controller to make it suitable for non-generating applications in power systems.

As mentioned before, and confirmed in [20][21][49], the frequency droop loop has a stabilizing effect on a generator. From Fig. 3 it is straightforward to determine the following small-signal transfer function:

$$\Delta\omega/\Delta T = (1/D_p)/(1 + Js/D_p), \quad (3.1)$$

with $J = 2H\ (s)$, when the electrical- and mechanical-torque are given in p.u.. With (3.1) it can be understood that when [21] states that D_p contains the mechanical friction, it is the friction for small deviations around the operation point, ω_{ref}, since the part of the damping torque related to mechanical friction is linear with the angular velocity. With the linearization of the frequency droop loop of Fig. 3, the reference is eliminated, as can be seen in (3.1). Thus, in the small-signal equation, damping from the amortisseur or other damping circuits can be inserted in the damping coefficient, D_p, as well [50][51][52][53][54]. This statement cannot be sustained for the complete control diagram of Fig. 3, the large-signal model, where the frequency droop, D_p, only can stand for frequency droop as used in real generators, since the damping torque, T_D, in this diagram, is related to deviations with respect to a reference for angular speed, ω_{ref} [21]. Whereas the damping of the amortisseur, which operates similarly as a squirrel cage in an induction machine, is related to the time derivation of the difference between the angular velocity of the rotor and the bus. Therefore, when controlling the converter as a synchronous machine, the torque originated from the amortisseur should be obtained with frequency measurement at the bus. This idea is running away of the original idea of utilizing a synchronverter to avoid the use of PLLs. At last, the part of the damping torque related to mechanical friction and windage is linear with the own angular velocity, thus in this case, referring to Fig. 3, ω_{ref}, should be zero.

For all non-generating converters with synchronverter control, the frequency droop, D_p, has to be zero when related to ω_{ref} as given by secondary controllers or fixed preset values [42], since these converters can´t contribute in steady state with electrical power due to the lack of an energy source at the dc-side of the converter. Damping from amortisseurs is not considered either to avoid the need of PLLs as mentioned before.

This leaves the mechanical damping, from the three damping factors mentioned above, to utilize as a damping factor, since, when D_p is equal to zero, (3.1) becomes purely integrative. Then, the main loop, responsible for synchronization with the grid,

from ΔT to $\Delta\theta$, becomes a double integration leading to an undamped oscillation. Although for electrical machines this damping factor in p.u. is typically between 0.0 and 0.05, where 0.0 means no frictional losses, for a static compensator this value at first can be chosen freely, since it is not related to a physical construction.

Utilizing (3.1) as a controller, thus besides an equation to describe small signal deviations, does not seem a very effective way to control a static compensator. This controller is a linear first order low band pass filter with gain $1/D_p$ for steady state and for frequencies higher than J/D_p the controller becomes a pure integrator 1/(Js) again. Therefore, another solution will be investigated in item 3.3, where this solution is proposed to create virtual damping again to emulate damping effect.

Before the "Classic" solution is described in item 3.2, and the proposed one in item 3.3, some particularities in relation to the power system will be derived in the next item. Though, the developed transfer functions are valid for any network fed by two voltage sources at the extremities of passive series electric network elements, see Fig. 7, these are especially important for low resistance (X/R > 10) power systems.

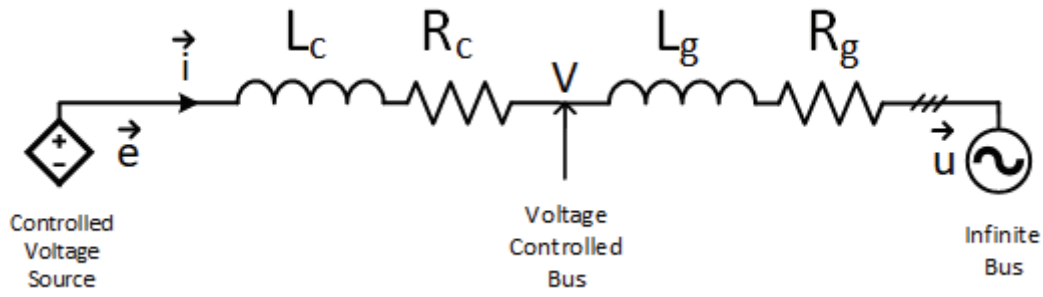

Fig. 7 Passive network with a controlled voltage source at one extremity controlling the voltage amplitude at the voltage controlled bus and an infinite bus, representing the grid, at the other extremity.

3.1 Power System

The authors of [31] determined a transfer function for $\Delta\delta$ to ΔP, $H_{P\delta}$ (s), considering the flux dynamics for a VSC connected to an infinite bus by impedance, Z. When the conventional equation for controller project is:

$$H'_{P\delta} = \frac{EU}{X}\cos\delta_0 , \qquad (3.2)$$

where many authors even consider worst case with $\delta_0 = 0$, no resonance effects will be obtained. Though, considering the flux dynamics and applying Park transformation, it becomes clear that when $s = -j\omega_s$, $jX + sL$ becomes zero. Hence, the denominator of the complete transfer function $H_{P\delta}$ will only have the term R for the system frequency.

From here on in [31], a swing equation is added in series with $H_{P\delta}$, and then the complete transfer function for the VSG, $H_{vsg}\ (s)$, is derived for the reference active power change, ΔP^*, to the actual active power change, ΔP. The authors show the relation between the gain of the total system and the parameters, active droop, Dp, the virtual inertia, J, and, the resistance, $R = R_c + R_g$, of the impedance between the two voltage sources.

The droop D_p is normally given by the operator, and, in case of STATCOM or active filter operation D_p is even equal to zero. So, the experiments were conducted with increased J and R. Increasing J is easy, since it is already a virtual parameter. Though, a controller is applied with virtual resistance, R_v, to avoid dissipating energy in a real inserted resistance.

Now, this contribution is valid to determine the cause of the resonance. It is straightforward to see that this resonance only is relevant in case of fast controllers/converters acting in the range of the system frequency. And, since, for the system frequency the denominator of $H_{P\delta}\ (s)$ is equal to the resistance value, the effect will be more relevant in relatively low resistance networks like power systems.

Although, STATCOM and active filters do have a power control block diagram, since the dc-voltage has to be controlled, it is not the main function of these FACTS. Both mentioned above have the same main function, which is controlling the voltage on a bus, were the latter also compensates harmonics, which is out of the scope of this thesis. Therefore, the other three transfer functions, $H_{\delta Q}$, for $\Delta\delta$ to ΔQ, H_{EQ}, for ΔE to ΔQ, and H_{EP}, for ΔE to ΔP, have to be derived with which a minimum time constant for the reactive power loop can be determined.

Firstly, the transfer function for $\Delta\delta$ to ΔP, $H_{\delta P}$, where in this thesis the more common annotation is adopted for transfer functions where the first symbol in the subscript indicates the input deviation, $\Delta\delta$, and the second subscript the output deviation, ΔP, is repeated for facilitation:

$$\mathrm{H_{\delta P}} = \frac{\Delta \mathrm{P}}{\Delta \delta} = \frac{3}{2} \cdot \frac{\mathrm{a_{\delta P} s^2 + b_{\delta P} s + c_{\delta P}}}{(\mathrm{R+sL})^2 + \mathrm{X}^2}\,, \tag{3. 3}$$

where

$$a_{\delta \mathrm{P}} = \frac{EL^2}{R^2 \div X^2}(-EX + UR\sin\delta_0 + UX\cos\delta_0)$$
$$b_{\delta P} = 2 \cdot \frac{ERL}{R^2 \div X^2}(-EX + UR\,sin\,\delta_0 + UX\,cos\,\delta_0) \quad (3.4)$$
$$c_{\delta \mathrm{P}} = EUR\sin\delta_0 + EUX\cos\delta_0\ ,$$

where the subscript "0" indicates the equilibrium point where around the linearization has been performed. When neglecting *R*, *R≈0*, and for the low frequency range, *s≈0*, (3.3) becomes (3.2) again as expected.

The transfer function for $\Delta\delta$ to ΔQ, $H_{\delta Q}$, can be derived in a similar way as $H_{\delta P}$ has been derived in [31]. Therefore starting with the instantaneous reactive power of the VSG [55][56][57]:

$$\mathrm{Q} = \frac{3}{2}(\mathrm{e_q}.\mathrm{i_d} - \mathrm{e_d}.\mathrm{i_q}) \quad (3.5)$$

For small deviation (3.5) becomes:

$$\Delta\mathrm{Q} = \frac{3}{2}(\Delta\mathrm{e_q}.\mathrm{i_{d0}} + \mathrm{e_{q0}}.\Delta\mathrm{i_d} - \mathrm{e_{d0}}.\Delta\mathrm{i_q} - \Delta\mathrm{e_d}.\mathrm{i_{q0}}) \quad (3.6)$$

Since the terms of (3.6) are all equal to those for the linearized equation for ΔP in [31] the algebraic manipulation leads to $H_{\delta Q}$ with the same denominator as $H_{\delta P}$ and with similar numerator terms as in (3.4):

$$\mathrm{H_{\delta Q}} = \frac{\Delta\mathrm{Q}}{\Delta\delta} = \frac{3}{2} \cdot \frac{\mathrm{a_{\delta Q}s^2 + b_{\delta Q}s + c_{\delta Q}}}{(\mathrm{R+sL})^2 + \mathrm{X}^2}, \quad (3.7)$$

where

$$a_{\delta \mathrm{Q}} = \frac{EL^2}{R^2 \div X^2}(ER + UX\sin\delta_0 - UR\cos\delta_0)$$
$$b_{\delta Q} = 2 \cdot \frac{ERL}{R^2 \div X^2}(ER + UX\,sin\,\delta_0 - UR\,cos\,\delta_0) - E^2L \quad (3.8)$$
$$c_{\delta Q} = EUX\,sin\,\delta_0 - EUR\,cos\,\delta_0$$

Now, for small input deviation ΔE, $\vec{e}$ and $\vec{i}$ must be linearized with respect to ∂E. Repeating the expressions of [31] given for $\vec{e}$ separated in the d and q axes:

$$e_{do} = E \cos \delta_0 \ , \ e_{qo} = E \sin\delta_0 \ , \tag{3. 9}$$

where the infinite bus voltage $\vec{u}$ is positioned entirely in the d-axis. Then applying the partial derivation with respect to ∂E on (3.9) leads to the following linearization:

$$\begin{aligned} \Delta e_d &= \frac{\partial e_d}{\partial E}\Delta E = \cos \delta_0 \\ \Delta e_q &= \frac{\partial e_q}{\partial E}\Delta E = \sin \delta_0 \end{aligned} \tag{3. 10}$$

After linearizing $\vec{i}$ from [31] with respect to ΔE the small deviation expressions utilizing (3.10) follow as:

$$\begin{aligned} \Delta i_d &= \frac{(R+sL)\cos \delta_0 + X \sin \delta_0}{(R+sL)^2+X^2}\Delta E \\ \Delta i_q &= \frac{-X \cos \delta_0 + (R+sL) \sin \delta_0}{(R+sL)^2+X^2}\Delta E \end{aligned} \tag{3. 11}$$

With (3.9), (3.10), (3.11) and the steady state operating points for $\vec{i}$ given in [31], the transfer function for ΔE to ΔQ is given by:

$$H_{EQ} = \frac{\Delta Q}{\Delta E} = \frac{3}{2} \cdot \frac{a_{EQ}s^2 + b_{EQ}s + c_{EQ}}{(R+sL)^2+X^2} \tag{3. 12}$$

where

$$\begin{aligned} a_{EQ} &= \frac{L^2}{R^2 \div X^2}(EX - UR \sin \delta_0 - UX \cos \delta_0) = \frac{-a_{\delta P}}{E} \\ b_{EQ} &= 2 \cdot \frac{RL}{R^2 \div X^2}(EX - UR\, sin\, \delta_0 - UX\, cos\, \delta_0) = \frac{-b_{\delta P}}{E} \end{aligned} \tag{3. 13}$$

$$c_{EQ} = -UR\,sin\,\delta_0 - UX\,cos\,\delta_0 + 2EX = \frac{-c_{\delta P}}{E} + 2EX$$

For the fourth and final transfer function from ΔE to ΔP, H_{EQ}, the linearized equation of the instantaneous active power equation of [31] have to be used again as was used to determine (3.3). Only this time the derivations should be as in (3.10) and (3.11) as for the determination of H_{EQ}, since the linearization is with respect to ΔE. Then H_{EQ} follows as:

$$\mathrm{H_{EP}} = \frac{\Delta \mathrm{P}}{\Delta \mathrm{E}} = \frac{3}{2} \cdot \frac{\mathrm{a_{EP}s^2 + b_{EP}s + c_{EP}}}{(\mathrm{R+sL})^2 + \mathrm{X}^2} \tag{3.14}$$

where

$$\begin{aligned} a_{EP} &= \frac{L^2}{R^2 \div X^2}(ER + UX\,sin\,\delta_0 - UR\,cos\,\delta_0) = \frac{a_{\delta Q}}{E} \\ b_{EP} &= 2 \cdot \frac{RL}{R^2 \div X^2}(ER + UX\,sin\,\delta_0 - UR\,cos\,\delta_0) + EL = \frac{b_{\delta Q}}{E} + 2EL \\ c_{EP} &= UX\,sin\,\delta_0 - UR\,cos\,\delta_0 + 2ER = \frac{c_{\delta Q}}{E} + 2ER \end{aligned} \tag{3.15}$$

Although the complete expressions are utilized for numeric analysis in the next chapter, one approximation for visual analysis can be made for non-generating devices. Whereas, the load angle, δ_{gb}, between the infinite bus and the controlled voltage bus can be large, caused for example by loads on this voltage controlled bus, the load angle, δ, caused by loading the non-generating device in relation to the infinite bus is very small. In a linear network with respect to small deviations this load angle can be considered equal to zero. Equations (3.4), (3.8), (3.13) and (3.15) then become:

$$\begin{aligned} a'_{\delta \mathrm{P}} &= \frac{EL^2X}{R^2 \div X^2}(U - E) \\ b'_{\delta P} &= 2 \cdot \frac{ERLX}{R^2 \div X^2}(U - E) \\ c'_{\delta \mathrm{P}} &= EUX \end{aligned} \tag{3.16}$$

$$a'_{\delta \mathrm{Q}} = \frac{EL^2R}{R^2 \div X^2}(E - U)$$

$$b'_{\delta Q} = 2 \cdot \frac{ER^2L}{R^2 \div X^2}(E - U) - E^2L \tag{3.17}$$
$$c'_{\delta Q} = -EUR$$

$$a'_{\mathrm{EQ}} = \frac{L^2X}{R^2 \div X^2}(E - U) = \frac{-a'_{\delta \mathrm{P}}}{E}$$
$$b'_{EQ} = 2 \cdot \frac{RLX}{R^2 \div X^2}(E - U) = \frac{-b'_{\delta P}}{E} \tag{3.18}$$
$$c'_{EQ} = UX + 2EX = \frac{-c'_{\delta P}}{E} + 2EX$$

$$a'_{EP} = \frac{L^2R}{R^2 \div X^2}(E - U) = \frac{a'_{\delta Q}}{E}$$
$$b'_{EP} = 2 \cdot \frac{R^2L}{R^2 \div X^2}(E - U) + EL = \frac{b'_{\delta Q}}{E} + 2EL \tag{3.19}$$
$$c'_{EP} = R(2E - U) = \frac{c'_{\delta Q}}{E} + 2ER$$

The poles are given in [31] and for facilitation are repeated here:

$$s_{1,2} = -\frac{R}{L} \pm j\omega_s \tag{3.20}$$

With (3.17) the natural frequency, ω_n, and the damping, ξ, can be calculated:

$$\omega_n = \sqrt{{\omega_s}^2 + \frac{R^2}{L^2}} = \omega_s\sqrt{1 + (\frac{R}{X})^2} \tag{3.21}$$

$$\xi = \frac{\frac{R}{L}}{\sqrt{{\omega_s}^2 + \frac{R^2}{L^2}}} = \frac{\frac{R}{X}}{\sqrt{1 + (\frac{R}{X})^2}} \tag{3.22}$$

With (3.18) and (3.19) it is evident that in power systems, which have *X/R > 10*, the natural frequency of the system, for transfer from δ or E to either P or Q, is close to the system frequency. Besides, the system frequency resonance for those power systems are poorly damped with $\xi < R/X < 0.1$.

3.2 Classic solution

Here the solution of Nguyen, Zhong, Blaabjerg and Guerrero [24] will shortly be presented and commented. This is the only paper found with respect to a STATCOM with synchronverter controller. After Zhong has repeated his classical synchronverter controller [21], the contribution in this paper related to the synchronverter is an option with two switches for choosing between reactive power control, voltage control and voltage-droop control. Then the feedback of the electrical torque is abandoned and the angular velocity is directly derived with a PI-controller from the dc-voltage difference. This concept is based on changing the load angle, δ, between the STATCOM terminals and the controlled bus to maintain the dc-link voltage constant, normally to cover switching losses and dissipation in the power circuit components of the STATCOM [58].

Only simulation results are presented in [24]. Two cases were simulated. Firstly, the STATCOM switches between reactive power control to voltage control and then droop control. Secondly, when the STATCOM enters in voltage control, 4% step-changes on the angular velocity of the ideal source, representing an infinite bus, are applied. When simulated with values more typical of a transmission grid the performance seem to be poor because of higher X/R values. The gains were adjusted by PSCAD simulations, as shown in item 4.2, to the best. Compromise between oscillation of dc-voltage controller, needing higher loop gain, and synchronous frequency resonance [31], limiting the bandwidth because of resonance peak on system frequency.

3.3 Proposed solution

As mentioned before, a STATCOM without energy storage doesn't have an active power droop controller, since its function is only to support with reactive power. A derivative operator on the frequency droop avoids contribution in steady state, though pure derivations applied in digital signal processing can lead to nasty spikes. This can be mitigated by adding a real pole to the pure derivation operator, as shown in Fig. 8, hence, leading to delays, which can be significant for applications where energy contributions are expected just for transients. Furthermore, while it might work for transient power contribution, because of the lagging derivation there is no indication that it can be effective for internal angular velocity damping.

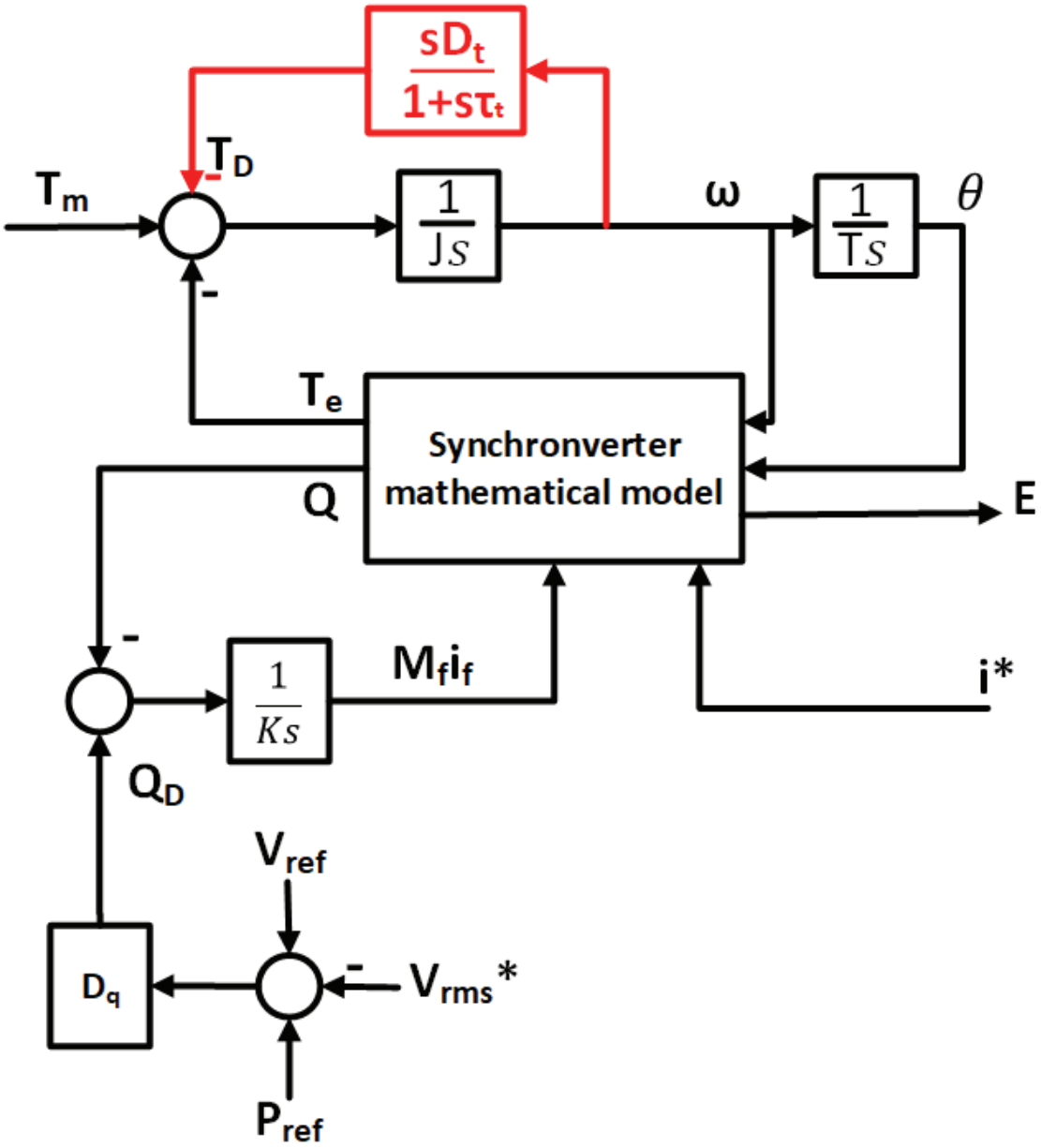

Fig. 8 Diagram of original synchronverter controller [21] with a derivative droop in red.

To avoid this problem, dynamics can be improved by utilizing a PI-controller instead of a pure integrator to calculate ω, as shown in Fig. 9. Hence, a PLL is found as in [43] and all of the experience gained with this PLL can be applied to dimension the PI-controller in the synchronverter. Later it was found that the concept of adding a proportional gain P in an indirect way in [32] was applied to VSG. Positive results in this control concept were obtained.

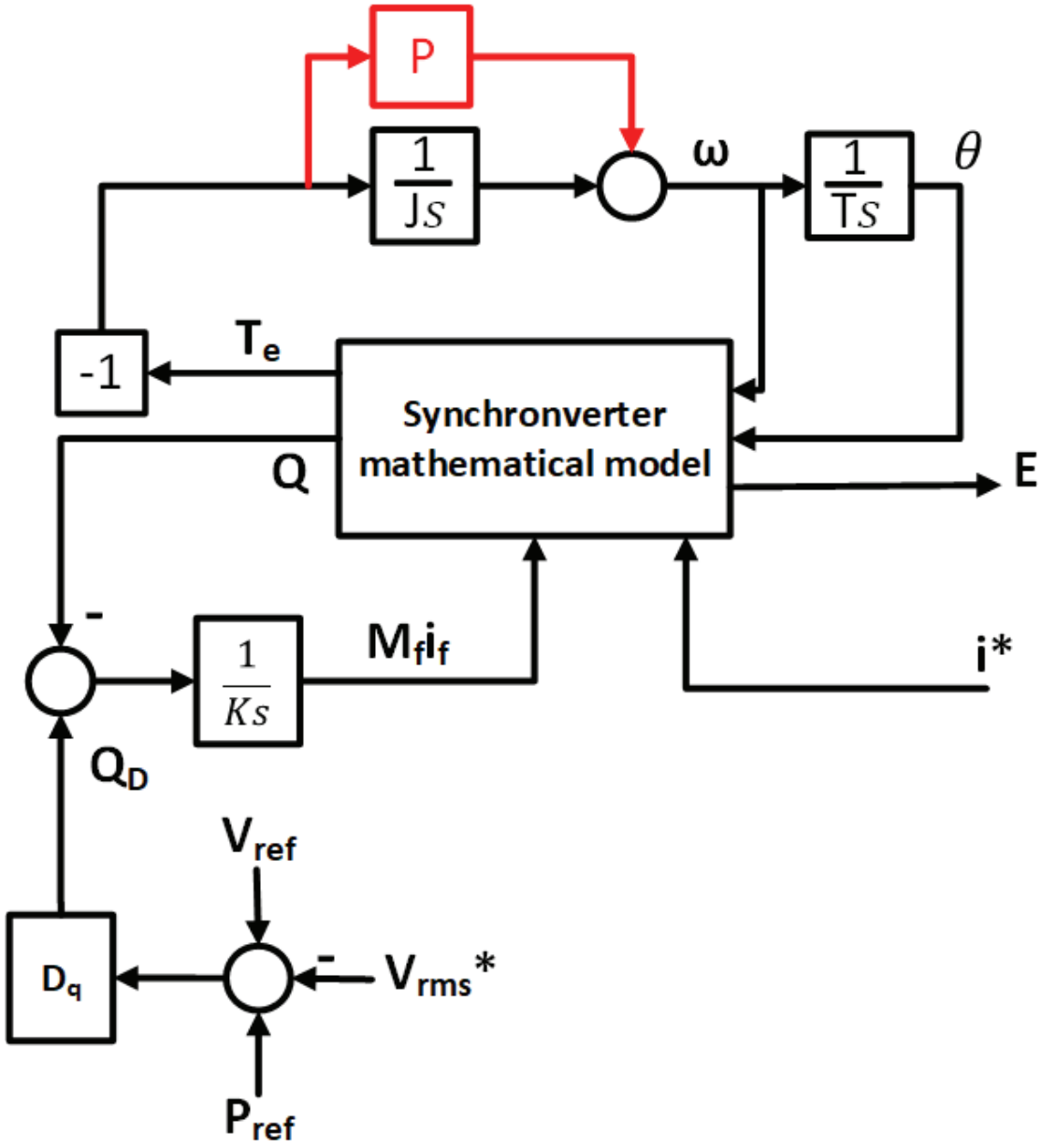

Fig. 9 Diagram of original synchronverter controller for STATCOM in black as in [22] with proposed proportional gain in red for stability purposes and speeding up transients.

While in [22] and [23] the dc-capacitor was considered infinite and, thus the diagram of Fig. 4 was utilized to control the converter, in this thesis a dc-capacitor is considered. Therefore, the mechanical torque signal was introduced again as in the original synchronverter configuration as shown in Fig. 3.

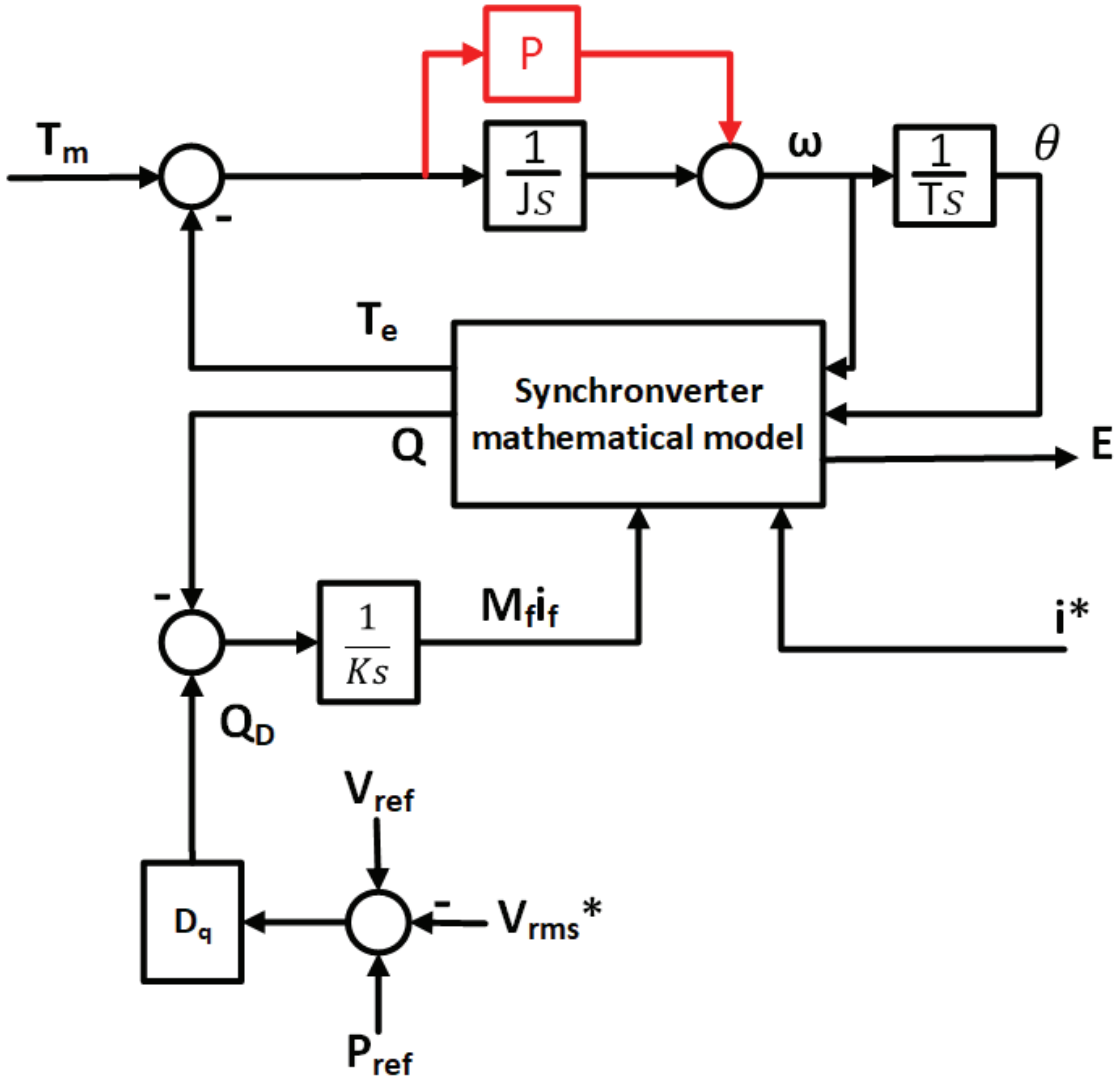

Fig. 10 The proposed synchronverter controller with signal for virtual mechanical torque, T_m, to compensate for physical losses in the VSC.

The last stage of the diagram is given in Fig. 11. Three differences with Fig. 10 can be noted. Firstly, the diagram was converted from generator to motor convention and parameter name adaptations, since a STATCOM has no generator unit at its dc-side. Some papers can be found with generation configurations, though, to the author´s knowledge, in practice such an operative configuration is inexistent and not object of this thesis. Thus, a STATCOM, in steady state, only absorbs active power.

Secondly, the mechanical torque signal is detailed by a simple proportional controller applied to a voltage difference on the capacitor. An integrator with high time constant, in relation to $J = 2H$ (s), can be applied in parallel to the proportional gain when a zero steady state error is desired. This can be considered as a secondary

controller [42] when a dc-capacitor is seen as an equivalent of mechanical inertia of synchronous generators, which contains a kinetic energy in function of the angular velocity. The time constant of the integrator can be seen as an equivalent of the time constant of a secondary controller and the reference signal, V_{dcref}, has its equivalent in the frequency reference signal of synchronous generators.

Finally, the reactive loop gained two additional parameters. A set-point for the reactive power, Q_{set}, was added. And an own gain, D_Q, for the difference between the reactive power with its set-point was included according to [24]. In Fig. 10, Q_{set} was considered equal to zero and D_Q equal to one.

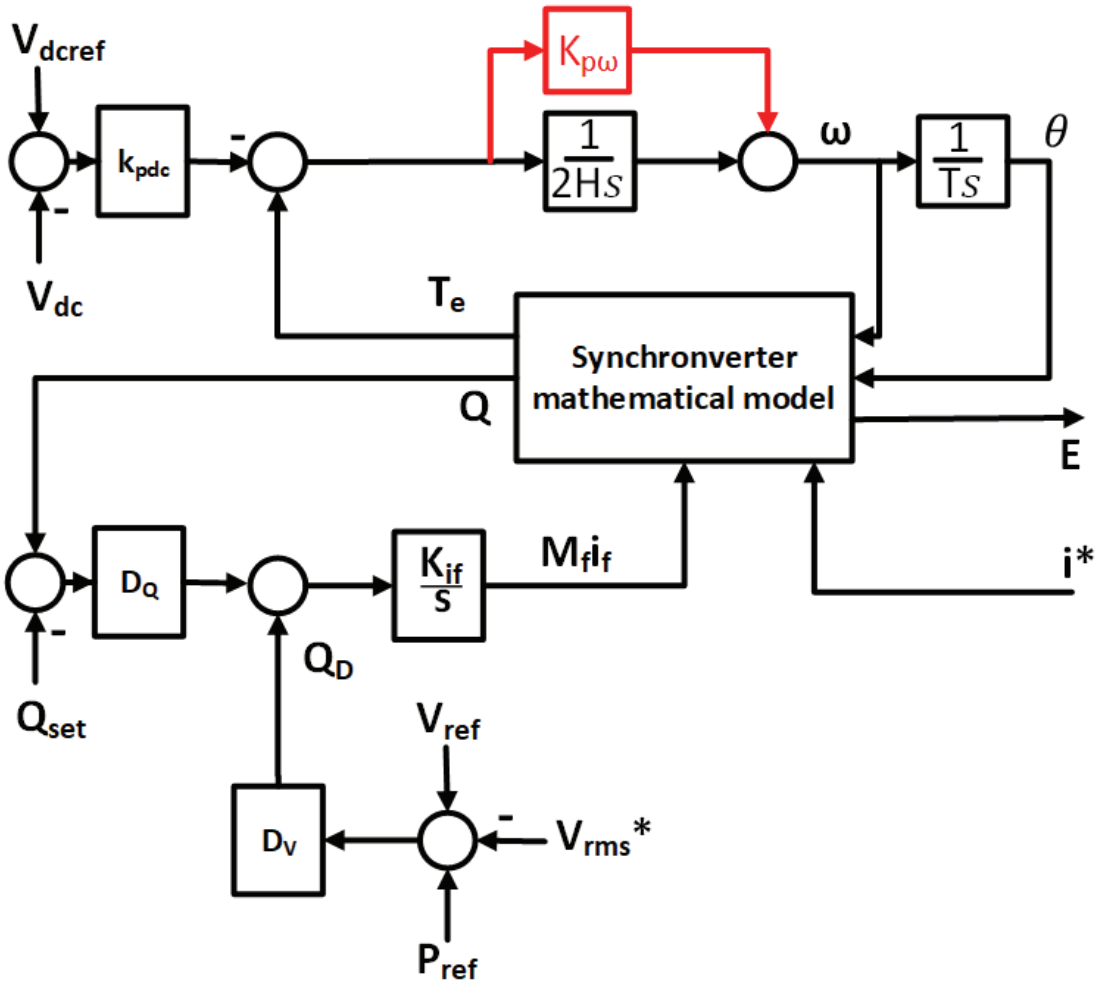

Fig. 11 The proposed synchronverter controller adapted to motor convention and parameter name adaptations, with input for dc-voltage control to compensate for physical losses in the VSC, and reactive power control.

The loop for small deviations in active power reference, ΔP^*, to small deviations in output active power, can be closed with the synchronverter based controller for STATCOM, as given in Fig. 11, and the plant for the relation between small deviations in load angle, $\Delta\delta$, and small deviations in active power, ΔP, transfer function $H_{\delta P}$, as given in (3.3) and (3.4). The active power control block diagram is given in Fig. 12. With this diagram, root locus for different values of the proposed gain $K_{P\omega}$ and the inertia $2H$ can be obtained as well as for different X/R values.

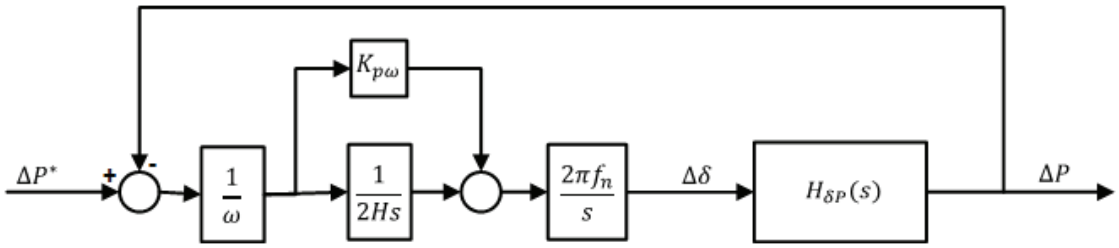

Fig. 12 Active power control block diagram with linearized plant $H_{\delta P}$ for controller project for STATCOM with proposed controller.

The newly developed transfer function, H_{EQ}, for small deviations in the generated amplitude of the converter voltage, ΔE, to small deviations in reactive power, ΔQ, as given in (3.12) and (3.13) was used to close the loop for reference signal for reactive power, ΔQ^*, to actual reactive power, ΔQ. The reactive power control block diagram can be found in Fig. 13. Limit value for gain $D_q.K_{if}$ can be obtained, giving thus the smallest possible time constant that can be applied.

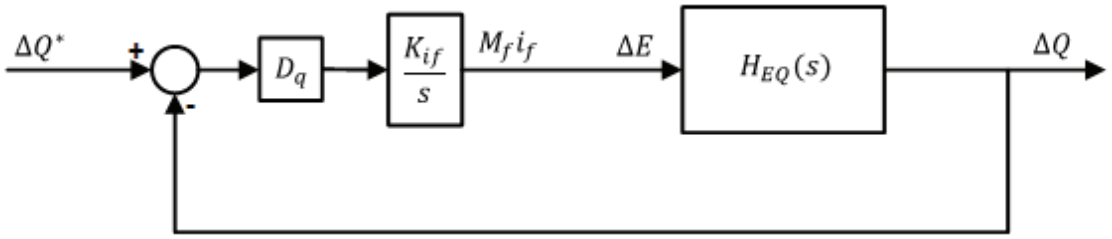

Fig. 13 Reactive power control block diagram with newly developed linearized plant H_{EQ} for controller project for STATCOM.

The block diagrams of Fig. 12 and Fig. 13 can be connected together utilizing the disturbance transfer functions from $\Delta\delta$ to ΔQ, $H_{\delta Q}$, as in (3.7) and (3.8), and from ΔE to ΔP, H_{EP}, as in (3.14) and (3.15). The obtained result is given in Fig. 14 and was

implemented in Simulink to verify the significance of these disturbances on the results of the isolated power control blocks of Fig. 12 and Fig. 13.

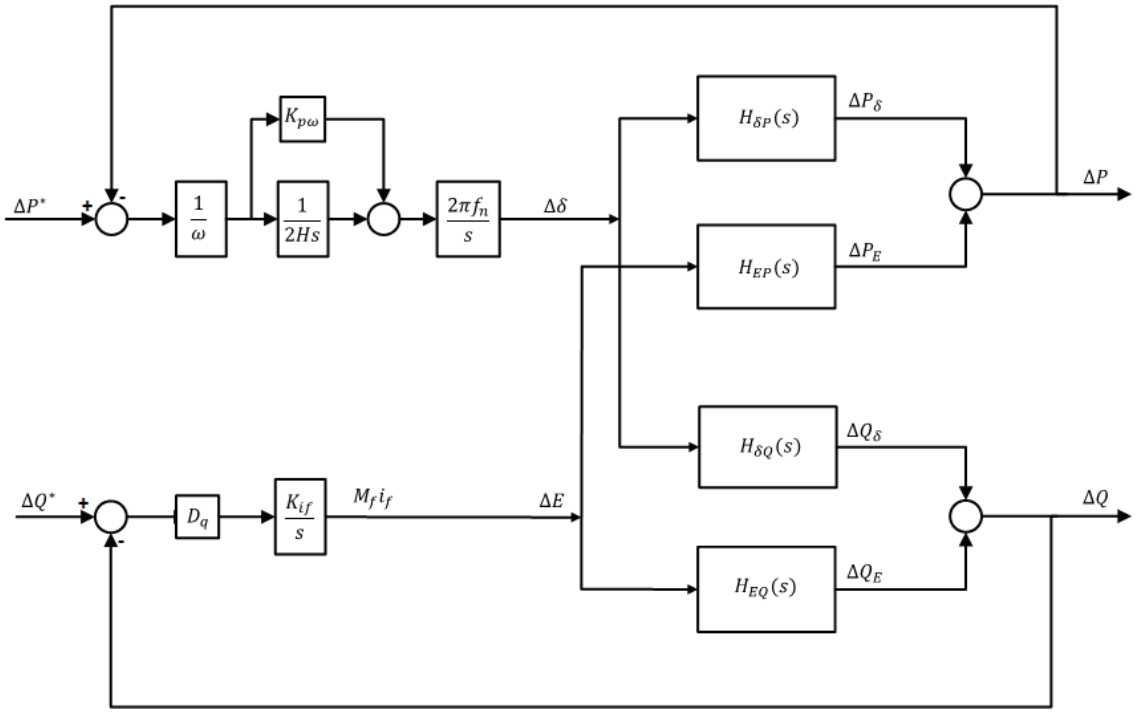

Fig. 14 Active- and reactive-power control block diagram connected with the disturbance transfer functions between the active- and reactive-loops as modeled in Simulink.

4 Results and analysis

This chapter gives the results of both classic and proposed non-generating synchronverter controllers. These results are represented in both the frequency- and time-domain and is accompanied by analyses and suggestions

4.1 Frequency domain

In this item some results can be found for the proposed synchronverter, item 3.3, considering system frequency resonance, item 3.1, for the frequency domain. For the active- and reactive-power loops, root loci, and phase- and gain-margin plots were generated in function of the controller gain. The presented results serve as a base for the simulations of the Brazilian National Grid in item 4.2. The plots were made for the following parameters: $J = 2H = 1$ s, $X/R = 50$ at 60 Hz. This ratio is equal to the actual transformer at Bom Jesus de Lapa where nowadays a SVC is connected to the 500 kV grid. In the simulations the converter inductor was considered with the same X/R ratio.

In Fig. 15 the root loci for the closed loop of $\Delta P/\Delta Pref$ can be found for different values of $k_{p\omega}$. For zero value of this proposed gain the poles are located on the black crosses. While increasing the value, the path via the blue dots is heading to the red crosses. As expected, 2 pole pairs are found for each gain $k_{p\omega}$. One pole pair is related to the system frequency resonance and has a value close to the system frequency of 377 rad/s and starts on the stable side of the s-plane. Whereas, the pole pair related to the virtual inertia starts at the right half side of the s-plain. While increasing the proposed gain, $k_{p\omega}$, the virtual inertia becomes a stable pole pair as well. Nevertheless, when increasing the gain too much, the system frequency resonance becomes unstable. As can be seen in the figure, indicated by the last sixteen blue dots before the red crosses, this will occur before the swing equation becomes overdamped.

For every calculated root locus as a function of $k_{p\omega}$ the phase- and gain-margins were calculated as well. The results for open loop transfer function belonging to the roots of Fig. 15 can be found in Fig. 16. The system was found to be stable for $0.00107 < K_{p\omega} < 0.0122$.

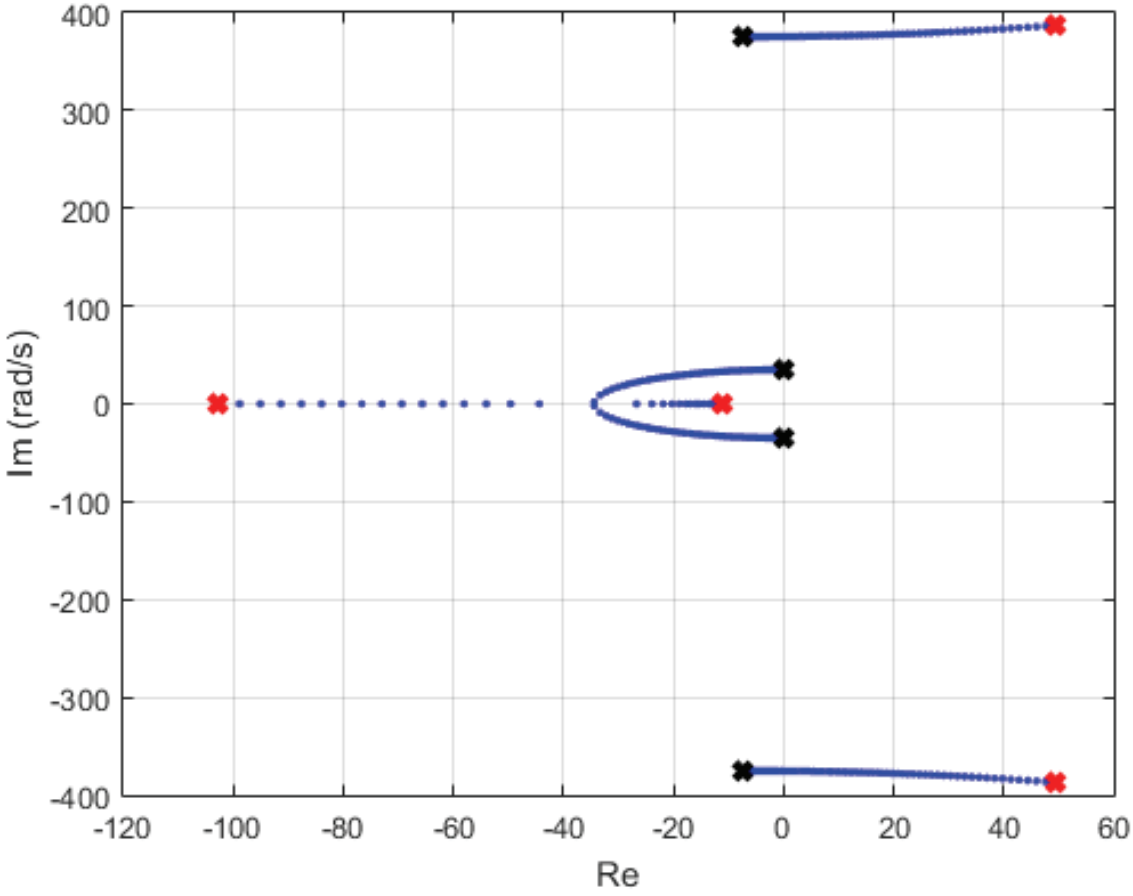

Fig. 15 P_{ref} to P. System frequency resonance pole pair starts (black cross) stable and goes with higher gain $k_{p\omega}$ towards (red cross) instability. Pole pair of synchronverter starts instable and goes with higher gain towards stability. R = 0.00686 Ω. L = 0.00091 H. J = 2H = 1 s. $K_{p\omega}$ from 0 to 0.1.

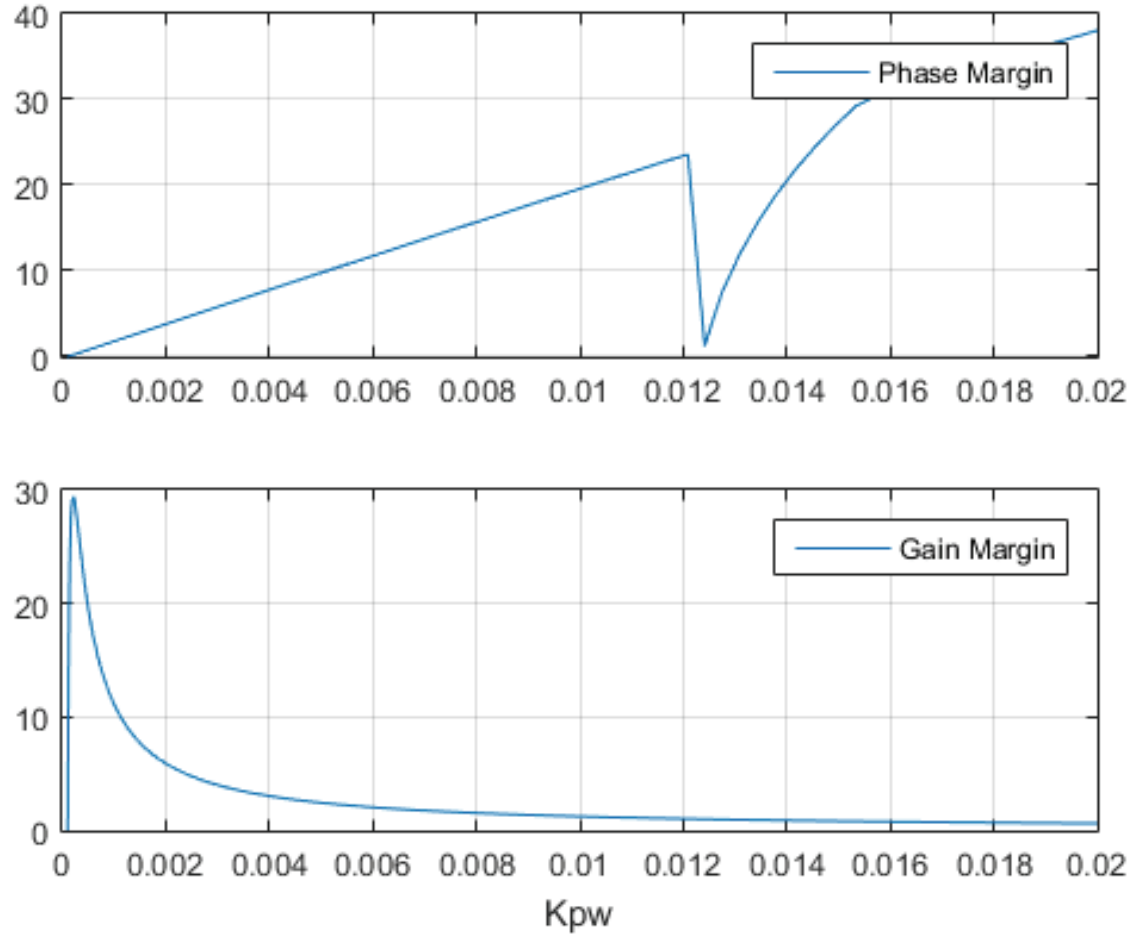

Fig. 16 P_{ref} to P. Phase and Gain Margin as a function of $K_{p\omega}$. R = 0.00686 Ω, L = 0.00091 H, J = 2H = 1 s. Stable for 0.00107 < $K_{p\omega}$ < 0.0122.

For the reactive power loop the root loci as a function of Ki_f, see Fig. 13, can be found in Fig. 17. The reactive loop only has one pole of the controller integrator and the pole pair of the system frequency resonance. Thus the pole starts in zero for zero gain. The pole pair for the transfer function related to the open loop transfer function is similar to the one for the active power, since the denominators are equal. Again the gain is limited by the pole pair related to the system frequency resonance.

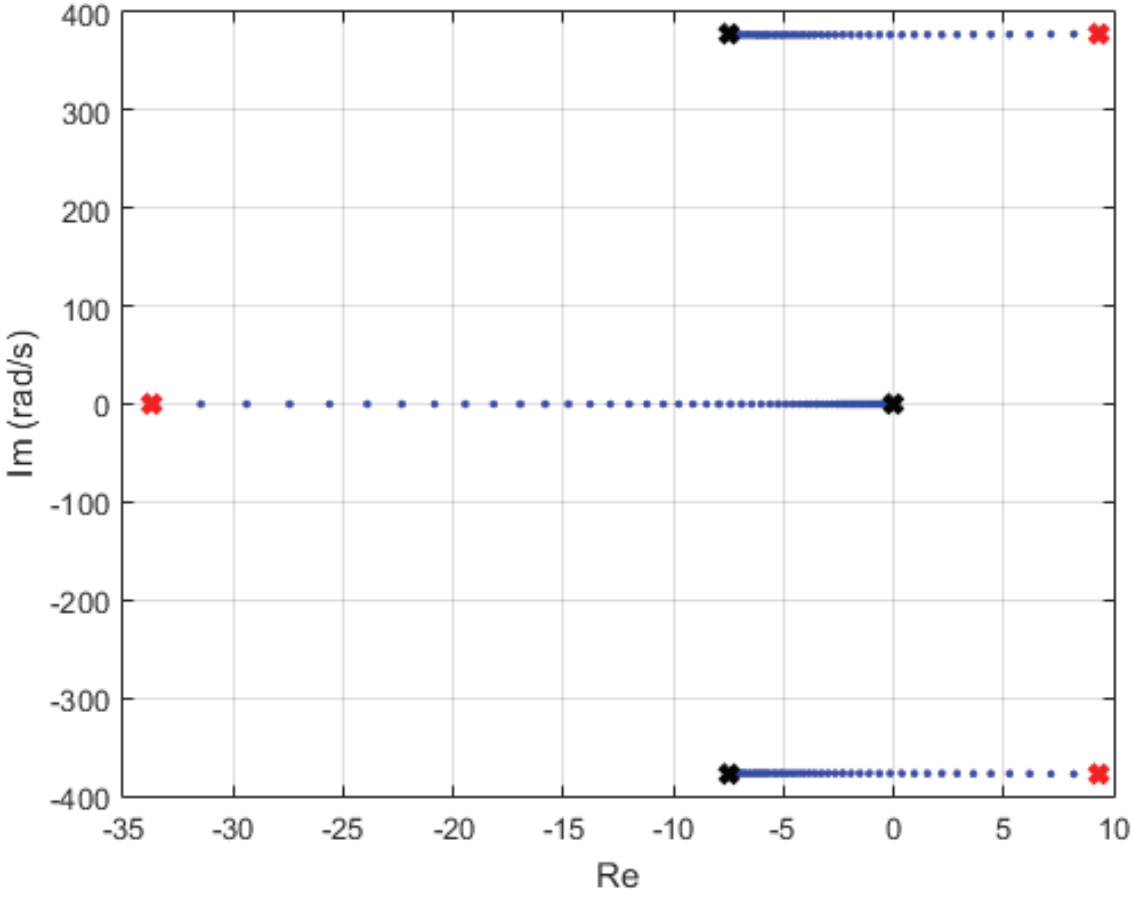

Fig. 17 Q_{ref} to Q. System frequency resonance pole pair starts (black cross) stable and goes with higher gain Ki_f towards (red cross) instability. Pole of synchronverter starts in zero. R = 0.00686 Ω, L = 0.00091 H. Ki_f from 0 to 10.

The phase- and gain-margins were calculated for the reactive power loop as well in function of gain Ki_f as can be found in Fig. 18. For value of $Ki_f < 4.37$ the system frequency resonance is stable. This means that the time constant for the reactive control has to be greater than 230 ms for grids with *X/R* higher or equal to 50.

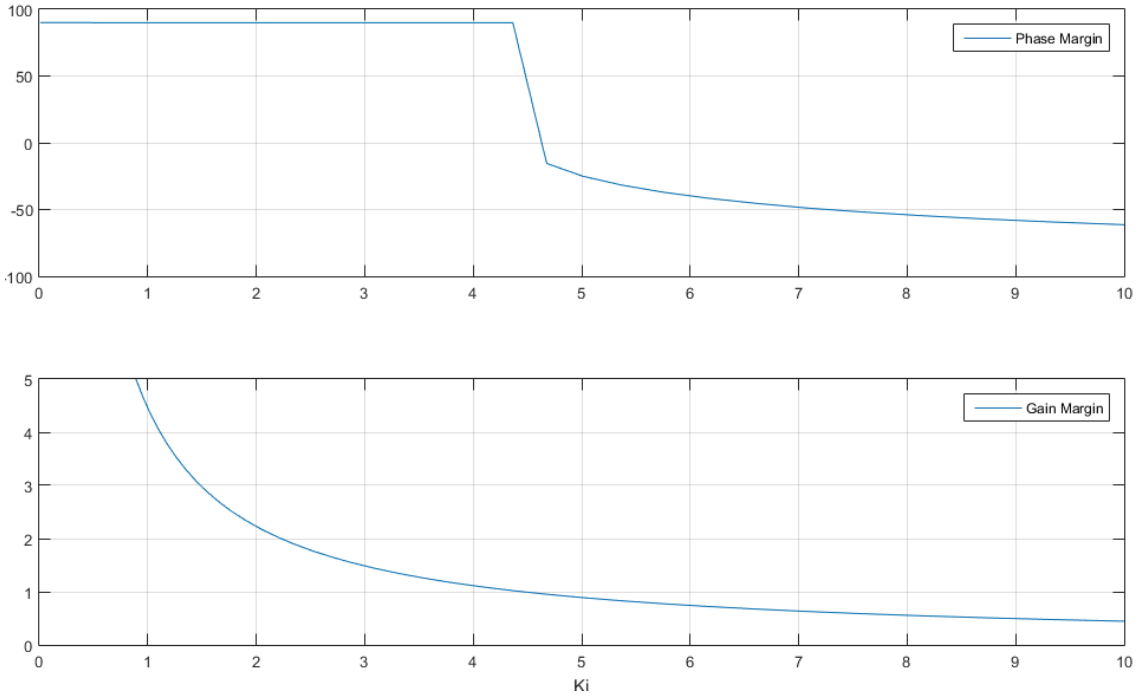

Fig. 18 Q_{ref} to Q. Phase and Gain Margin as a function of Ki_f. R = 0.00686 Ω, L = 0.00091 H. Stable for Ki_f < 4.37.

4.2 Time domain

Firstly, simulations of the proposal for STATCOM with synchronverter based control of Nguyen, Zhong, Blaabjerg and Guerrero [24] (see item 3.2) are compared with the proposal of this thesis (see item 3.3). No other references were found with synchronverter based controllers for STATCOM operation. After the comparison, the power system is simplified to examine rapidly the influence of parameters of the synchronverter/STATCOM. At last simulations are performed with a significant part of the Brazilian Power system with the synchronverter in STATCOM operation and power oscillation damping function based on [22] and [23].

For a fair comparison with [24], the model for the power system used in that paper was the base for the model used in PSCAD for the comparison between the classic solution and the proposed solution. [24] gives information on voltage levels, nominal active and reactive powers, transmission line length and feeder length. No information is given on the *R* and *X* values of the grid.

Therefore, the elements of the modeled Brazilian power system were utilized as a base for modeling the system of [24]. The real transformer at Bom Jesus de Lapa connecting nowadays a 250 MVA/17.5 kV SVC to a 500 kV bus, was base for the *L* and *R* values in the system (see Fig. 19). Therefore, all the elements have been scaled to 500 kV, with exception of the STATCOM elements which were scaled to 17.5 kV (see Fig. 20). The impedances of the transmission line and feeder are based on the short-circuit impedance, 0.178 H and 4.77 Ω, seen nowadays (2007) by the SVC. To obtain values for the grid angle, θ_g, on the voltage controlled bus in Bom Jesus de Lapa, comparable with the results in [24], this short circuit was doubled and 10% of the short-circuit impedance was added to represent the feeder. Though, the *X/R* ratio was kept unaltered in 14.1. The simulations in [24] were performed with a STATCOM configuration with an apparent power, $S_{STATCOM\ CLASSIC}$, of 5 MVA. Since, in this thesis all the simulations were performed with a STATCOM with an apparent power, S_{SVC}, of 250 MVA, all the powers of the loads in the model of [24] were multiplied with 50.

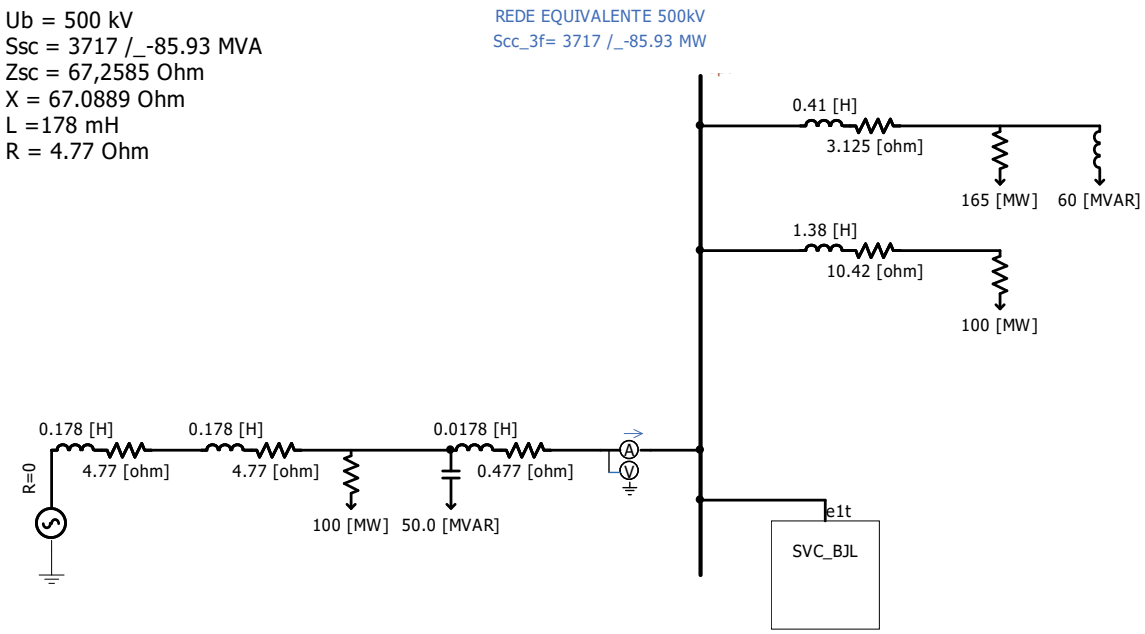

Fig. 19 Test bed based on [24]. Values of series elements were not given. Loads were scaled with S_{nom}.

All simulated variables in the simulation were utilized in their instantaneous form, with only one exception. Although the voltage at the 500 kV side at Bom Jesus de Lapa is also calculated and shown in its aggregated form, this cannot be used as a control signal for the synchronverter [21], since the ripples caused by unbalances on the

terminal voltages can imply instability. Therefore, the digital measurement function of the PSCAD meter was used (Fig. 20). This signal, an aggregate value of a moving average of the three line voltages, was transmitted to the “Ideal Statgen” module.

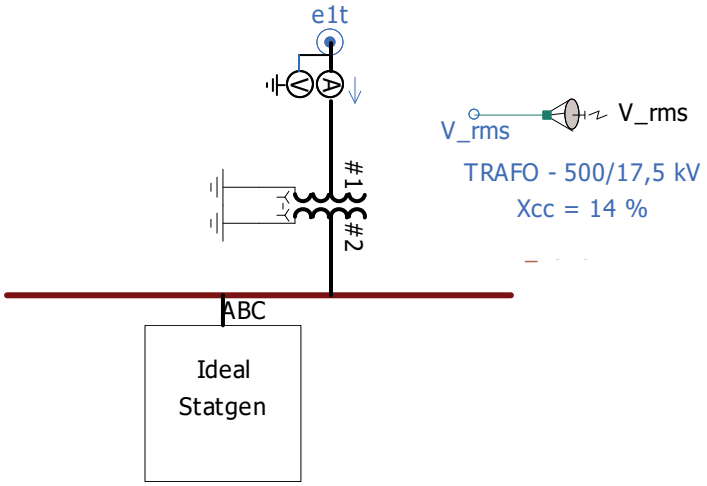

Fig. 20 Inside of the module SVC_BJL of Fig. 19. Transformer data based on transformer in operation at Bom Jesus de Lapa (BH), connecting SVC to the 500 kV transmission grid. Signal V_rms, RMS value of the voltage at the high-voltage side, #1, of the transformer, measured at the AV-meter is sent to the module “Ideal Statgen”.

The modeling of the hardware part inside this module is shown in Fig. 21. For not studying the switching behavior, also [24] used the IGBT models in average mode, a capacitor is omitted in the LCL-filter and the L-values were considered to be equal, which was found to be a common practice. The capacitor of an LCL-filter does not give significant reactive support at the system frequency.

The generated voltages are considered to be independent of the voltage level on the dc-link. In other words, the switching strategy is based on a division of the amplitude modulation ratio by the capacitor voltage. Therefore, the generated voltages, *Vref_A,B,C*, are equal to $e_{a,b,c}$, and only dependent of the variables as given in (2.2). The meter in Fig. 21 is only utilized for synchronization purposes and for analysis of the calculated load angle. The converter current is measured through the breaker, *BRK*. With exception of the Brazilian power system simulation, at all simulations the breaker closes at 0.9 s, and remains closed.

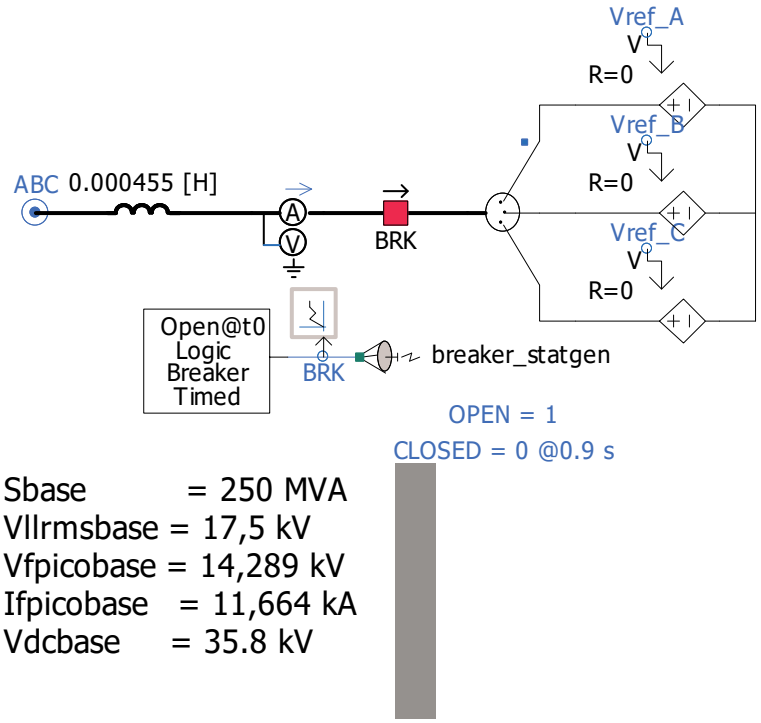

Fig. 21 Inside of the module Ideal Statgen of Fig. 20. Motor convention is adopted. Synchronverter current is measured at breaker BRK.

Since, electronic switches, e.g. IGBTs, are not modeled, because harmonics are out of the scope of this thesis, a mathematical model of the dc-link capacitor was developed, as can be found in Fig. 22. The energy, *Einv*, entering the converter at the ideal voltage sources, is a result of integrating the instantaneous power, which is calculated by the inner product of the measured current in the breaker, *BRK*, and the reference voltages, *Vref_A,B,C*. The model is derived from the equation $Etot=½CV_{dc}^2$.

The total energy, *Etot* = *Einv* – *Erdc*, is equal to the energy entering the converter terminals less the energy dissipated in a resistor in parallel with the capacitor. The dissipated energy is equal to the integral of the dissipated power, *Prdc*, in the resistor, where $Prdc= V_{dc}^2/R$. The parallel resistor stands for an approximation of the switching losses and dissipation in all the elements of the converter and the power loss is only a function of the capacitor voltage. For studies with focus on the influence of the capacitor voltage on the system, the converter current should be considered as well. In the case of a STATCOM this current is practically linearly related to the reactive power generation and therefore a time constant in the order of seconds for power systems.

Thus, the value of *Rdc* was assumed to be constant and equal to 316 Ω. This value gives a loss of 1.6% of the nominal apparent power of the converter at a nominal

dc-voltage, *Vdcbase*, of 35.8 kV. The capacitance *C* of the dc-link capacitor is assumed to be 10 mF, which corresponds to $2H$ = 50 ms, though the small signal behavior is not influenced by the capacitor value. These three values remain constant in these thesis.

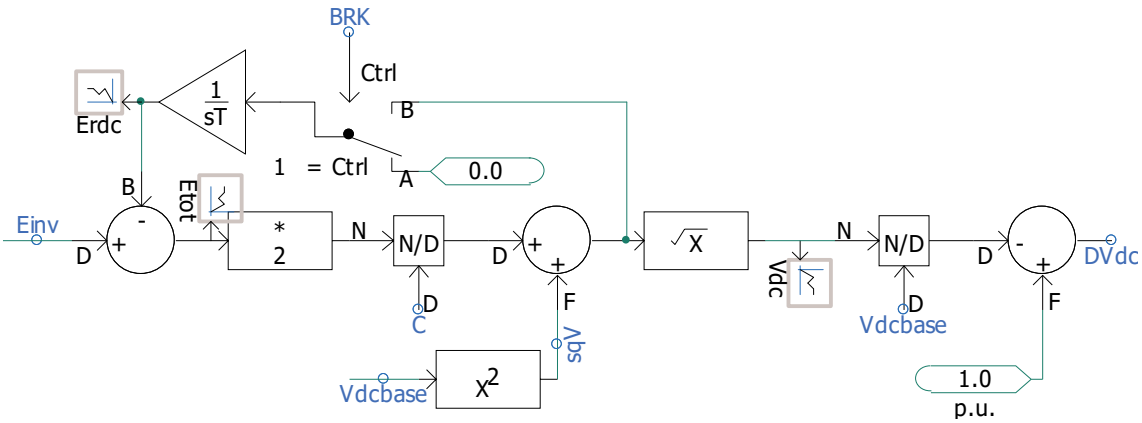

Fig. 22 Mathematical model to calculate the voltage difference, in p.u., on the dc-capacitor, DV_{dc}, based on the integrated active power entering the converter, E_{inv}, and the integrated power consumption in a resistor parallel to the capacitor, E_{rdc}, representing energy losses due to switching and thermal losses in all the components behind the converter terminal (motor convention).

Comparison between [24] and thesis proposal

For the first simulations on the comparison with the proposal of [24], the only found publication for synchronverter based controllers applied to STATCOM operation, the generator convention was adopted for better comparison with [24]. As mentioned before, two simulations were performed. The first simulation is on voltage control variations without mentioning when the converter connects. Thus, the converters, both classic as thesis proposal, are connected at t = 0.9 s, which was found to be early enough for the system entering in steady state at t = 1.5 s. Both simulation sessions in [24] show the results starting from this time.

The STATCOM starts to control voltage at t = 2 s, firstly with Q-control with Q_{set} from 0 to -150 Mvar. At t = 3 s, the control was switched to V-control to control V_g to 1 p.u. While at t = 4 s, the droop-control, both Q- and V-control, was actioned. Finally, the simulation stops at t = 4.5 s.

The results with this thesis proposal are shown in Fig. 23 and the same format and order was maintained to facilitate comparison with [24]. As mentioned before, the grid values are different and scaling of the power has been applied. The time constant of

the Q- and V-control could not be made smaller with respect to the system frequency resonance (see item 4.1).

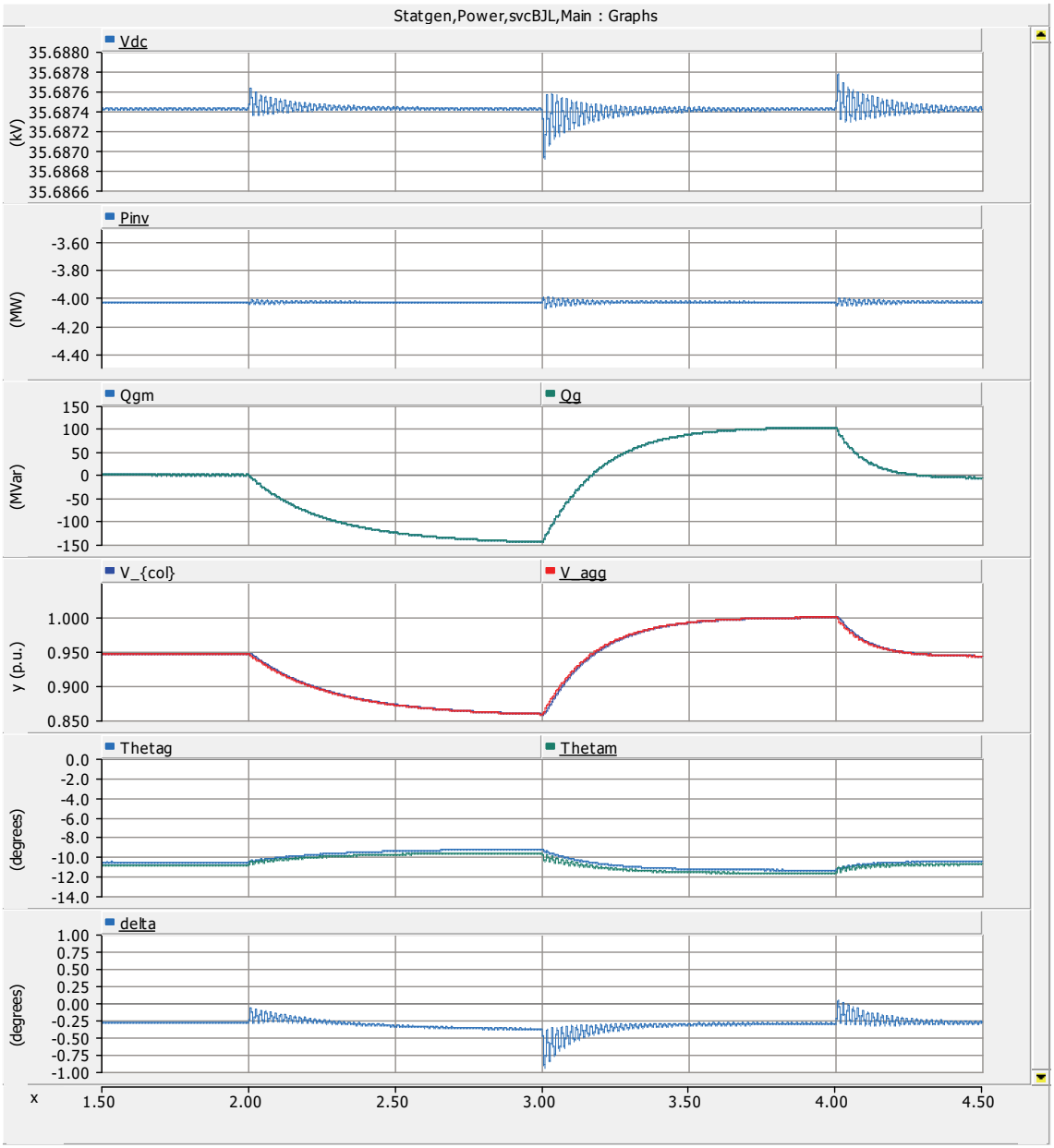

Fig. 23 Results to compare with the first simulation set concerning the voltage regulation of Nguyen et al in paper [24]. Generator convention.

Besides the variables as presented in Fig. 23, other variables more related to the synchronverter are presented in Fig. 24. The first window displays the electrical torque at the converter terminals, *T_e*, the generated power in p.u., *Pinvpu*, which is equal to $\omega.T\_e$, and, the mechanical torque, *Tm*. The last was determined not only by a gain applied to the dc-voltage difference, *DVdc*, see Fig. 11 and Fig. 22, but parallel to k_{pdc}

was placed an integrator for better comparison with [24], where the dc-voltage also returns to the nominal value in steady state. The second window displays the calculated reactive power, Q, of the synchronverter, while the measured one at the breaker of the converter with a simple LP-filter (lagging real pole), *Qinvpu*. The instantaneous reactive power, *Qgpu*, was calculated going out of the controlled bus. At the third window a representation of the filtered voltage, *V_{col}*, at the controlled bus and the aggregated value, *V_agg*. Below that one, the aggregated voltage before the LCL filter, *Vl_agg*, and the virtual flux amplitude *Mfif*, *M_fi_f*. Since the angular velocity of the synchronverter, *w_{eag}*, is very close to 1 p.u., as shown in the last window, the voltage amplitude and *Mfif* are practically equal. With a standard PLL the frequency was measured too at the same place as *Vl_agg*, denominated as *w_{grid}*. The damped frequency oscillation on *w_{eag}* is according to item 3.1, and, therefore, the damping is determined by the grid elements and the value of ΔQ_{ref} determines the initial amplitude of the frequency oscillation. In Fig. 24 this is the largest at $t = 3$ s, as can be seen as well for *Qgpu*. Those are present as well on the torque, but are hardly visible on the chosen scale.

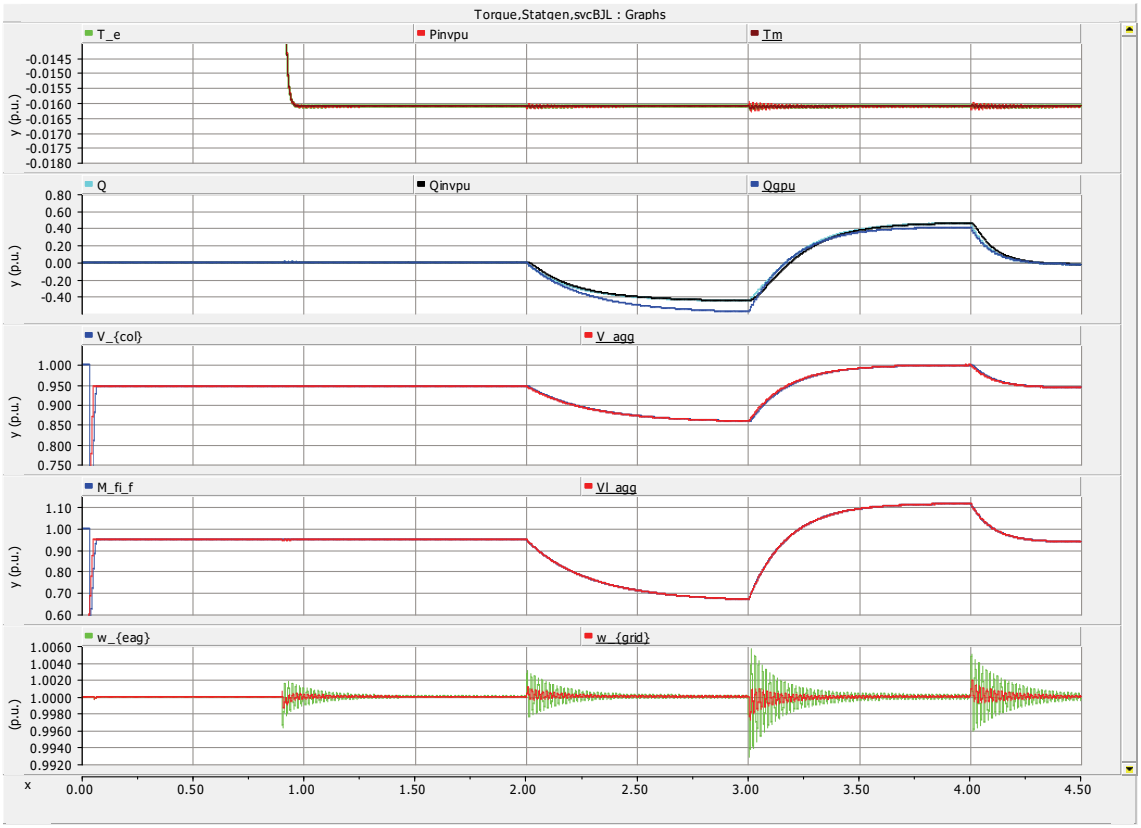

Fig. 24 Variables of the synchronverter during the simulation as in Fig. 23. Generator convention.

Thus, for a fairer comparison, the control strategy of [24] was implemented in PSCAD as well, to simulate it in the same grid. Their time constants and gains were used and scaled as a starting point. They were adjusted according to 4.1. See Fig. 25 for the active control loop as in [24]. As described in that paper, a PD-controller was put in series with the integrator for *theta* with a time constant 5 times the fundamental frequency (in [24] is equal to 50 Hz, but adapted in this thesis to 60 Hz). The given reason for this insertion is to speed up the simulation. For fair comparison this was tried for the thesis proposal as well. Though, since the proposal already has a proportional gain in parallel with the inertia (integrator), this gain had to be reduced to only 5.10^{-6}. Even appearing an insignificant value, later in simulations it was found to be the cause of small damped system frequency oscillations at connection of the converter and was removed. The system frequency oscillation at connection was smaller though than the ones caused by reactive power changes.

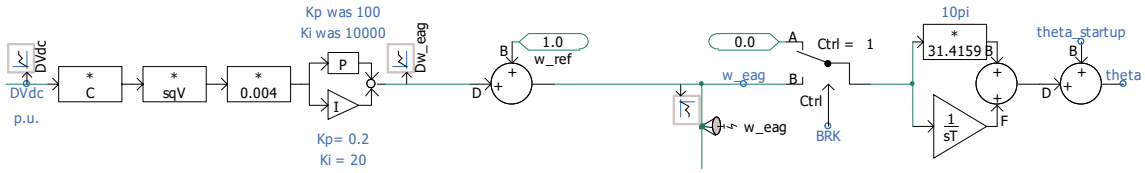

Fig. 25 The active control loop of [24] modeled in PSCAD for comparison with the thesis proposal.

In Fig. 26 the results of the controller solution of [24] are shown. The results of the thesis proposal shown in Fig. 23 present an overdamped inertia, or in fact what can be seen is that no oscillation related to the virtual inertia is present on the capacitor voltage or *Pinv*. Besides this fast capacitor voltage control of the thesis proposal, the system frequency resonance is still damped with the high controller gain. While the poorly damped oscillation, leading to a high overshoot, on the capacitor voltage from the control without electrical torque feedback needs a higher controller gain, Fig. 26 shows that this will lead to instability in the system frequency resonance with a high time constant.

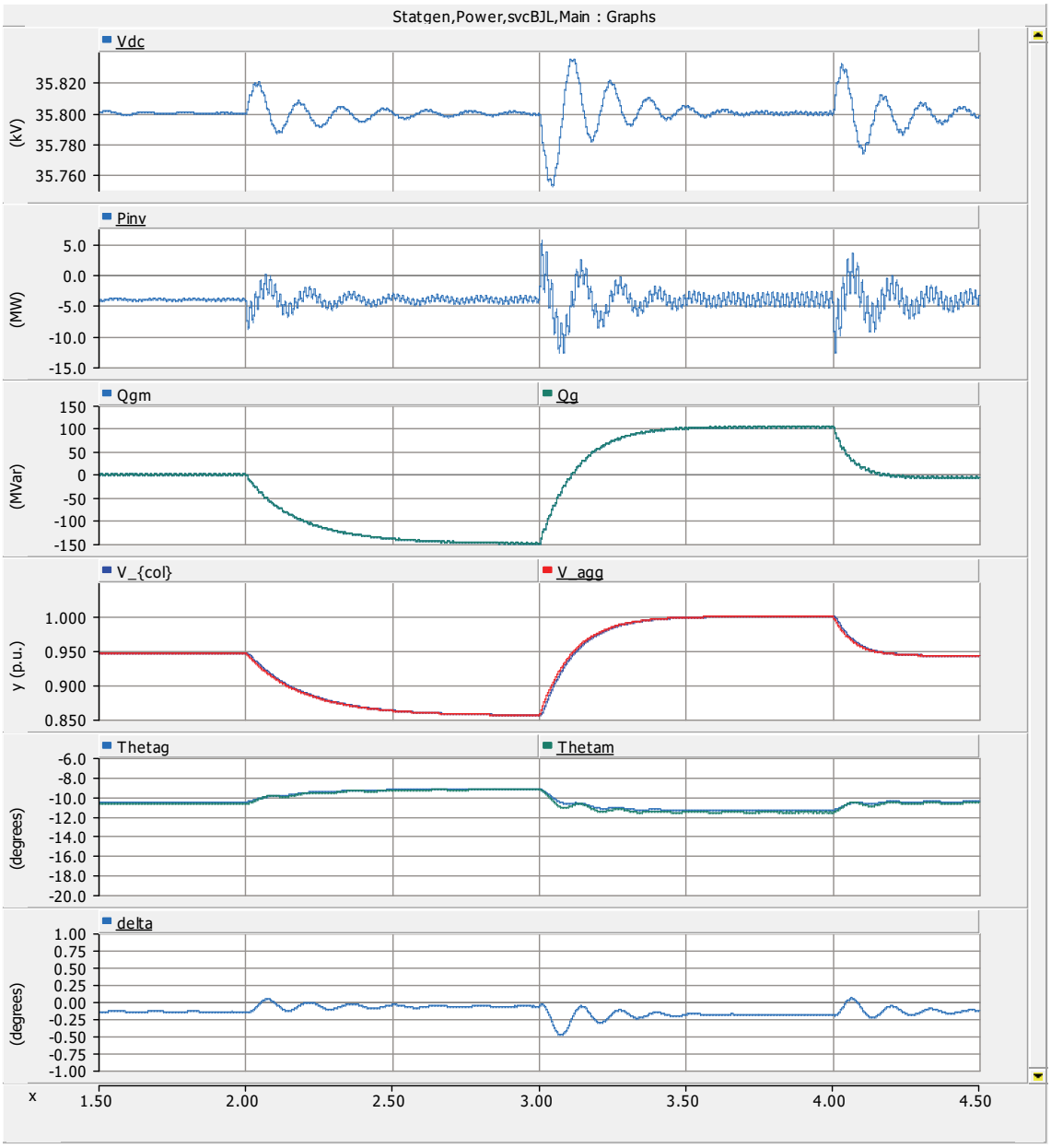

Fig. 26 Results from the controller of [24] applied to a system with high X/R values for the voltage control simulation.

The simulation from [24] related to frequency swings in the infinite voltage source are performed with the frequency profile, *fg*, as shown in Fig. 27. In a similar way as in that paper, the steps are 4% up and 4% down. The first step at $t = 2$ s occurs at the same moment as the habilitation of voltage control to 1 p.u.

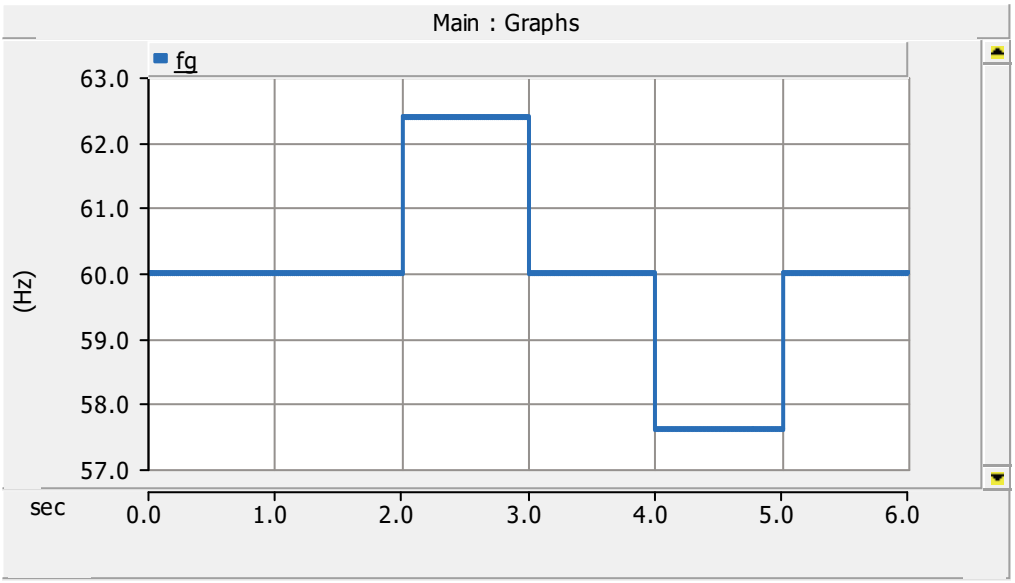

Fig. 27 Frequency variation on the infinite bus source.

Firstly, the results of the thesis proposal for the frequency steps are shown in Fig. 28. Clearly visible, the capacitor voltage rises at step ups of the grid frequency and declines when the grid frequency steps down. Although the contributions to inertia seem small, the idea is that if all converters are connected with this type of control, this contribution to inertia can be substantial. Further, for the comparison with the classic controller no special attention was given to increase this inertia contribution, though, adjusting the synchronverter parameters, this contribution can be increased as will be shown at the simulation results for the simple grid model.

The load angle in relation to the infinite bus based on a frequency of 60 Hz, θ_m, *Thetam* in Fig. 28, of the synchronverter follows very closely the load angle of the voltage controlled bus in relation to the infinite bus, θ_g, *Thetag* in Fig. 28. This can even better be seen in the last window of Fig. 28. The difference between these load angles, *delta*, only present the same damped system frequency resonance as in *Pinv* (second window), as expected.

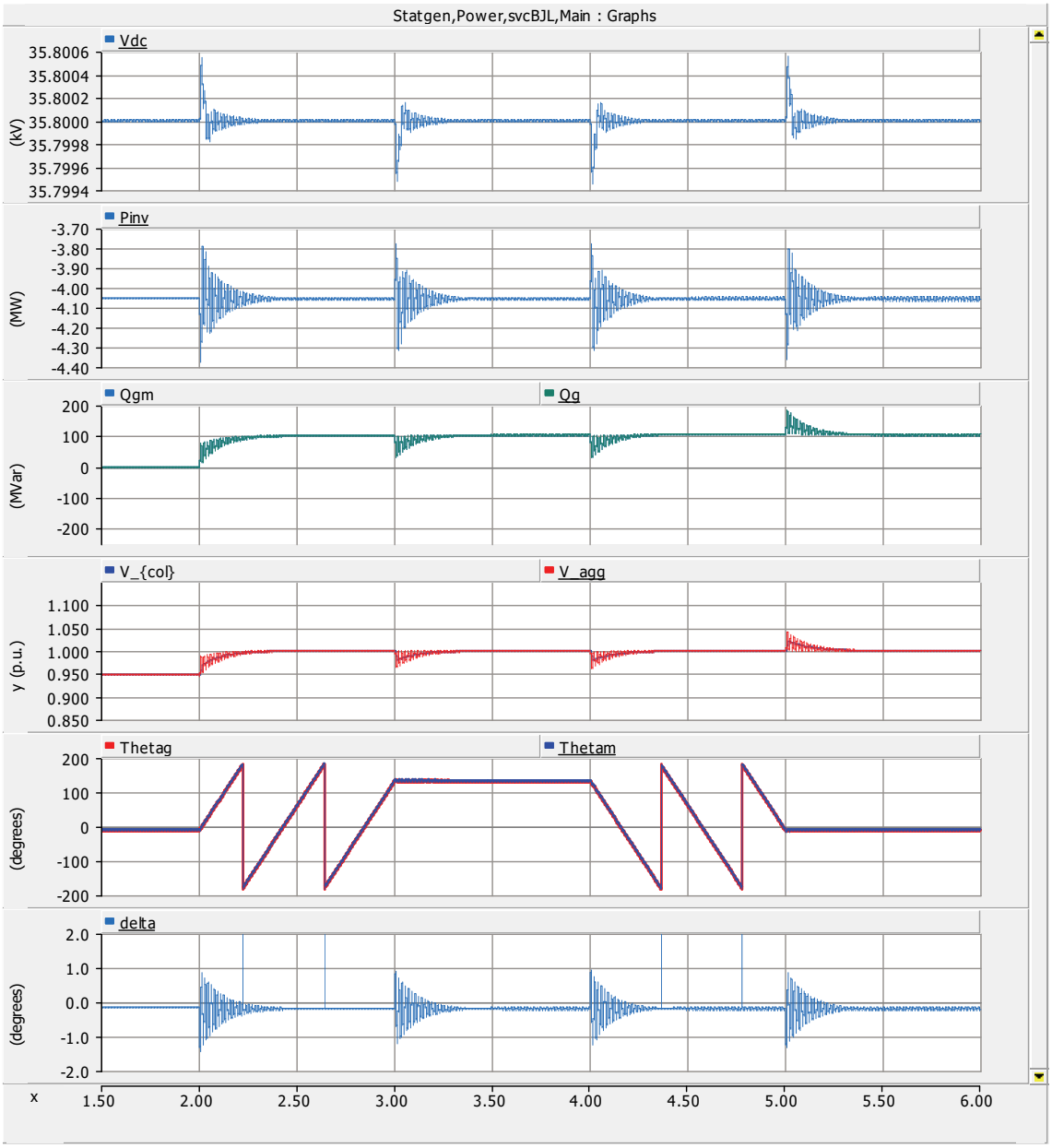

Fig. 28 Proposed controller of this thesis for the frequency track simulation in a system with high X/R.

The results for the frequency steps with the classic control are shown in Fig. 29. The oscillation of the PI-control to regulate the capacitor voltage remained the same as expected. Nevertheless, the frequency changes seem to cause even more instability to the system frequency resonance than the reactive power changes.

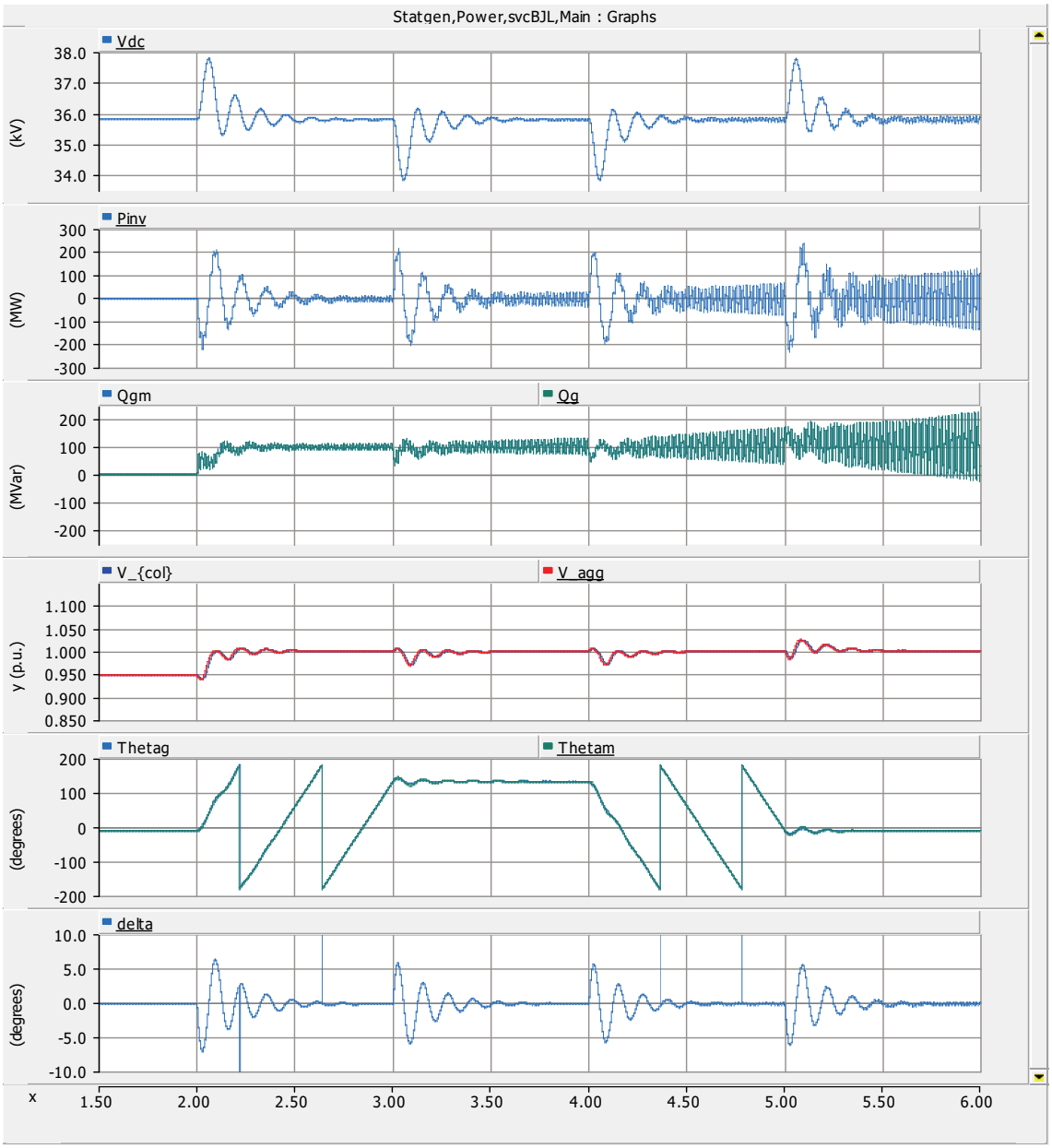

Fig. 29 Results with the controller of [24] for the frequency track simulation in a system with high X/R.

In Fig. 30 the simulation results are shown for the same case, but this time some resistance was added to the breaker. Now, it is evident that the controller can work properly too. The system frequency resonance is damped for lower X/R and the PI-controller can be applied with more gain to damp the capacitor voltage oscillation.

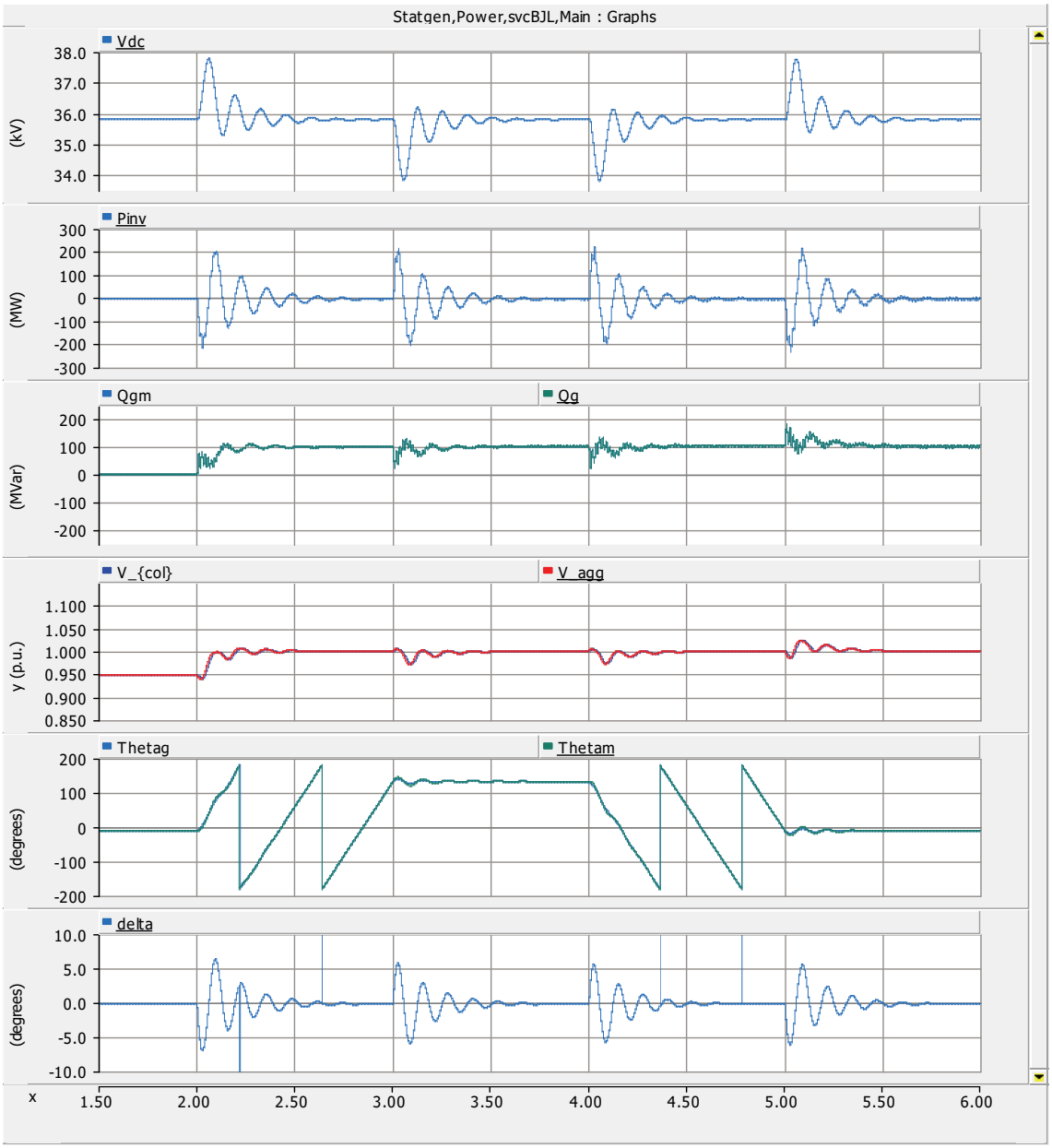

Fig. 30 Results with the controller of [24] for the frequency track simulation in a system with lower X/R.

Simple system simulations

Reactive control variations of STATCOM

After the presented comparison between the thesis proposal and [24], and before the Brazilian power system simulation, the grid has been simplified to quickly analyze some parameter influences. This basic grid model has been based on Fig. 19 and is shown in Fig. 31. The following simulations were performed with this grid and the only affected variables were θ_g and θ_m (see Fig. 23). Because the shunt load, 100 MW and 50 MVar as in Fig. 19, of the transmission line is omitted in the simplified grid model, these angles are about two degrees less negative.

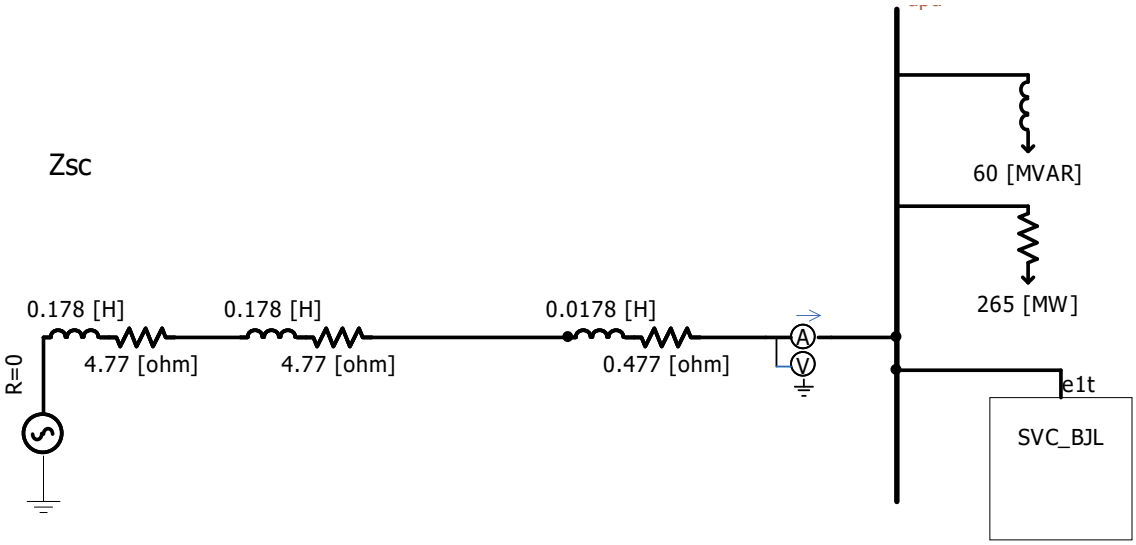

Fig. 31 Simplified model of Fig. 19.

The next step is to show the influence of the load on the bus. This load was reduced to only 10% of the active and reactive values to 26.5 MW and 6 MVar, respectively. The results are presented in Fig. 32 and Fig. 33. These are the only results with reduced load to verify if the linearized model as in Chapter 3 is correct in relation to omit the consideration of different load levels on the controlled bus.

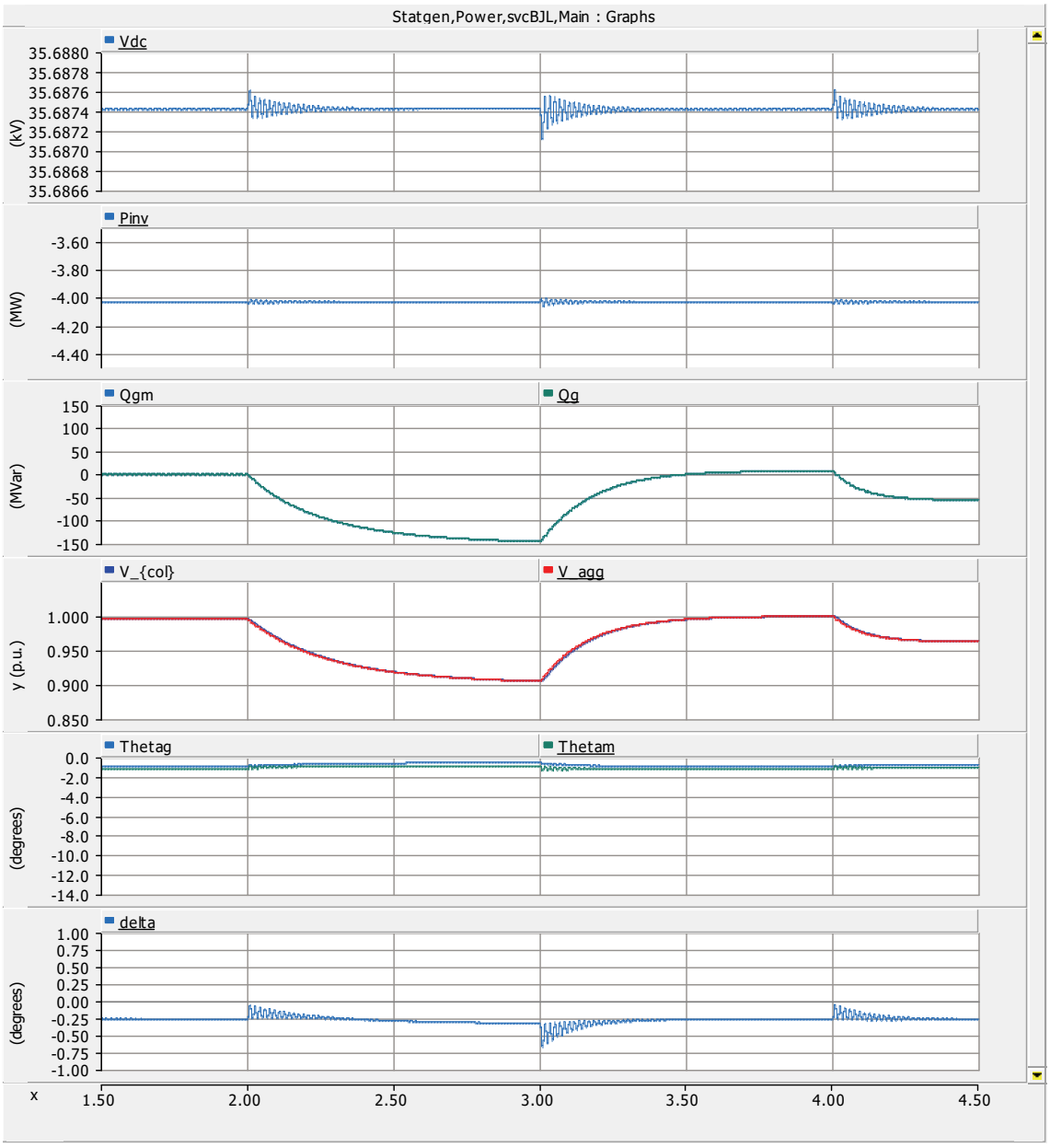

Fig. 32 Result of the first simulation case with only 10% of the load on the bus. To compare with Fig. 23 and Fig. 35. Generator convention.

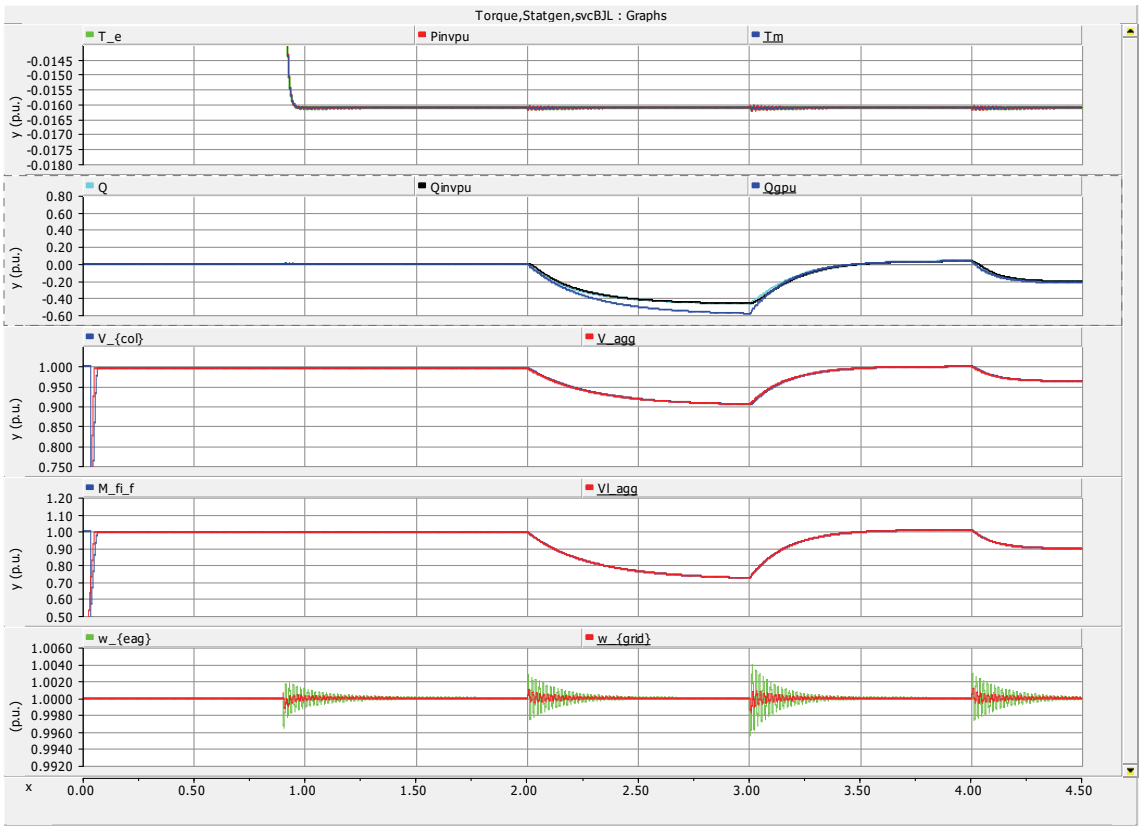

Fig. 33 Synchronverter variables with only 10% of the load on the bus. To compare with Fig. 24. Generator Convention.

The system frequency resonance, 60 Hz in these cases, is clearly reduced at the moments that V-control and D-control are applied, $t = 3$s and $t = 4$s, respectively. Whereas, at $t = 2$s, when the synchronverter after stabilizing from merely synchronizing jumps to Q-control, no change in system frequency resonance is found. This effect is best seen on the variable *w_{eag}* in Fig. 33 comparing with Fig. 24. The explanation is that for Q-control the change in reactive power, ΔQ, is the same for all loads on the bus. While for V- and D-control, the change ΔQ depends on the initial voltage values. And, for lighter loads, these changes in reactive load are smaller.

Another observation has to be made in relation to the connection of the synchronverter to the bus at $t = 0.9$s. From both cases, initial load and reduced load, it is found that the system frequency resonance amplitude is equal and during a period that the reactive power is unaltered. Therefore, the resonance is not only initiated by reactive power, though, also initiated by active power changes (connection of converter) as already noticed by [31].

One of the two proposals of [31] is to increase the virtual inertia to damp the system frequency resonance. Changing $J = 2H$ from 1s to 1000s does not have any

effect on any variable shown in the figures before. This is explained by the fact that the authors of aforementioned work use a pure integrator, as in the swing equation, while in this thesis the proportional gain is suggested parallel to the integrator, PI-control, to damp an oscillation mode related to its virtual inertia.

Nevertheless, making the inertia 100,000 times smaller than the base case, does not lead to instability in this case, as can be seen in Fig. 34.

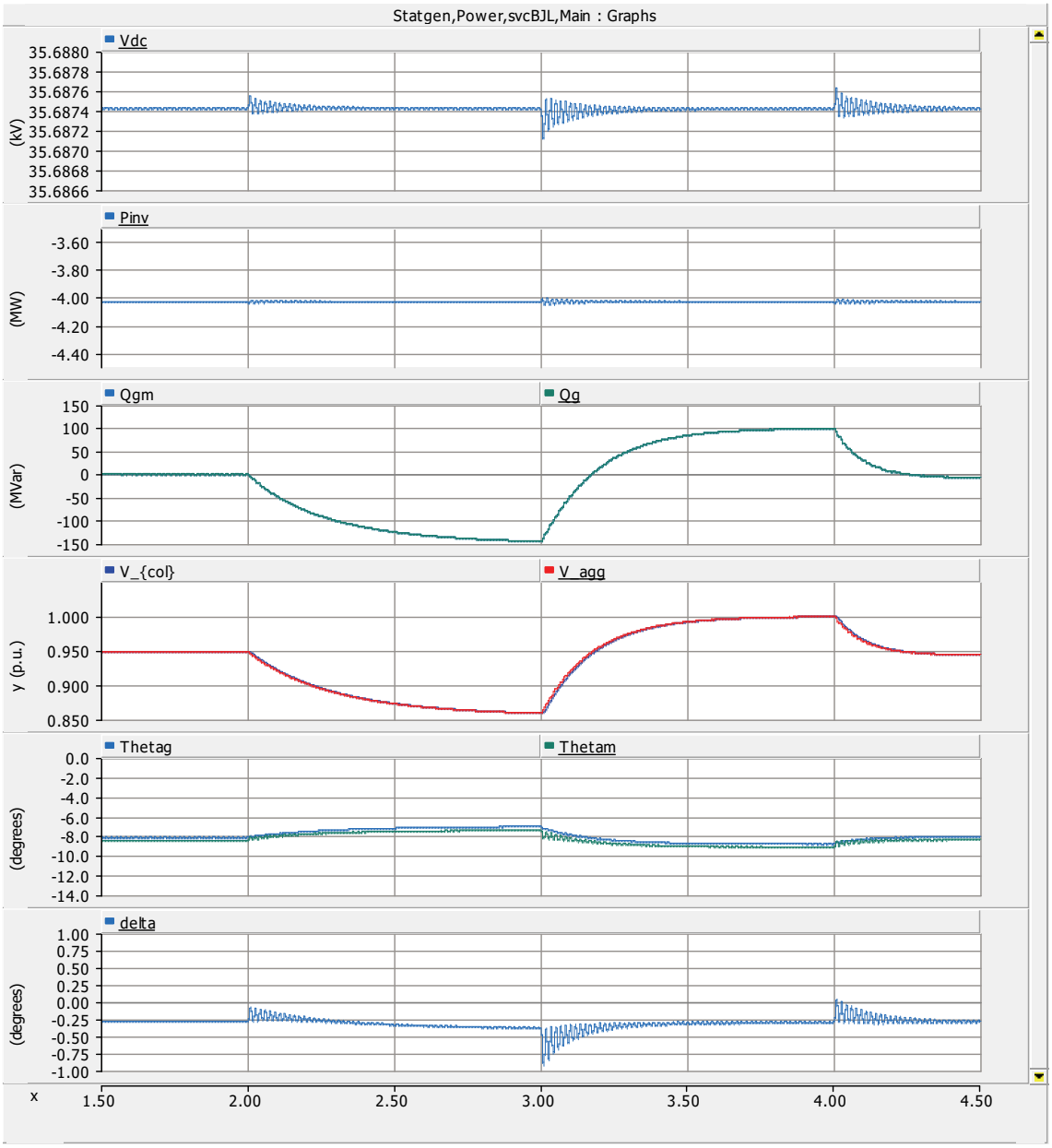

Fig. 34 Result of the first simulation case with J= 2H = 10 µs. To compare with Fig. 23. Generator convention.

In fact, in this case, the only variable that is influenced is the dc-voltage, V_{dc}. As expected, it is more stable with smaller inertia values, since the electrical torque, T_e, is following the virtual mechanical torque, T_m, much quicker. Three differences can be noted in relation to [31]. Firstly, the model here considers a variable voltage on the dc-link, while in [31] the dc-voltage is considered to be constant. Secondly, the virtual flux is variable in this work while in the cited work, the virtual flux is considered constant in 1.05 p.u. Finally, this thesis has proposed a proportional gain parallel to the virtual inertia to compensate the lack of the damp-effect of the active power droop controller.

To emulate virtual inertia, the controller should not be over-damped. Before testing the transient contribution of the synchronverter in relation to supporting the grid and testing the effect of the time constant of the virtual flux integrator, the simplified base case is presented in Fig. 35 and Fig. 36 for motor convention.

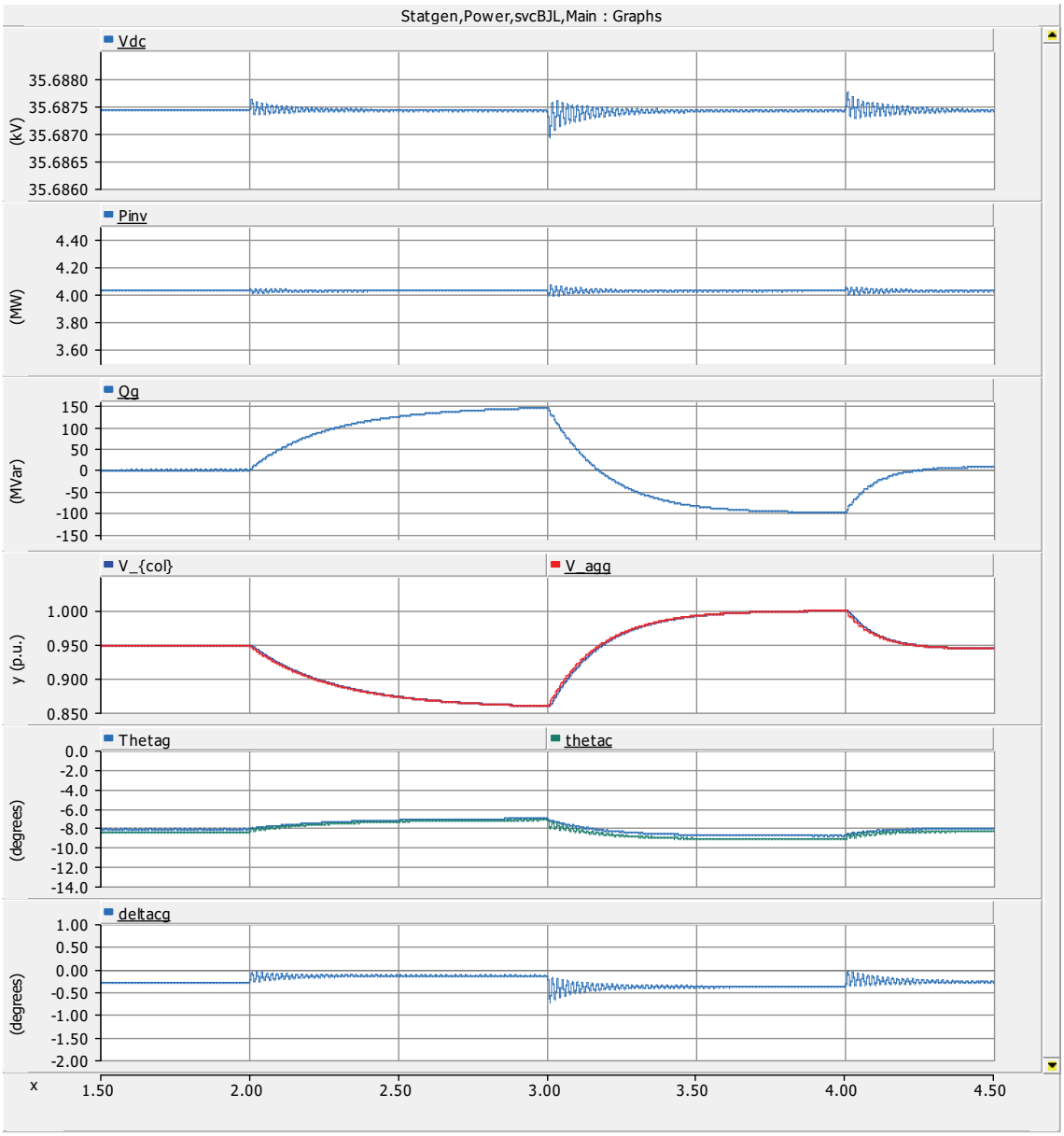

Fig. 35 Results of the simple model base case. To compare with Fig. 23.

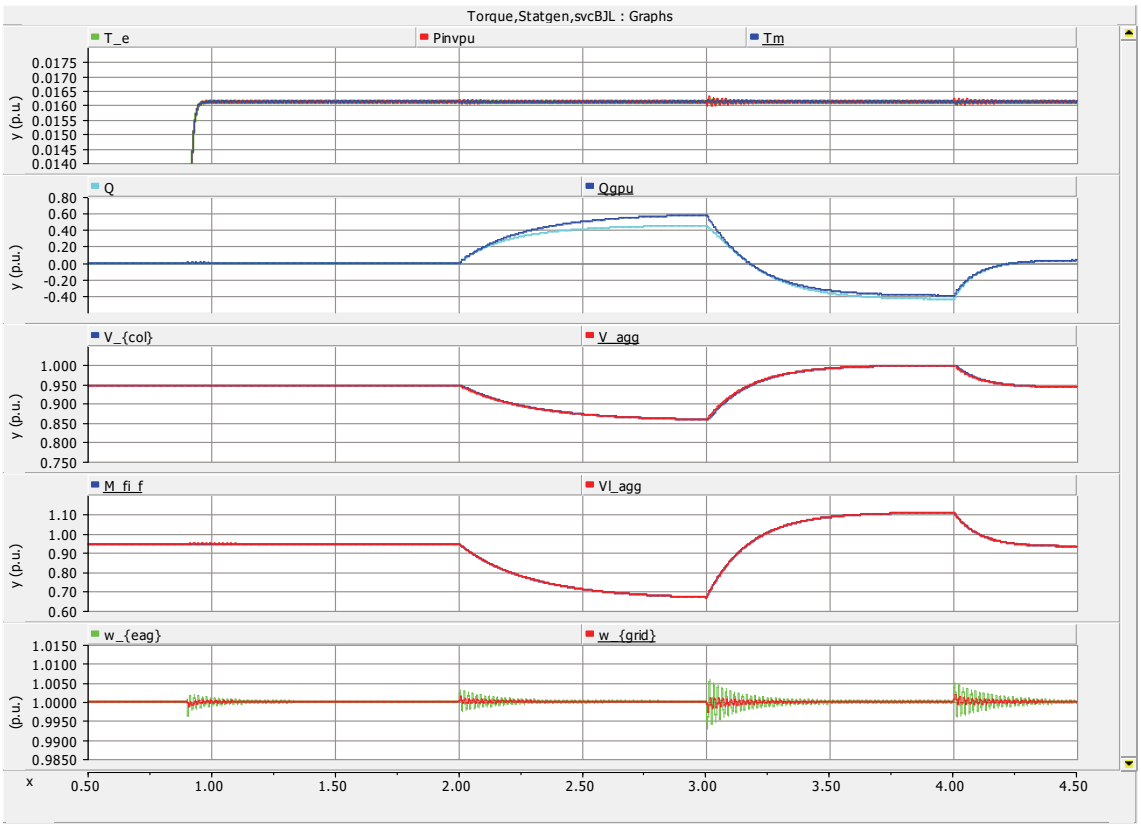

Fig. 36 Synchronverter variables of the simple model base case. To compare with Fig. 24

In Fig. 37 e Fig. 38 the effect of more rapid voltage or reactive power control is shown. For this case K_{if} was doubled from 1 to 2, is equal to making the time constant two times smaller.

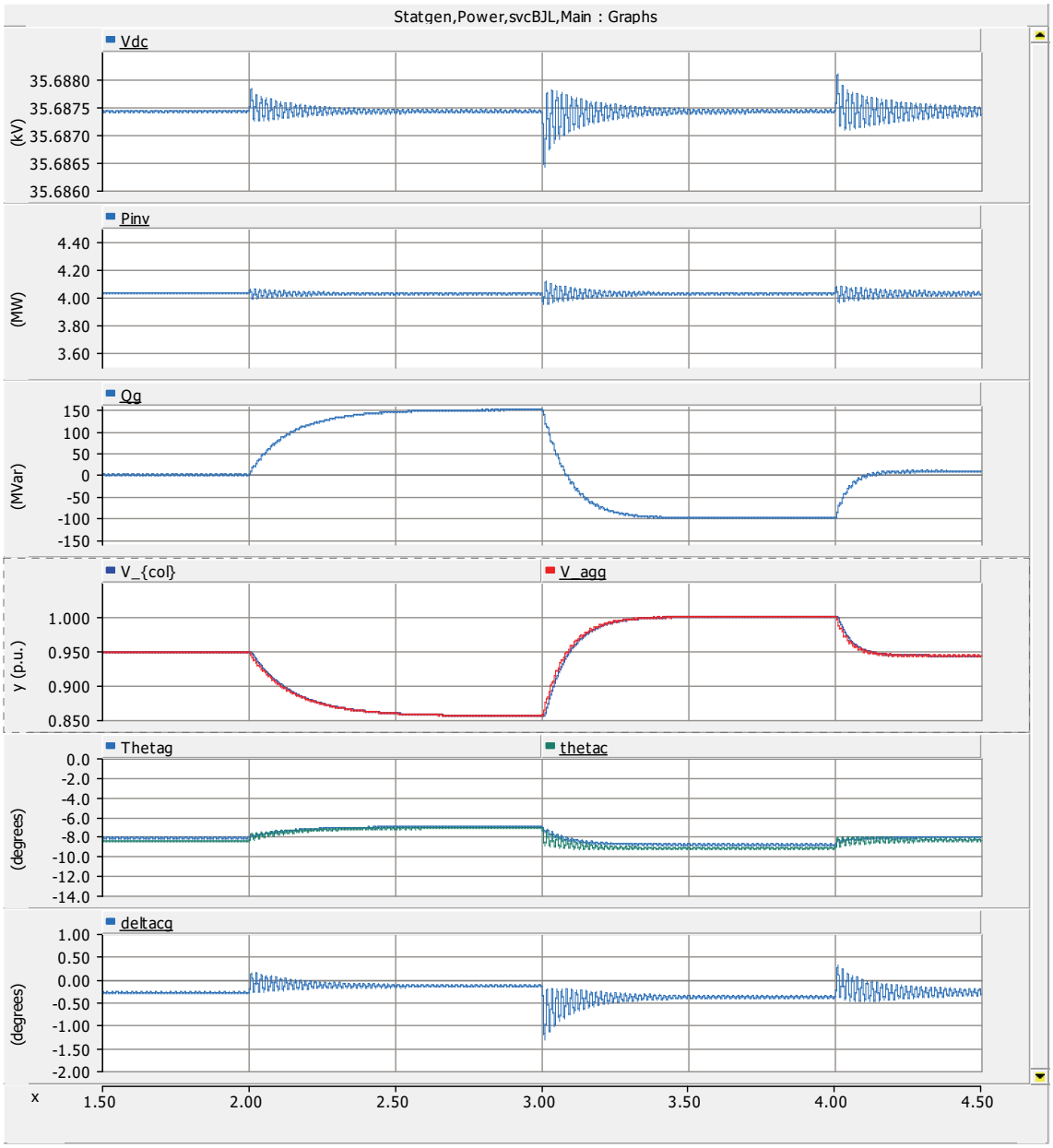

Fig. 37 K_{if} increased from 1 to 2. To compare with Fig. 35. Resonance frequency oscillation has increased twice as well.

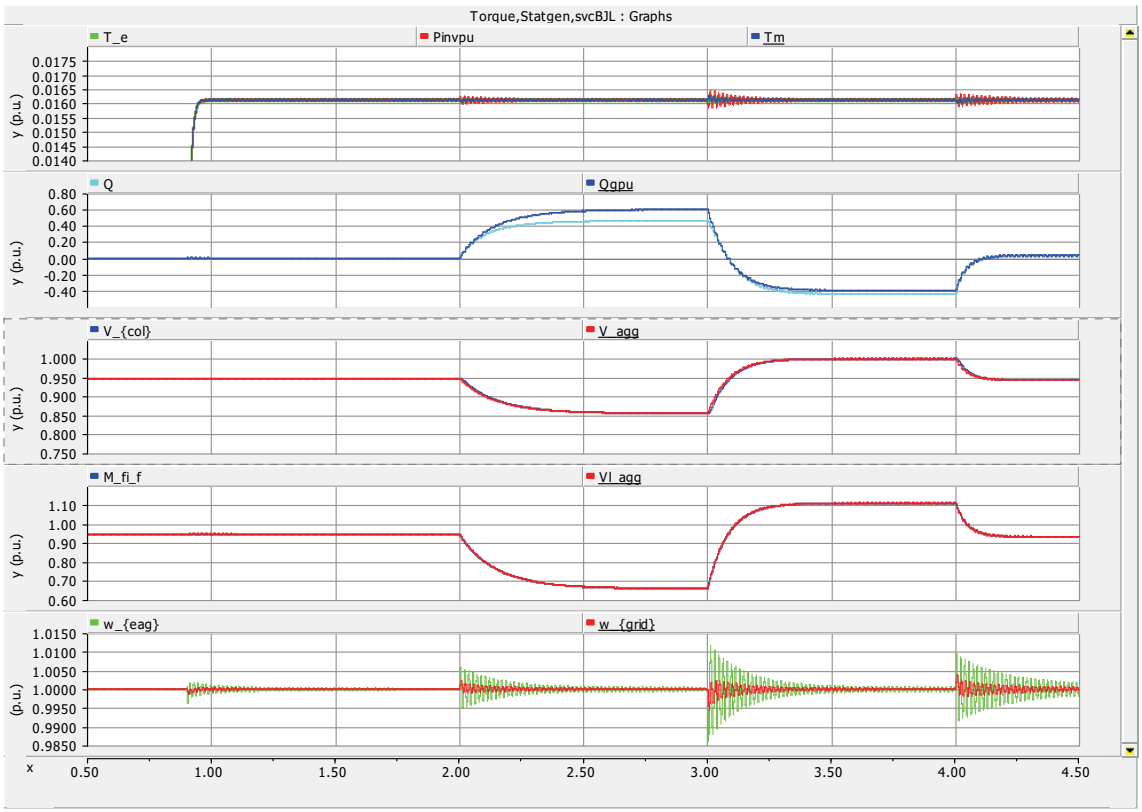

Fig. 38 K_{if} increased from 1 to 2. To compare with Fig. 36. Resonance frequency oscillation has increased twice as well.

Although the oscillation of the system frequency has doubled when doubling K_{if}, in all shown variables, the system is still stable. Nevertheless, when increasing K_{if} to 5 s^{-1}, the system becomes instable at connection, which represents a step in active power, and when Q- and D-control are activated. The results are shown in Fig. 39 and Fig. 40. Only when V-control is in operation, the system frequency resonance is damped. This means that the gain for the voltage loop is smaller than the one for the reactive power loop.

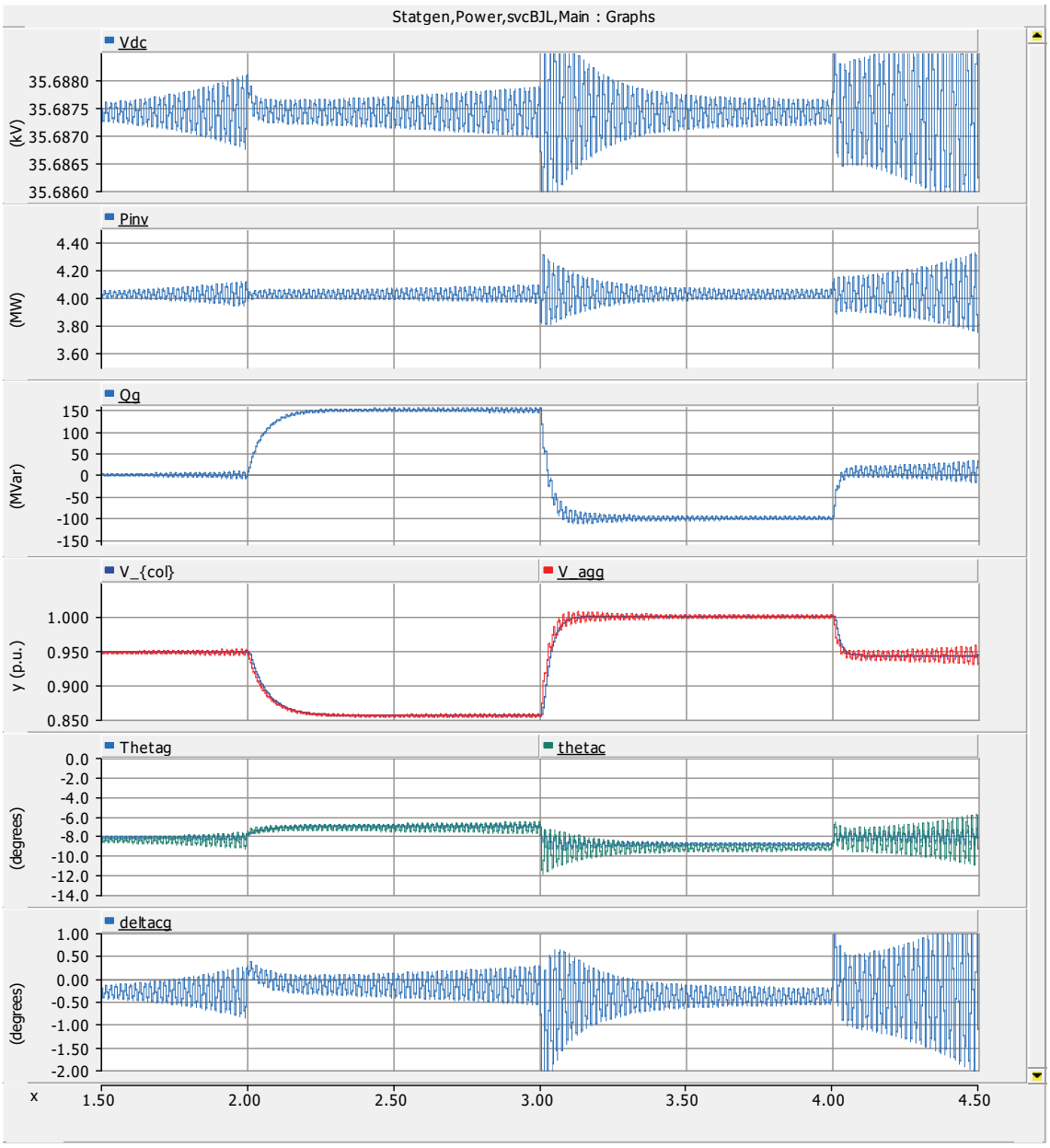

Fig. 39 K_{if} increased to 5 s^{-1}. System becomes unstable.

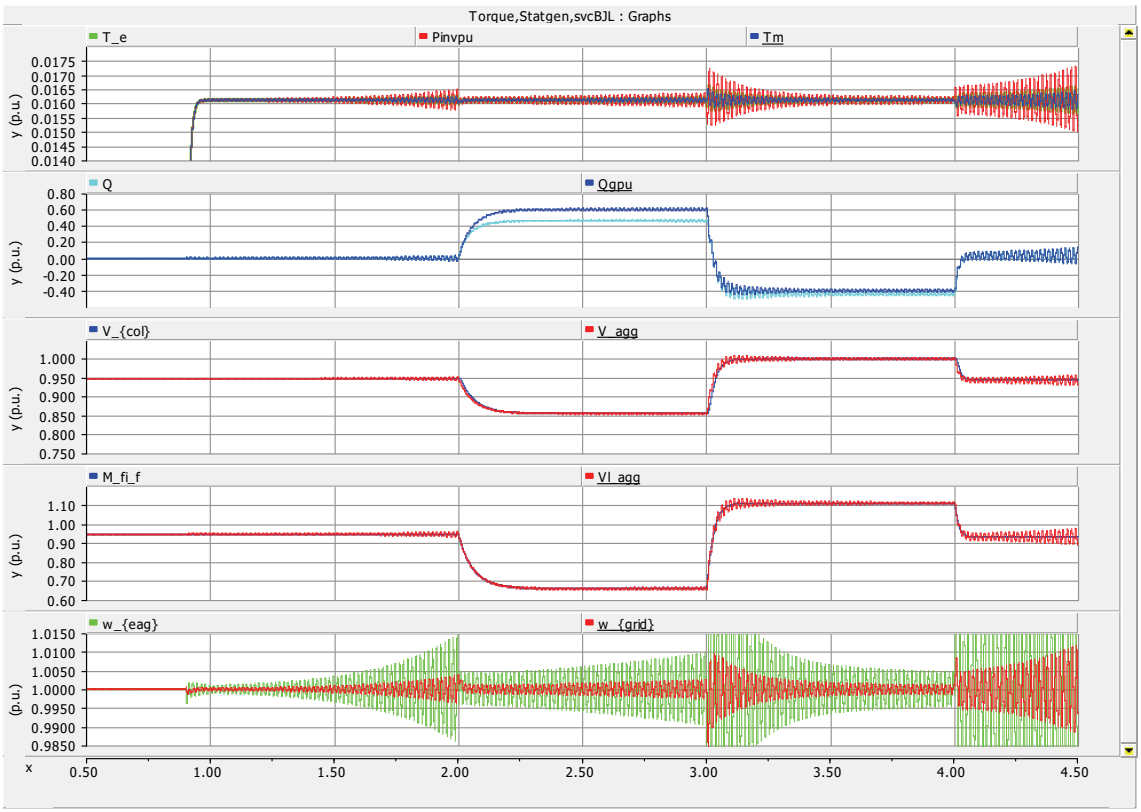

Fig. 40 Kif increased to 5 s^{-1}. System becomes unstable.

$K_{p\omega}$ has only influence on T_e and thus V_{dc} and P_{inv} as can be observed in Fig. 41 and Fig. 42. The system frequency resonance oscillation on the angular velocity, ω (*w_{eag}* in Fig. 42), stays unaltered in relation to variations of $K_{p\omega}$. As expected, since this oscillation is determined by (3.3) till (3.15), therefore by the impedance values and the voltage values of the sources.

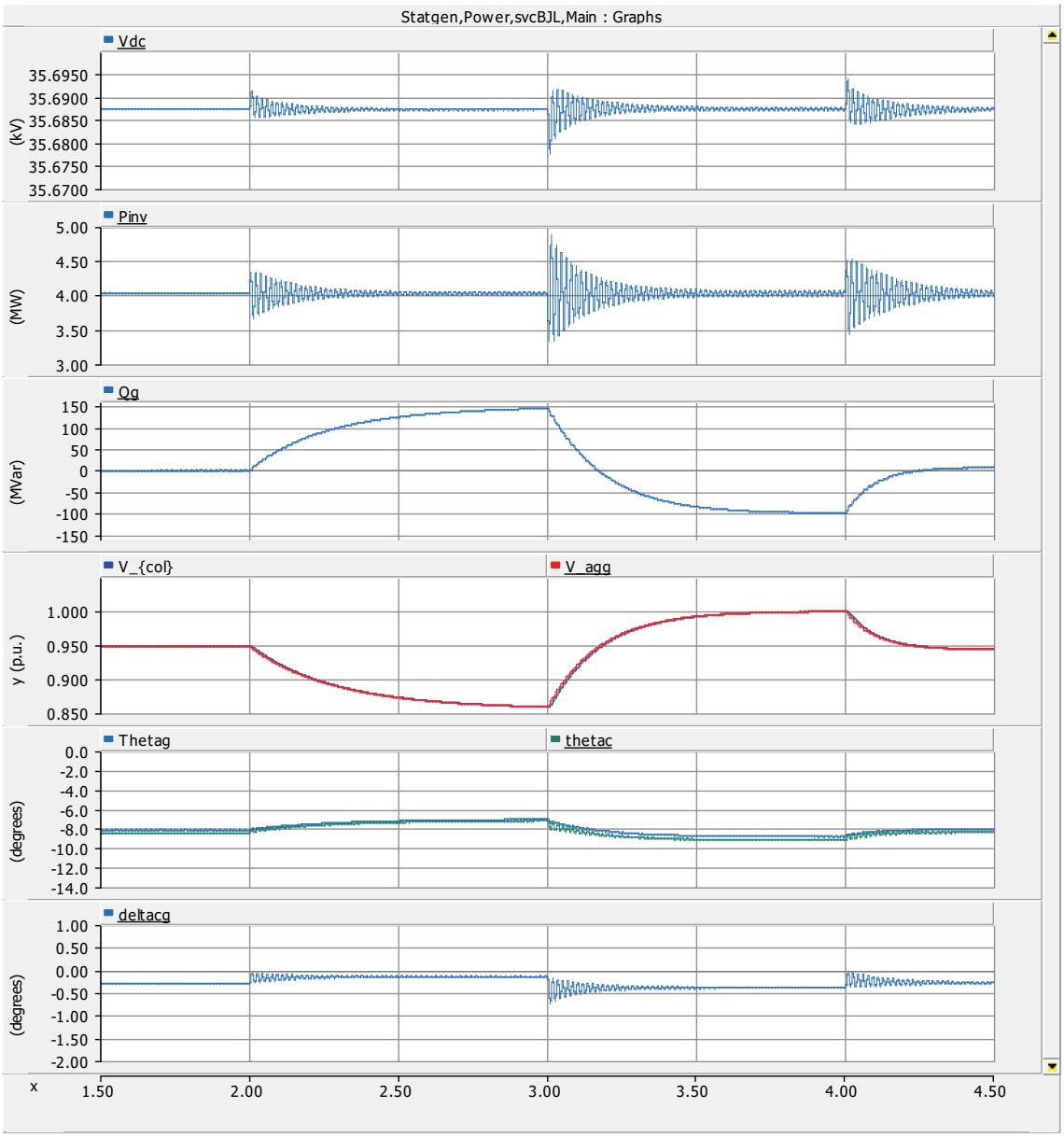

Fig. 41 $K_{p\omega}$ from 100 to 2. $K_{i\omega}$ = 1/(2H)= 20. Compare with Fig. 35.

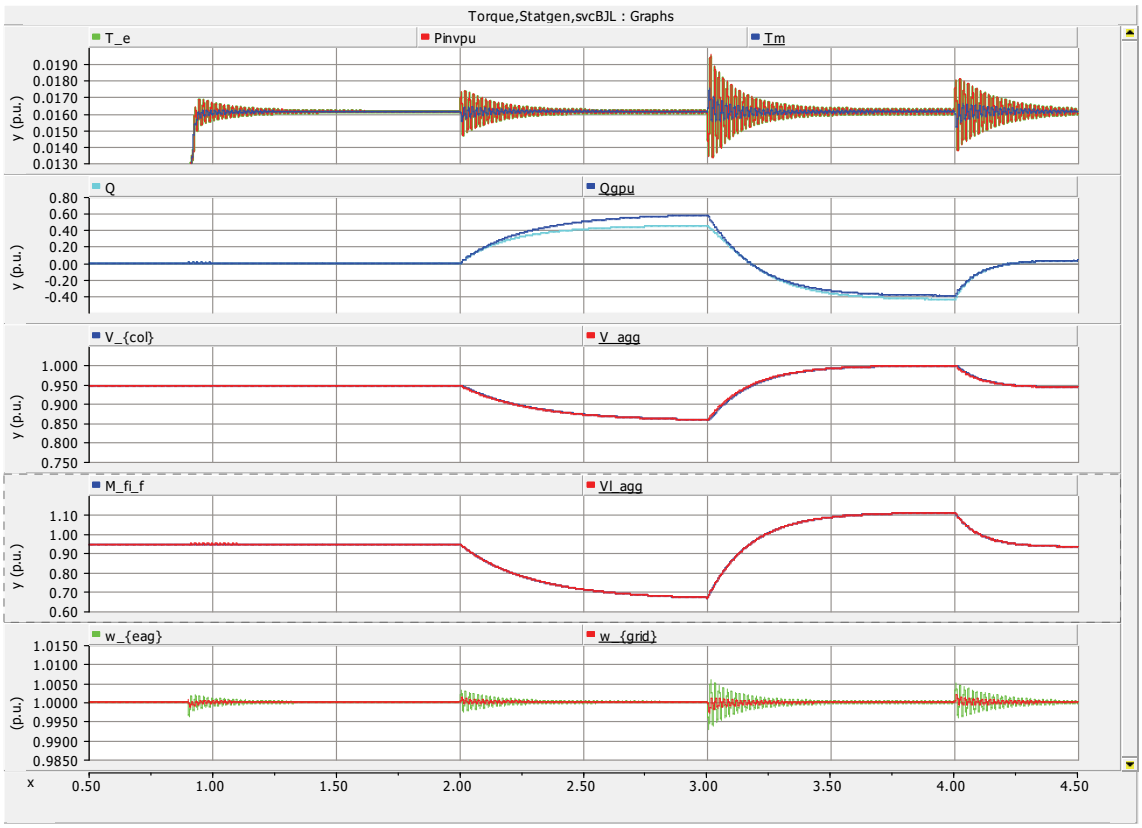

Fig. 42 $K_{p\omega}$ from 100 to 2. $K_{i\omega}$ =1/(2H)= 20. Compare with Fig. 36.

The influence of the parameter k_{pdc} (see Fig. 11) is shown from Fig. 43 till Fig. 48. It is the direct gain between the difference of the energy contained at the nominal voltage and the actual voltage, and, the virtual mechanical torque, T_m. It has a component that is linearly related with the square of the dc-voltage, as mentioned before, and a temporary part, which stores or supplies temporary differences between the mechanical and electrical torque, dictated by the virtual inertia, J (=$2H$), and $k_{p\omega}$. From the aforementioned figures it is clear, that the only affected variables are the ones related to active power within the converter, as expected, thus, *T_e*, *Pinv*, *Tm*, and *Vdc*. The small reduction of the average load angles are hardly observable on the chosen scale, which was dictated by the system frequency oscillation amplitude. This amplitude was not influenced by k_{pdc}. The effects on the active power related variables come from two sides; the dc-link and the ac-grid. From the dc-link it´s straightforward to see that with smaller gain k_{pdc} the signal *Tm* is smaller and thus, *Te* and so on *Pinv* are smaller as well, resulting in slower loading of the capacitor. Nevertheless, the system frequency resonance amplitude, and decay, did not suffer any alteration, since those were provoked by step changes on the reactive power.

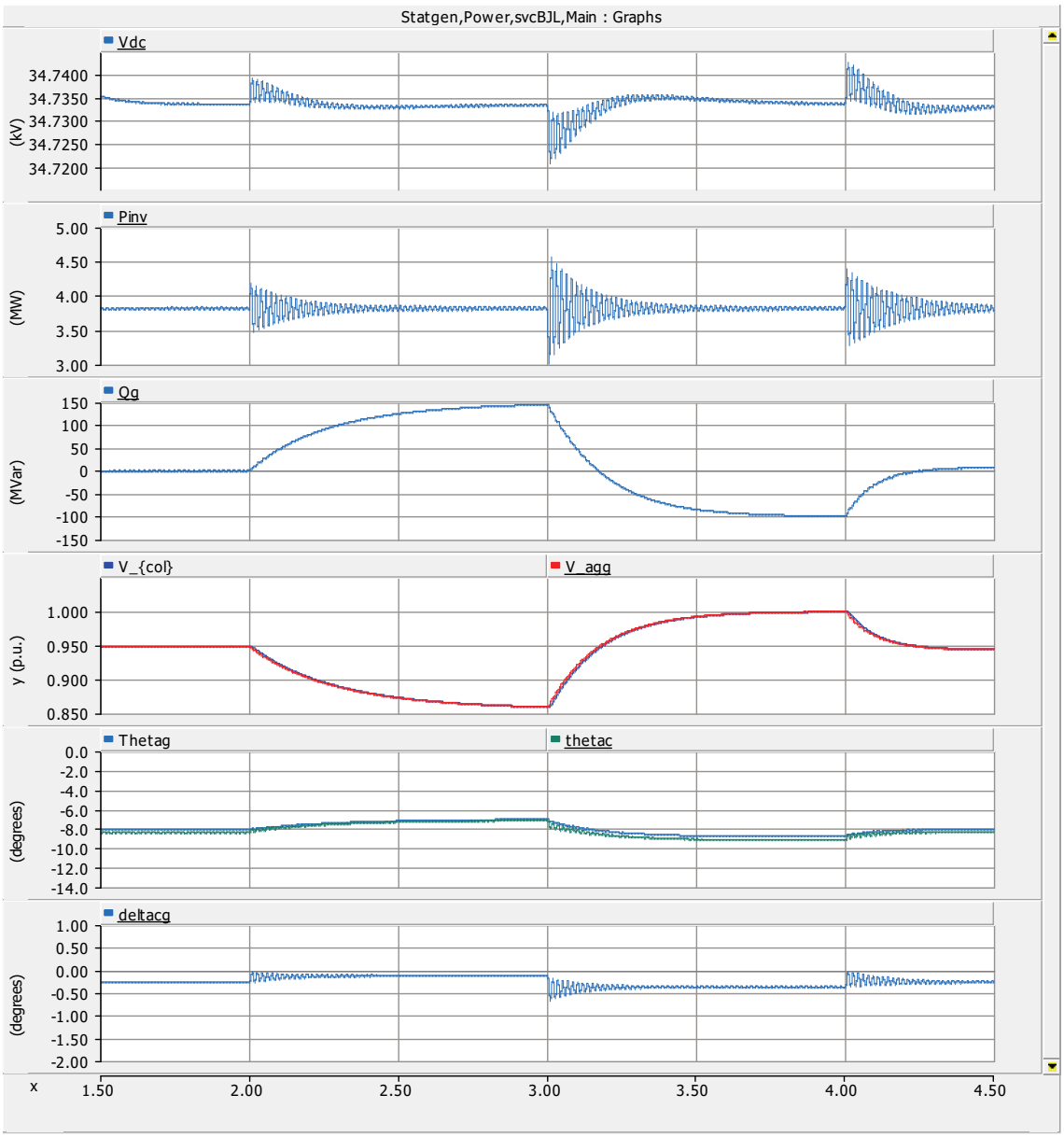

Fig. 43 K_{pdc} from 100 to 10. To compare with Fig. 41. $K_{p\omega\delta}$ was removed and resulted in elimination of oscillation at connection.

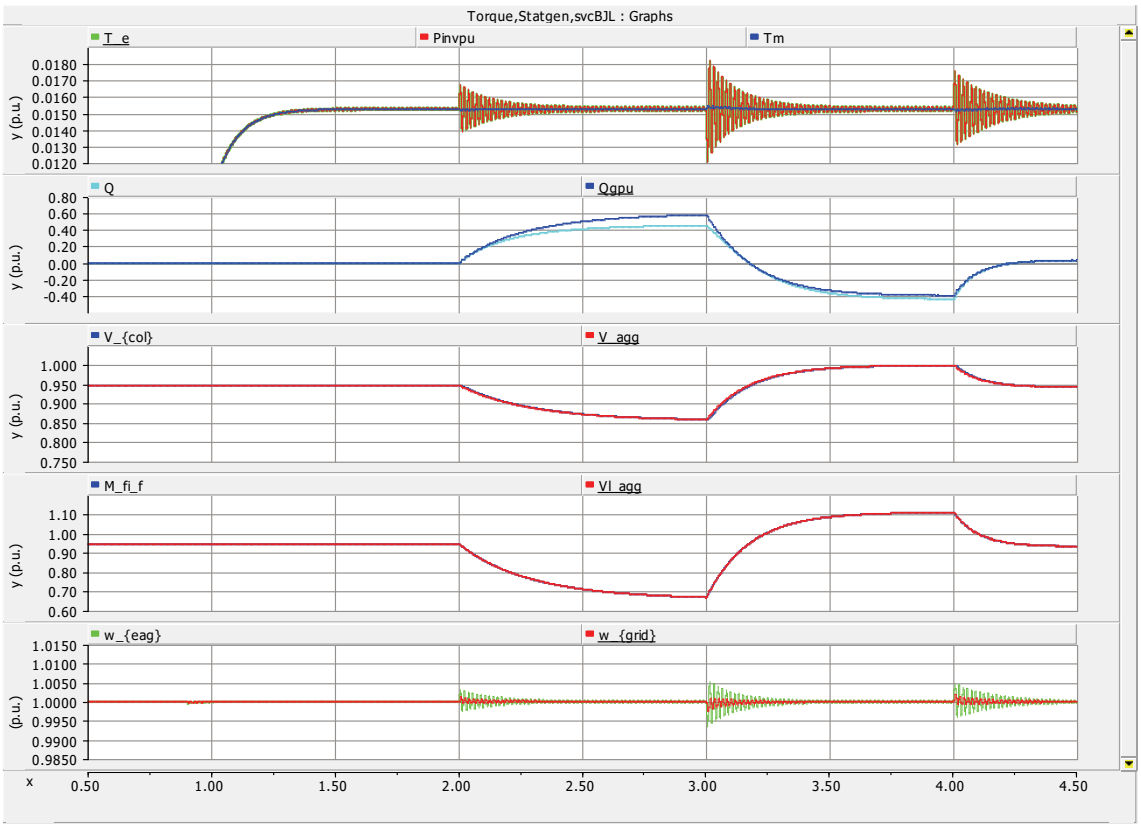

Fig. 44 K_{pdc} from 100 to 10. To compare with Fig. 42. $K_{p\omega\delta}$ was removed and resulted in elimination of oscillation at connection.

Fig. 41, where k_{pdc} = 100, shows that the voltage drop caused by the 1.6% resistive load is around 0.3% of the nominal value. With a 10 times smaller gain, this system part still behaves in a linear way as can be seen in Fig. 45, where the voltage drop is found to be 3%. Thus, the energy loss on the capacitor obeys still fairly the relation where $\Delta\bar{E}=2\Delta\bar{U}$.

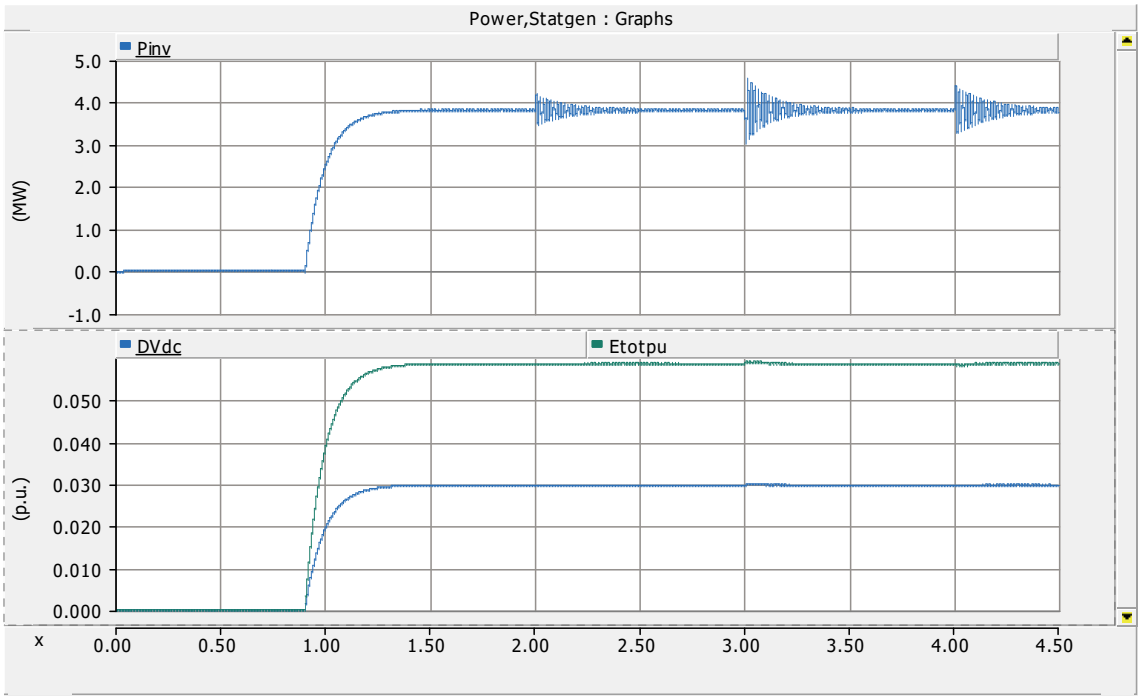

Fig. 45 K_{pdc} from 100 to 10. ΔV_{dc} increased 10 times (from 0.3% to 3%). The liquid total energy, Etotpu = Einv –Erdc, energy that entered the inverter minus dissipated energy, is still practically double of the voltage loss on the dc-link, as predicted by the linear model. $K_{p\omega\delta}$ was removed and resulted in elimination of oscillation at connection.

So, if the gain of the dc-link voltage control will decrease 10 times to gain 1, then the voltage loss is expected to be 30% in a linear case. Nevertheless, from Fig. 48 can be found that the voltage only drops 20%.

Fig. 46 shows that with a gain 10 times smaller the capacitor voltage drop leads to a significant reduction of the modeled loss in the parallel resistor and *Pinv* reaches in equilibrium already at 2.6 MW. In this case, neither the small signal equation $\Delta\bar{E}=2\Delta\bar{U}$ is valid anymore (see Fig. 48).

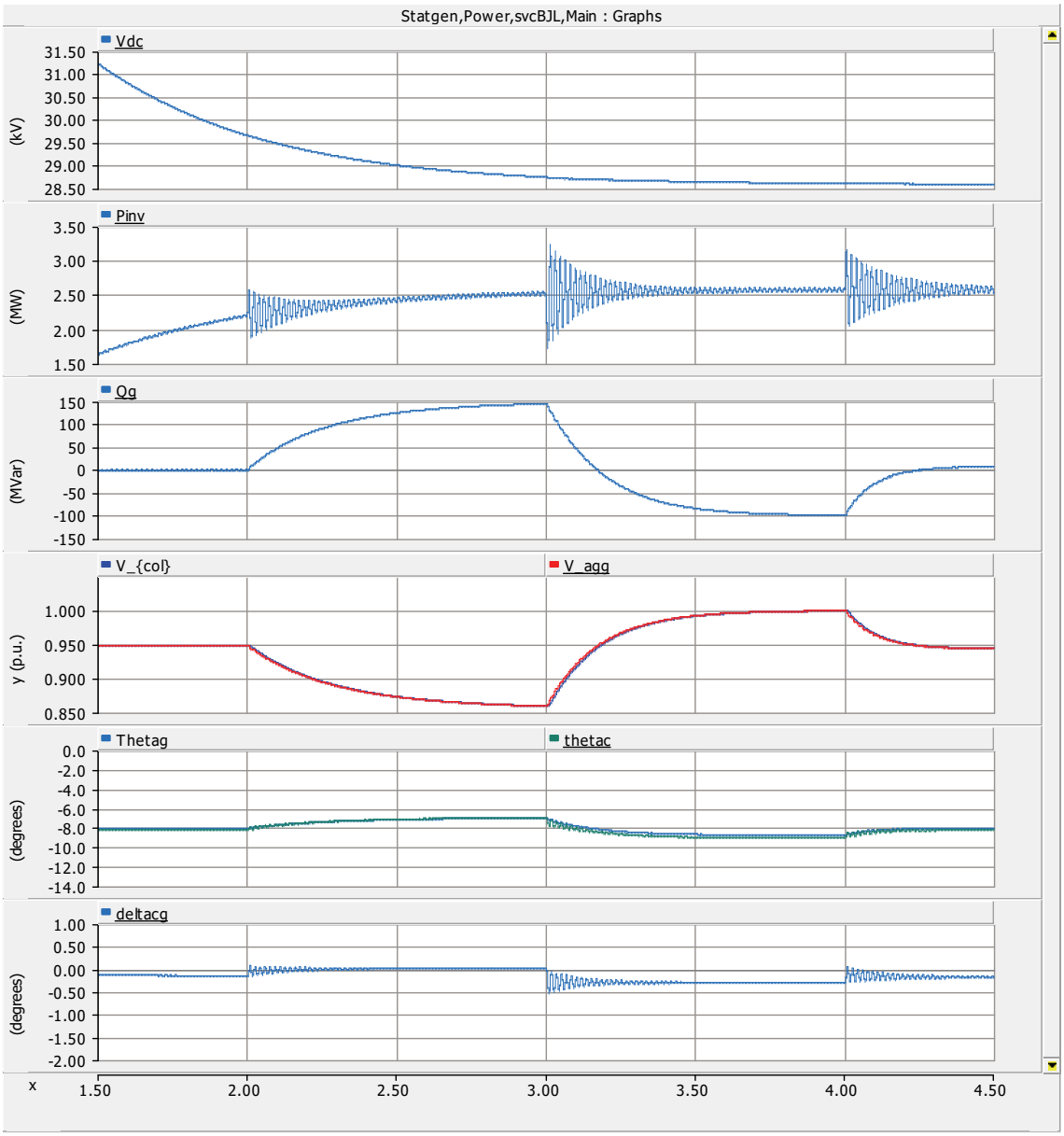

Fig. 46 K_{pdc} from 10 to 1. $K_{p\omega\delta}$ was removed and resulted in elimination of oscillation at connection.

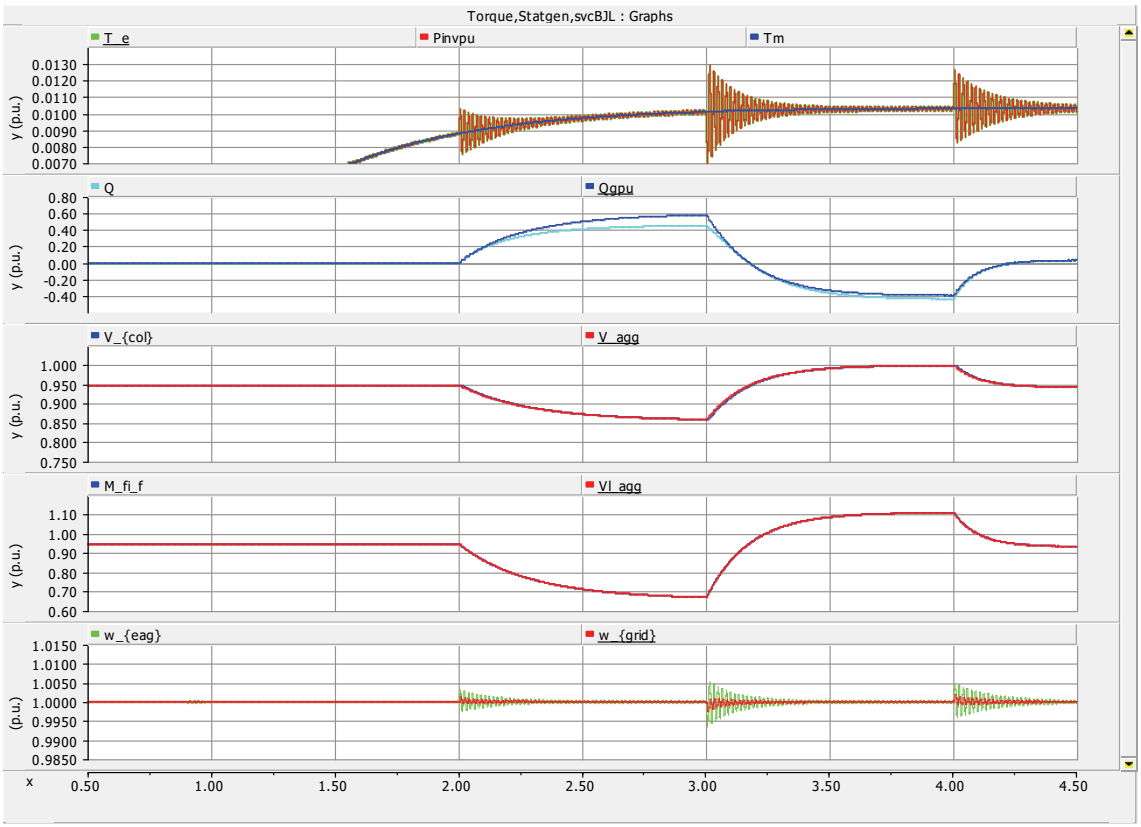

Fig. 47 K_{pdc} from 10 to 1. $K_{p\omega\delta}$ was removed and resulted in elimination of oscillation at connection.

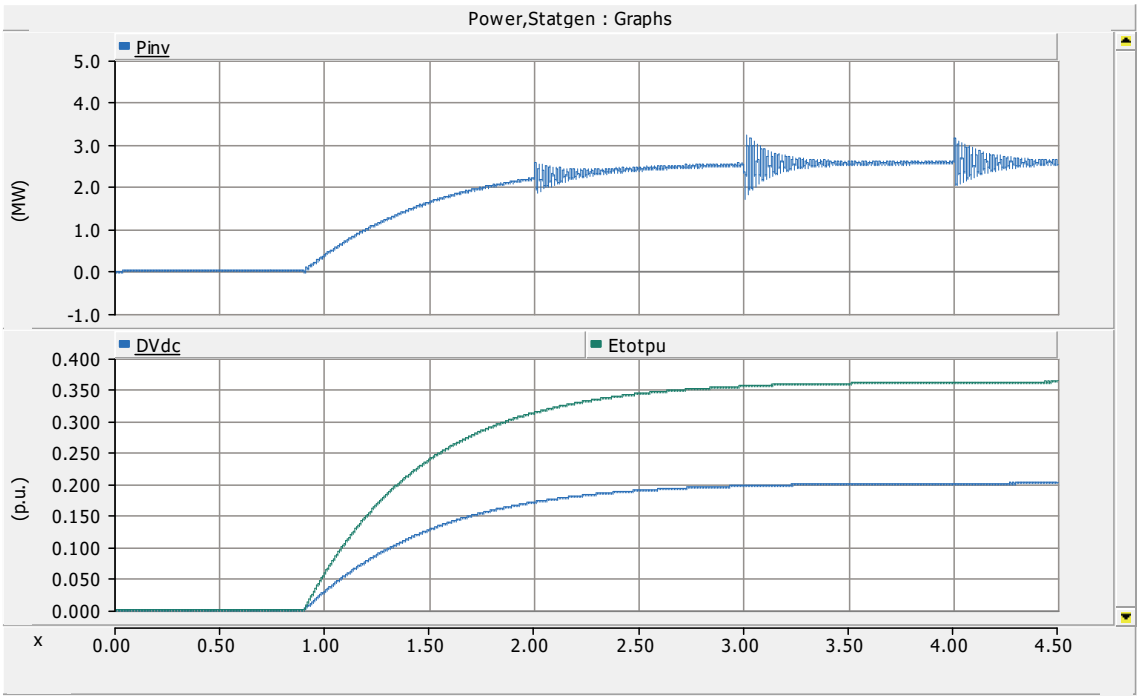

Fig. 48 K_{pdc} from 10 to 1. $K_{p\omega\delta}$ was removed and resulted in elimination of oscillation at connection.

Frequency variations in the grid

After examining the influence of the controller parameters for the reactive control variation simulations, some examining will be done as well for the frequency track simulations as in [24] with the proposed controller of this thesis.

The results of the first frequency track simulation are with the same parameters as the voltage control simulation for Fig. 43 and Fig. 44, K_{pdc}=10, $K_{p\omega}$=2, $K_{i\omega}$=20 ($2H$ = 0.05s), and are shown in Fig. 49 and Fig. 50. In relation to Fig. 28, results for the frequency track simulation to compare with [24], K_{pdc} and $K_{p\omega}$ have reduced with a factor 10. With these smaller gains the contribution to oppose to frequency changes has increased. As mentioned for the voltage control simulations, the system frequency resonance doesn´t suffer a significant alteration.

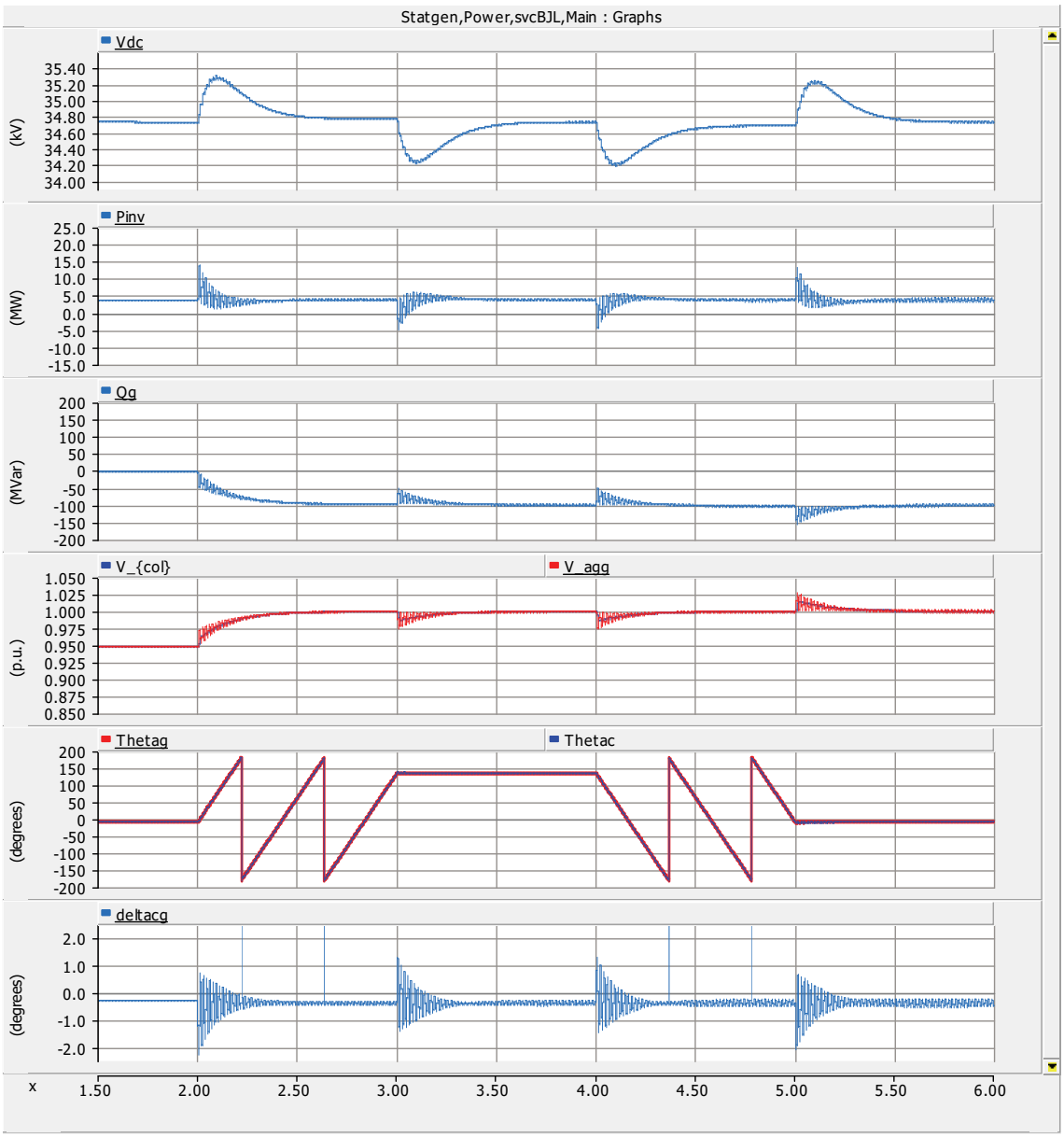

Fig. 49 K_{pdc} = 10. $K_{p\omega}$ = 2. $K_{i\omega}$ = 20 (2H = 0.05 s).

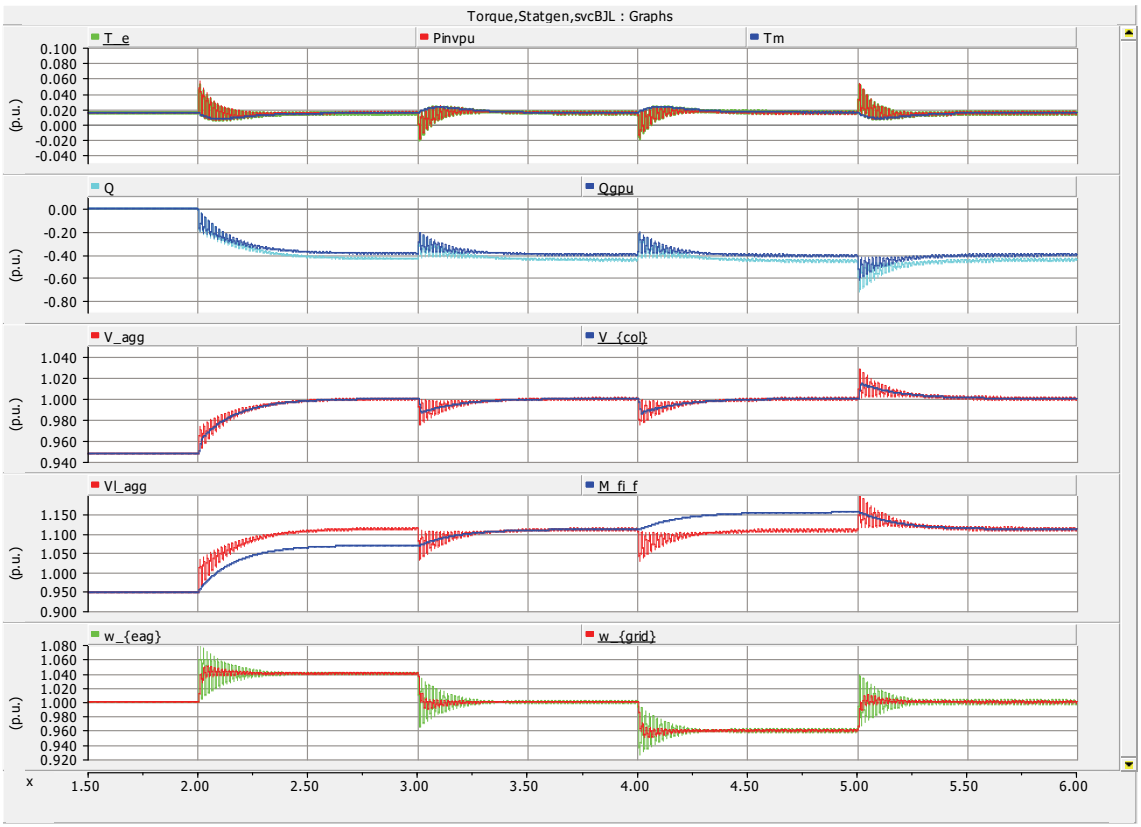

Fig. 50 K_{pdc} = 10. $K_{p\omega}$ = 2. $K_{i\omega}$ = 20 (2H = 0.05 s).

For every system frequency step, the angular velocity, *w_{eag}*, of the synchronverter has a system frequency resonance initiated, as was the case for reactive power step changes too. That it is really the system frequency resonance and not a 60 Hz resonance, zooms were made on the time scale, just after t = 2 s, fg = 62.4 Hz (see Fig. 51) and just after t = 4 s (see Fig. 52).

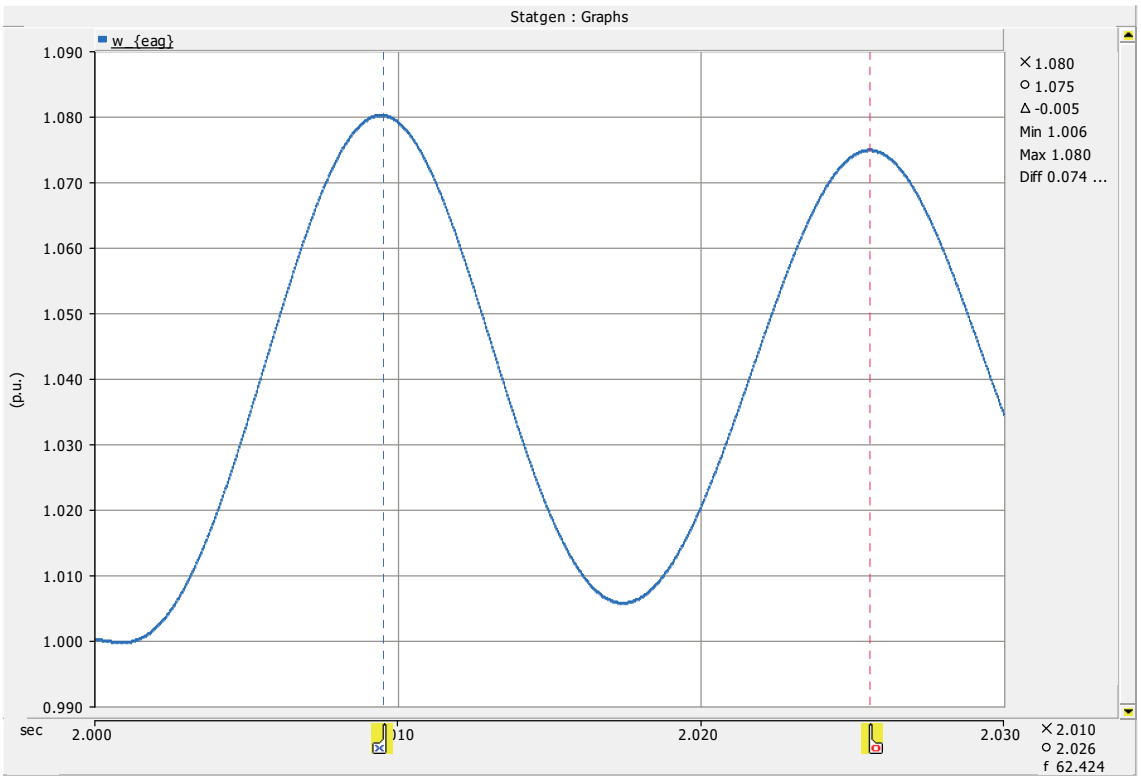

Fig. 51 The frequency of the resonance oscillation, 62.4 Hz is equal to the system frequency (see Fig. 27), 1.04 p.u. times 60 Hz.

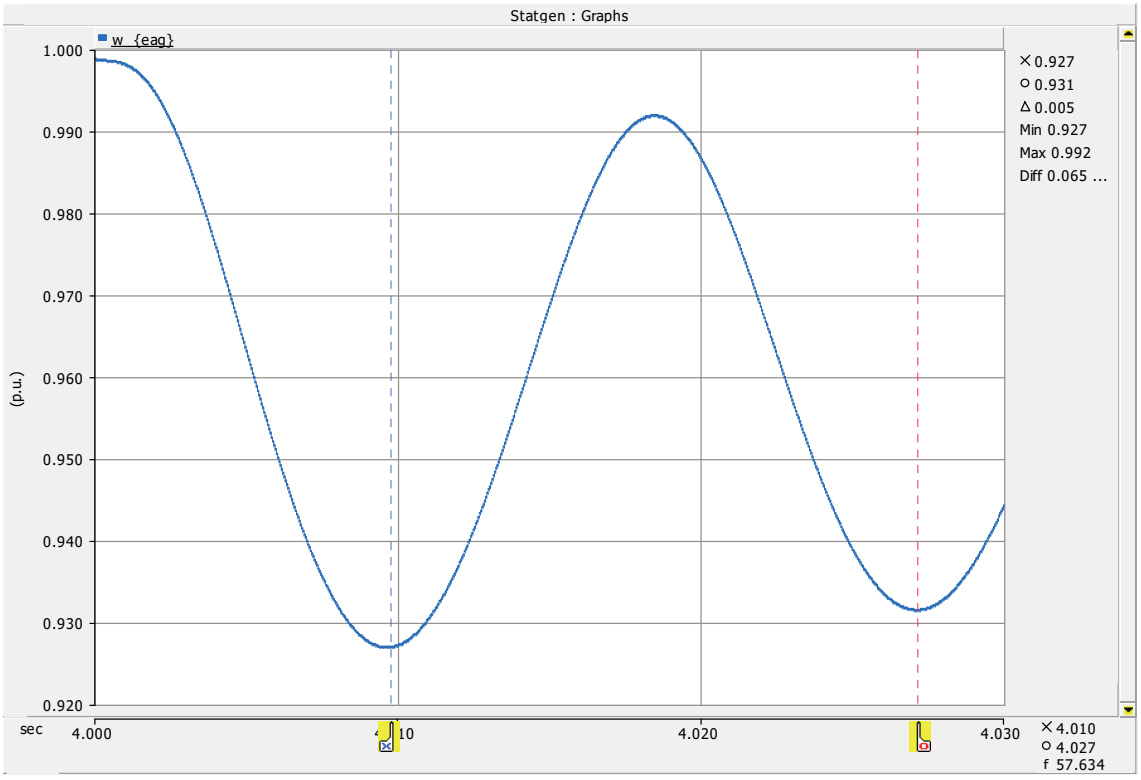

Fig. 52 The frequency of the resonance oscillation, 57.6 Hz is equal to the system frequency (see Fig. 27), 0.96 p.u. times 60 Hz.

So, with K_{pdc} = 10, as a lower limit, since smaller values lead to a poor capacitor loading response, remains $K_{p\omega}$ as a parameter to increase the inertia contribution as can be seen in Fig. 53 and Fig. 54.

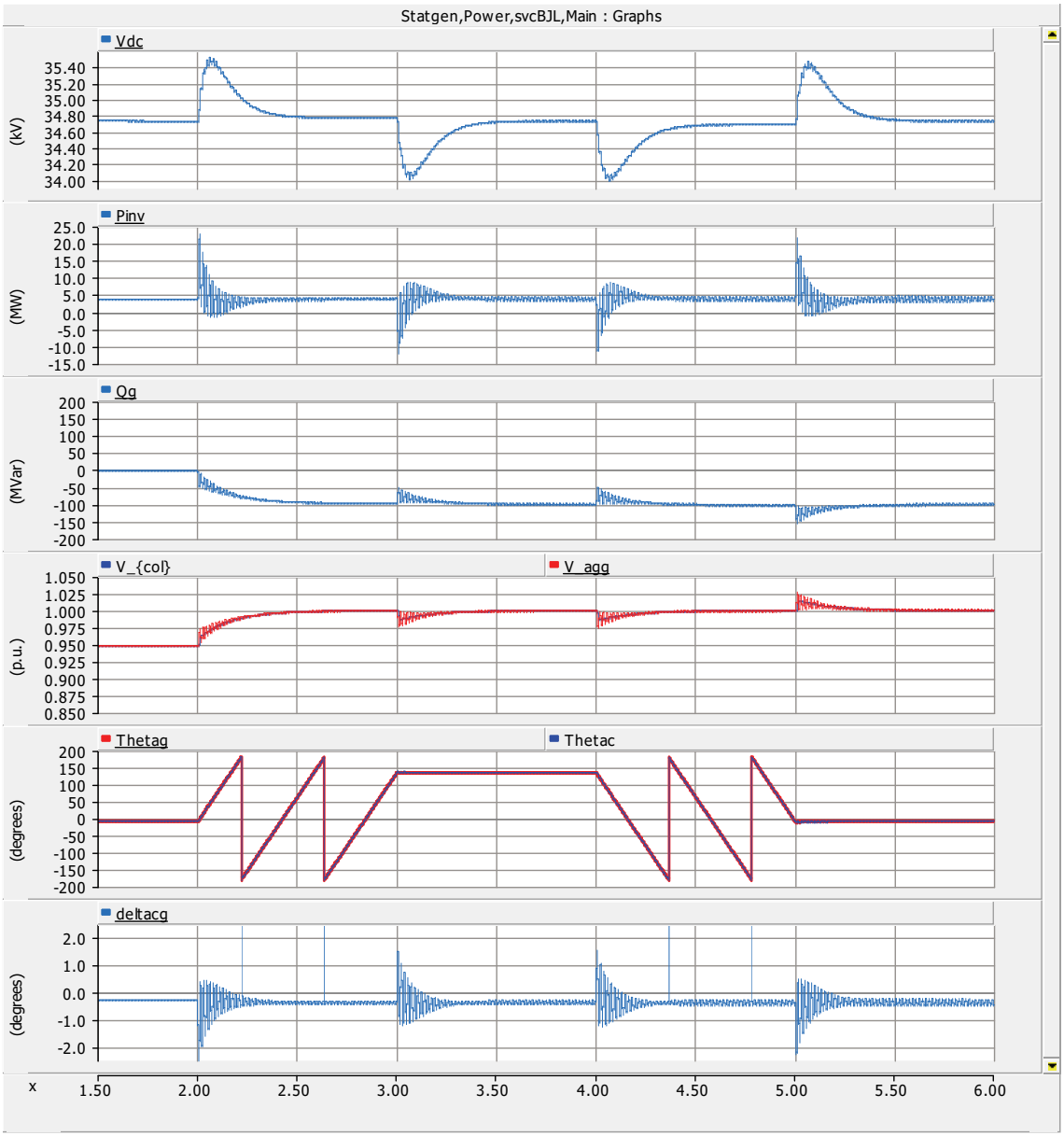

Fig. 53 K_{pdc} = 10. $K_{p\omega}$ = 1. $K_{i\omega}$ = 20 (2H = 0.05 s).

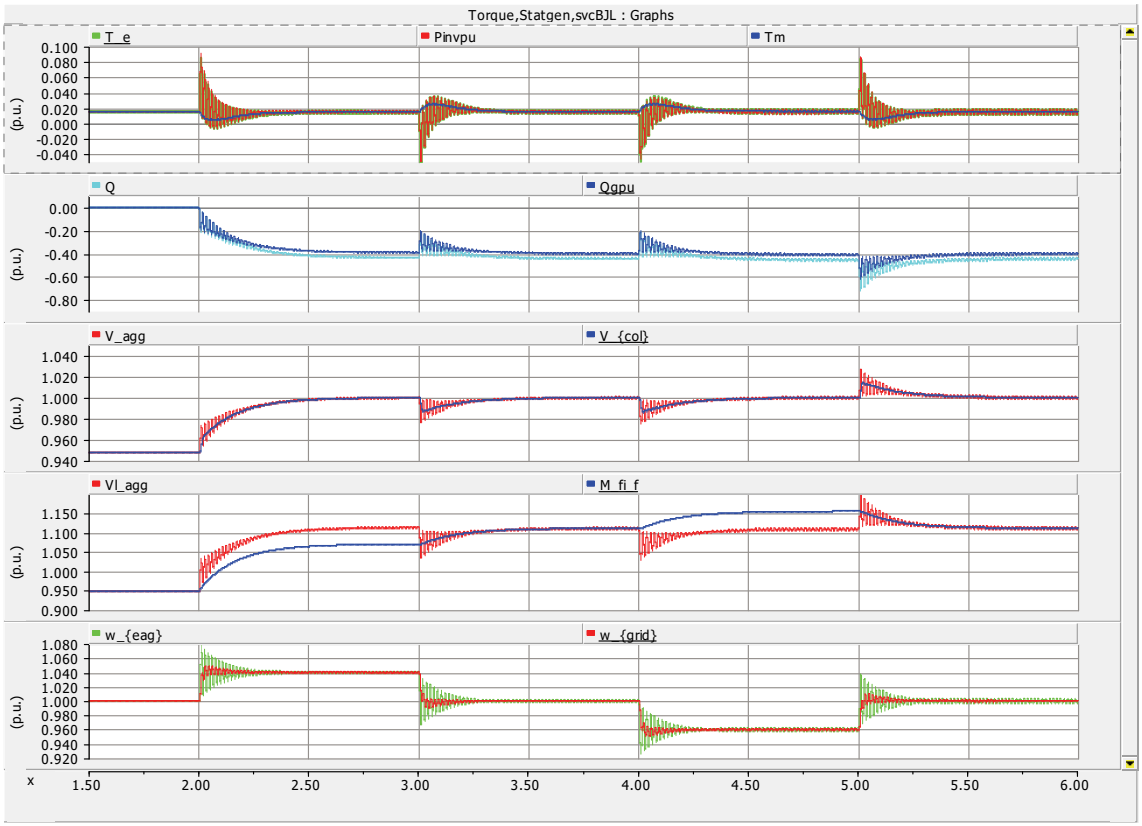

Fig. 54 K_{pdc} = 10. $K_{p\omega}$ = 1. $K_{i\omega}$ = 20 (2H = 0.05 s).

Though, $K_{p\omega}$ cannot be reduced to zero as foreseen in item 4.1 and the result is shown in Fig. 55 and Fig. 56. Without a parallel gain to the virtual inertia, the natural oscillation related to the inertia is revealed, since it is unstable and around 22 Hz.

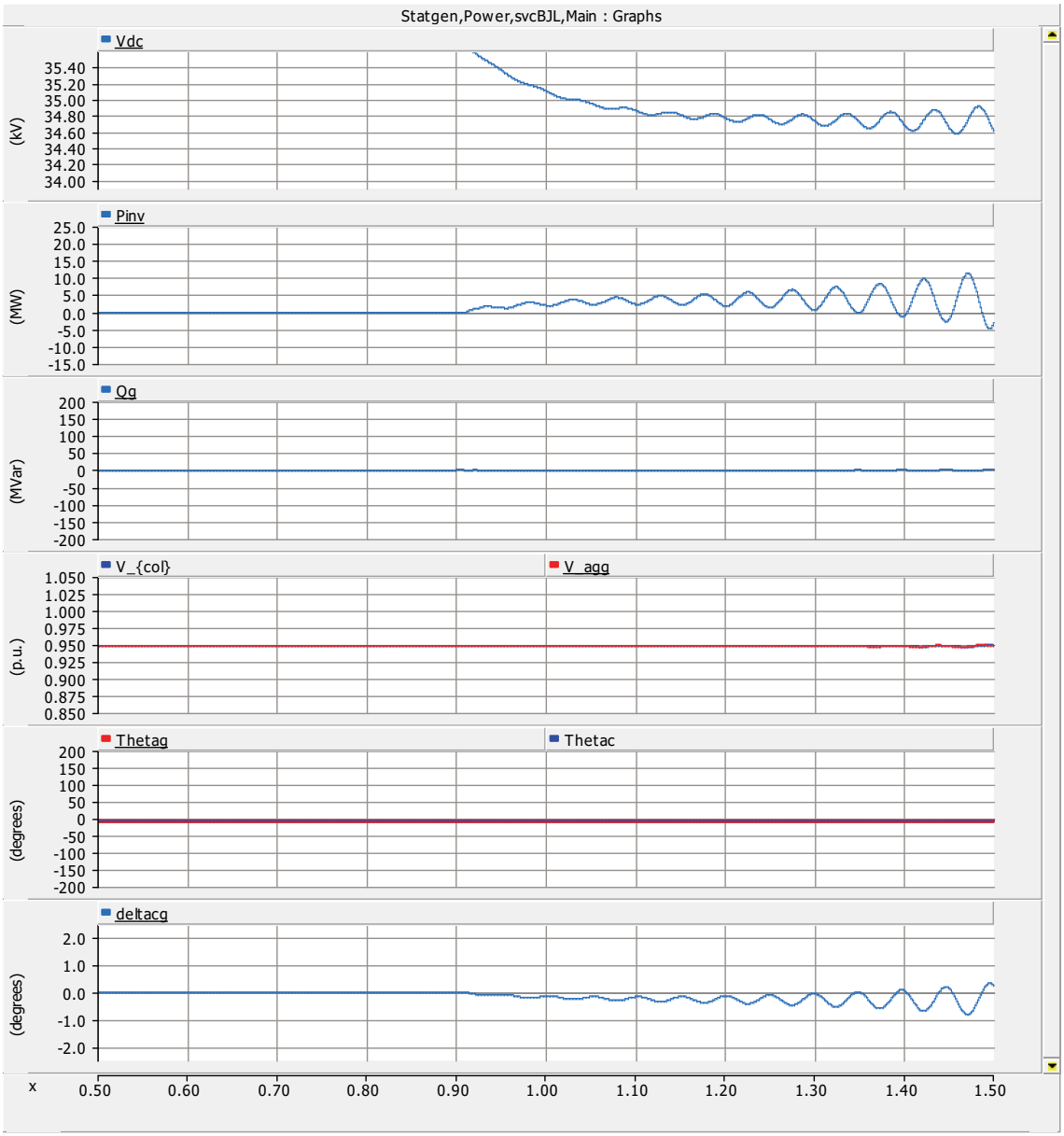

Fig. 55 K_{pdc} = 10. $K_{p\omega}$ = 0. $K_{i\omega}$ = 20 (2H = 0.05 s). Unstable right after connection with grid.

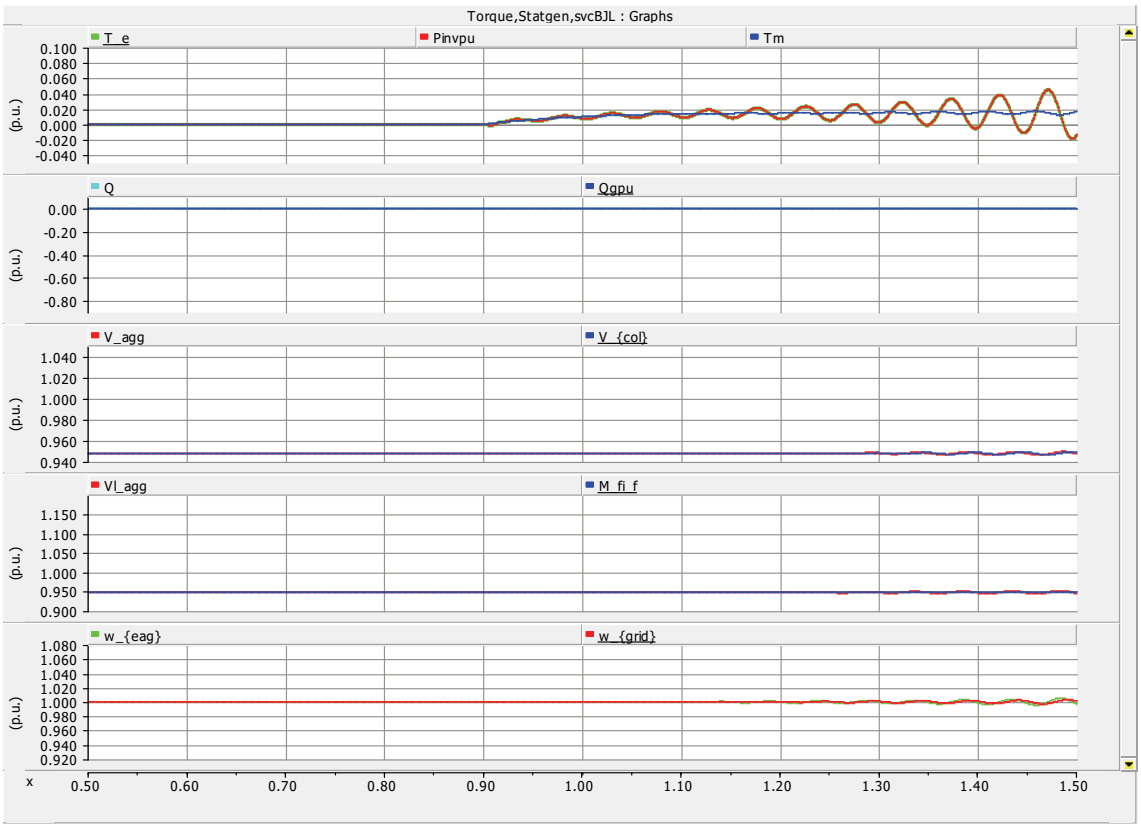

Fig. 56 K_{pdc} = 10. $K_{p\omega}$ = 0. $K_{i\omega}$ = 20 (2H = 0.05 s). Unstable right after connection with grid.

Although, one might think that J doesn´t have an influence on the contribution to the system frequency, this observation can be caused by utilizing high proportional gains, leading to an over damped system. With a proportional gain 10 times smaller than the integral gain, the effect of J variations is clearly shown in Fig. 57 and Fig. 58.

While with K_{pdc} the height of the peak contribution of V_{dc} was set as shown in Fig. 53, the parameter J has influence on the duration of the contribution as shown in Fig. 57. With this, the torques and active powers are influenced as well, as can be seen in Fig. 58.

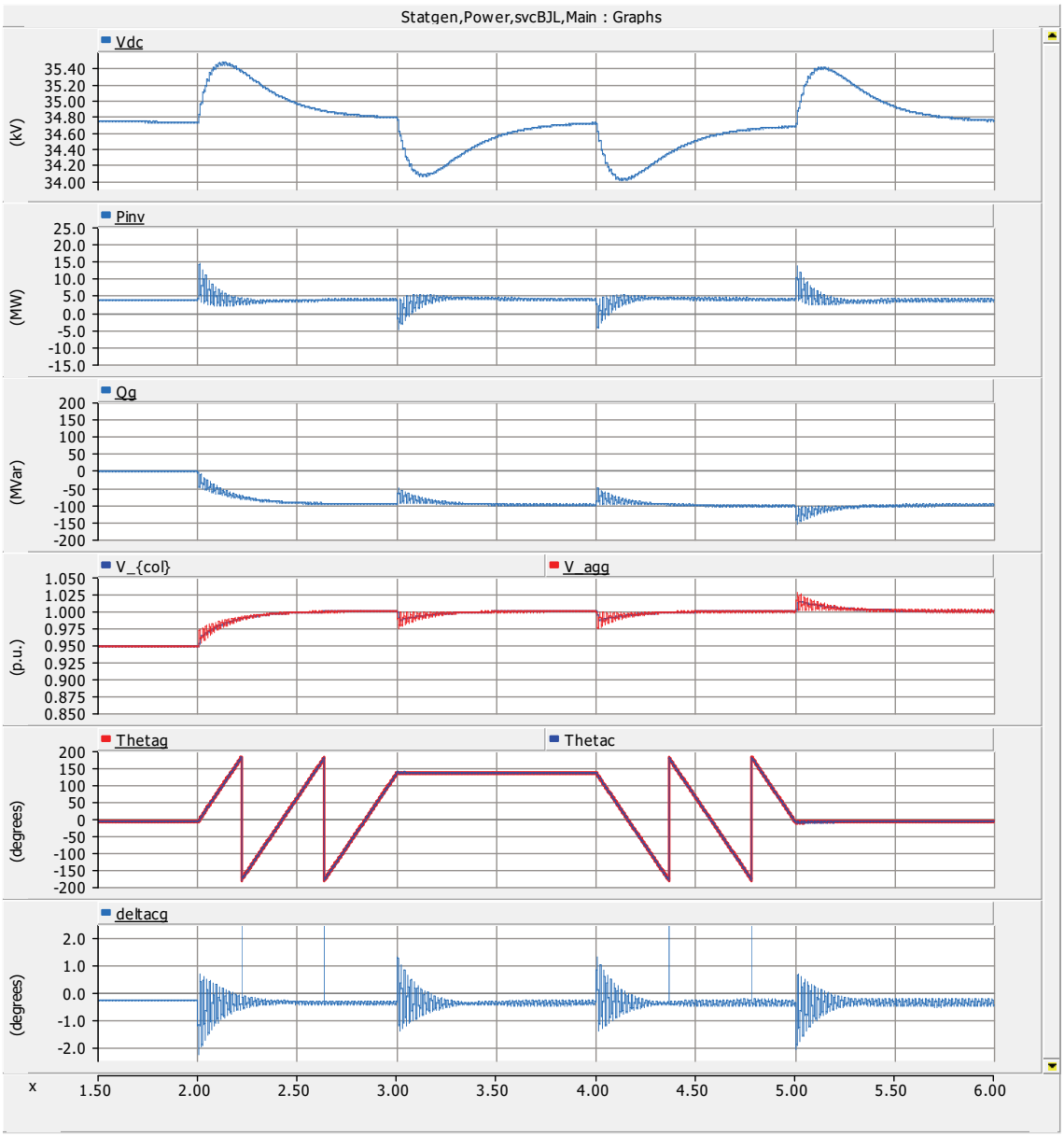

Fig. 57 K_{pdc} = 10. $K_{P\omega}$ = 2. $K_{I\omega}$ = 10 (2H = 0.1 s).

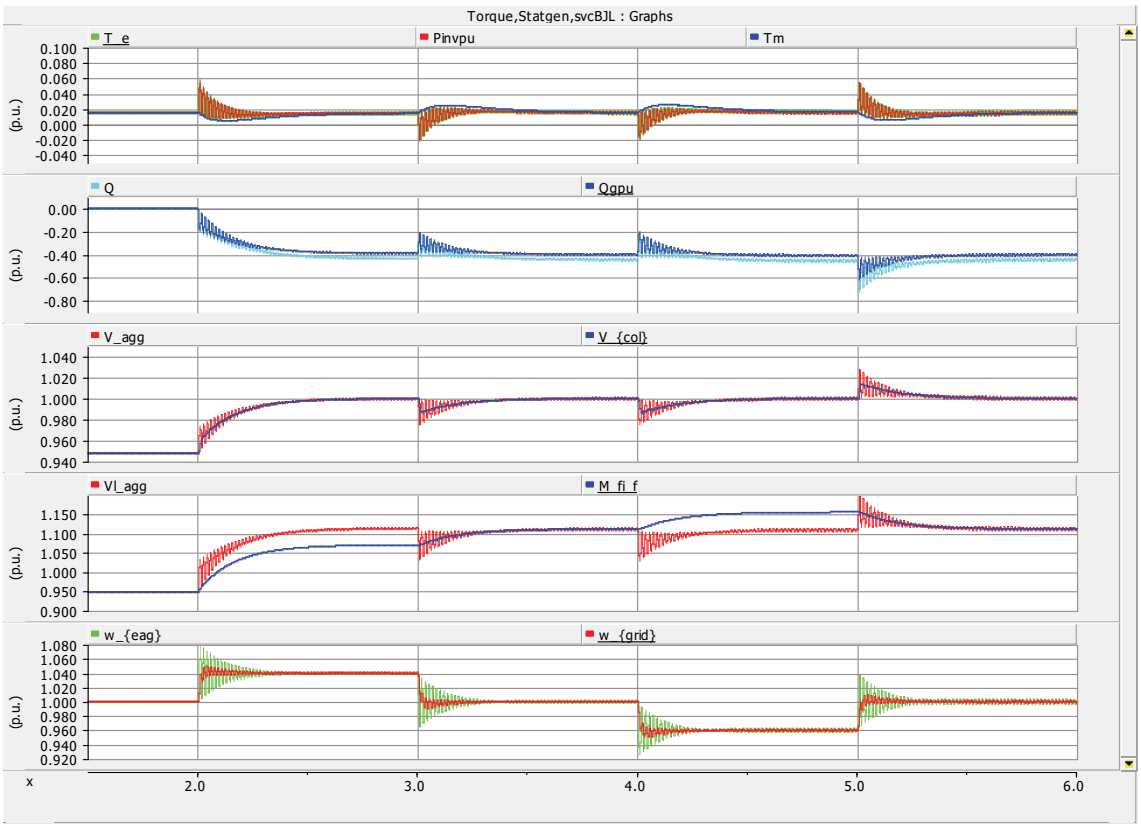

Fig. 58 K_{pdc} = 10. $K_{P\omega}$ = 2. $K_{I\omega}$ = 10 (2H = 0.1 s).

THE BRAZILIAN POWER SYSTEM

Final simulations are shown for testing the proposed controller at SIN in oscillation damping situation. The power oscillation damper as described in [23] was maintained. For this thesis, the mathematical capacitor was added as described in Fig. 22. And, of course the proposed gain $K_{p\omega}$, to damp the oscillation related to the virtual inertia, without provoking system frequency resonance.

The map of the part of the National Brazilian System that was modeled in PSCAD is given in Fig. 59. At three strategic points the system was cut and at these locations dynamic equivalents were inserted to represent the spinning generation in regions behind those points. These equivalents are placed in Serra da Mesa (South/South-East/Center-West), Xingó (North-East) and Marabá (North). In between Marabá and Serra da Mesa a fourth dynamic equivalent was placed to comply with the load flow. This equivalent is much smaller representing only the generation plant in Lajeado. The synchronverter is connected at Bom Jesus da Lapa with a 500 kV/17.5 kV transformer.

Fig. 59 Part of the National Interconnected System, configuration of January 2009, modeled in PSCAD – source: website of ONS (National System Operator).

The model in PSCAD is given in Fig. 60. This is the main page, since the system was constructed in a modular way. In this case all the transmission lines were modeled as PI-sections and some of them mutually coupled PI-sections. This is sufficient for electromechanical oscillations. Some observations will be made on transient behavior, though they are worst case observations, since for electromagnetic transient studies the frequency dependent transmission line model should be used. These simulations not only need a smaller time step than for electromechanical simulations, more time is also spent in calculating the travelling waves. To initiate significant electromechanical oscillations, short-circuit with 0.1 Ω resistance value is applied at t = 5 s during 10 ms on the bus of Miracema (see Fig. 60 for approximate location). The synchronverter is electrically connected at t = 3.1 s.

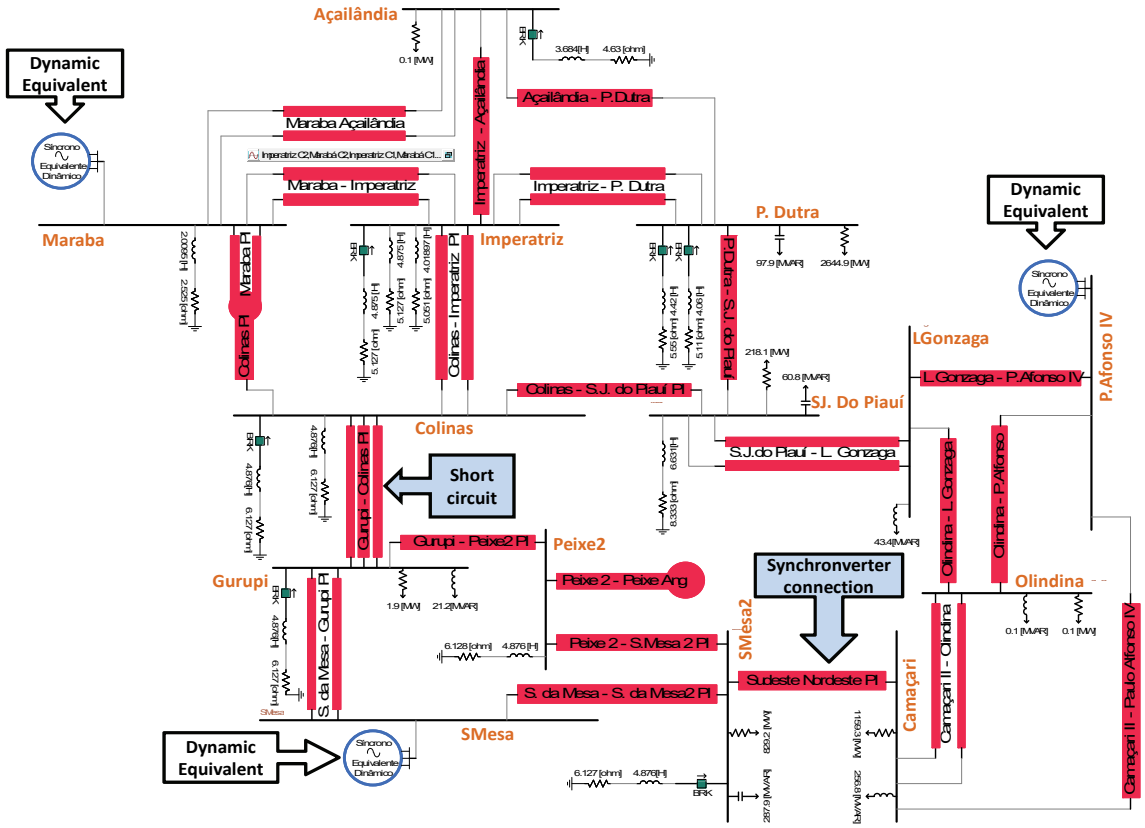

Fig. 60 Overview of the simulated system with modular construction based on data of Fig. 59 [22].

The block diagram for the signal treatment of the active power flow in the transmission line S. Mesa – Gurupi, which was used to sense the electromechanical oscillations, is repeated in Fig. 61 for convenience. The treatment consists of a low-pass filter with a damped resonance peak in 0.82 Hz and a washout filter to avoid interfering in the load flow. Both active power flows on the two transmission lines from S. Mesa to Gurupi were added. The filters are reset 100 ms before the entrance of STATCOM.

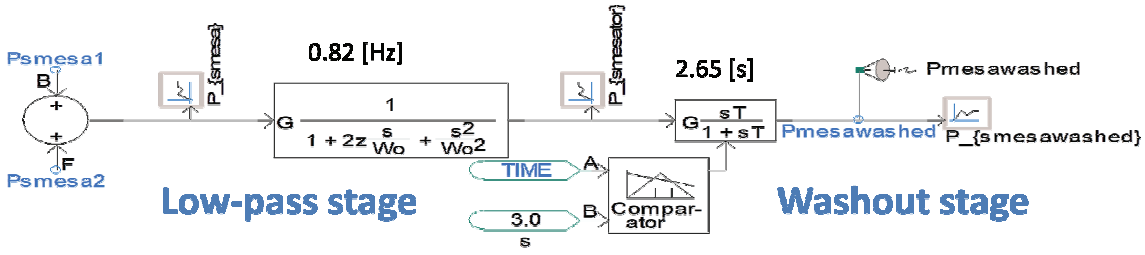

Fig. 61 Block diagram for the signal treatment of the active power flow in the transmission line S. Mesa – Gurupi.

This filtered signal was transmitted to the STATCOM location in Bom Jesus da Lapa where this signal passes through a delay stage to obtain the most effective damping for the electromechanical oscillations in this system. For four dynamic equivalents, besides the virtual inertia of the synchronverter, three electromechanical oscillations are expected. The one related to Lajeado has the highest frequency, about 2 Hz, and, normally is self damped. Fig. 62 shows the delay stage. To show the effectiveness of the POD, it was only activated at t = 30s, 25 seconds after short-circuit. The entire simulation time is 60 s. The used time step was 5 μs, while the plot step was set on 200 μs. The generated damping signal P_{ref} was added to the voltage control as shown in Fig. 11.

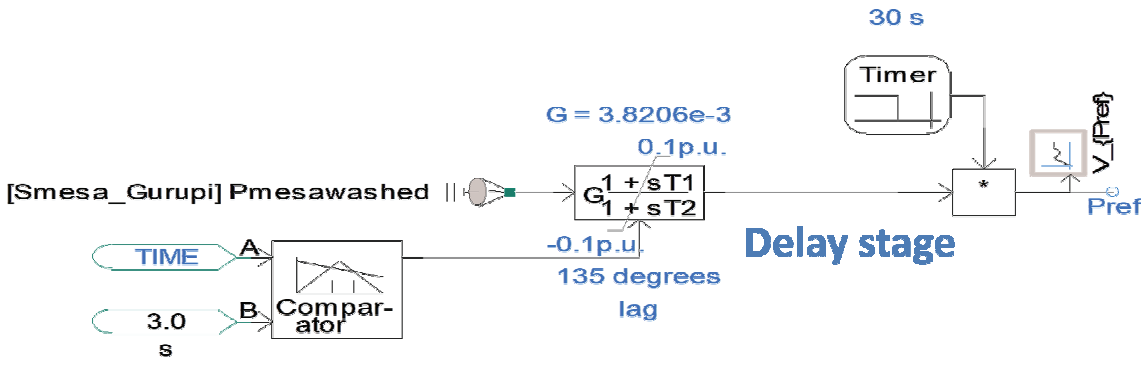

Fig. 62 Block diagram to delay the signal Pmesawashed and output the additional control signal Pref (see Fig. 11).

The following simulation results are in the same format as for the ones shown for the simple model simulations. Some minor alterations are made. In the simulation the reactive power, Q, utilized for voltage control is the internally calculated reactive power of the STATCOM. The reactive power, Q_{gpu}, at the voltage controlled bus is shown in the same window of the figures for comparison only. The STATCOM is connected and at the same time the droop control became operative. The reactive droop is 3% as utilized for the SVC. The voltage reference was set on 1.04 p.u. The angular velocity of the equivalent in Serra de Mesa, ω_{SM} (*omega_sm* in the figures), was added as a reference point for being the equivalent with the highest inertia.

The results for $K_{p\omega}$=0 are shown in Fig. 63 and Fig. 64. The STATCOM at connection is clearly unstable as predicted by the linear model in item 4.1. Therefore, the natural oscillation frequency of the virtual inertia $J = 2H = 50$ ms can be determined as approximately 22 Hz.

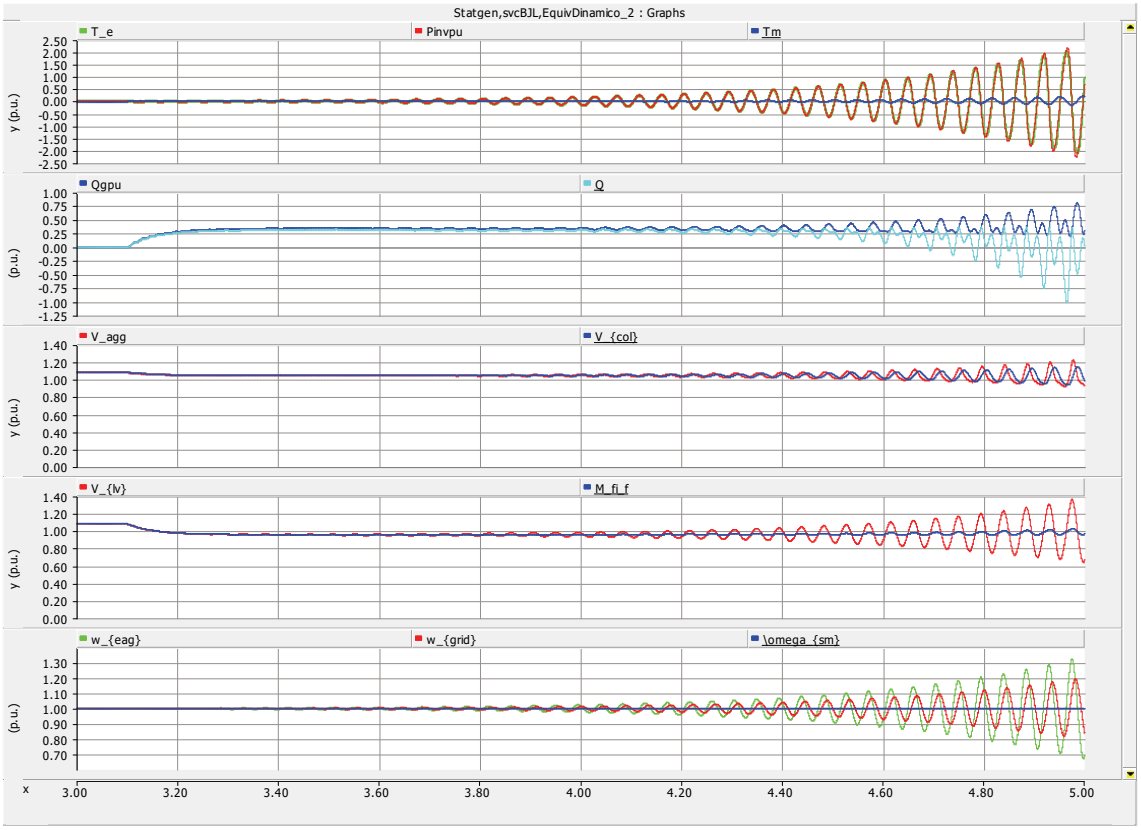

Fig. 63 Electrical torque, T_e, reactive power (+), Q, of the synchronverter (motor convention), controlled bus voltage, V_{col}, in droop mode with Vref = 1.04 p.u., synchronverter terminal-voltage, V_{lv}, virtual flux, M_fi_f, synchronverter angular velocity, w_{eag}, angular velocity calculated by a PLL at the synchronverter terminals, w_{grid}, and the angular velocity, omega_{sm}, of the dynamic equivalent representing the generation of region South/South-east/Center-West. $K_{p\omega}$=0.

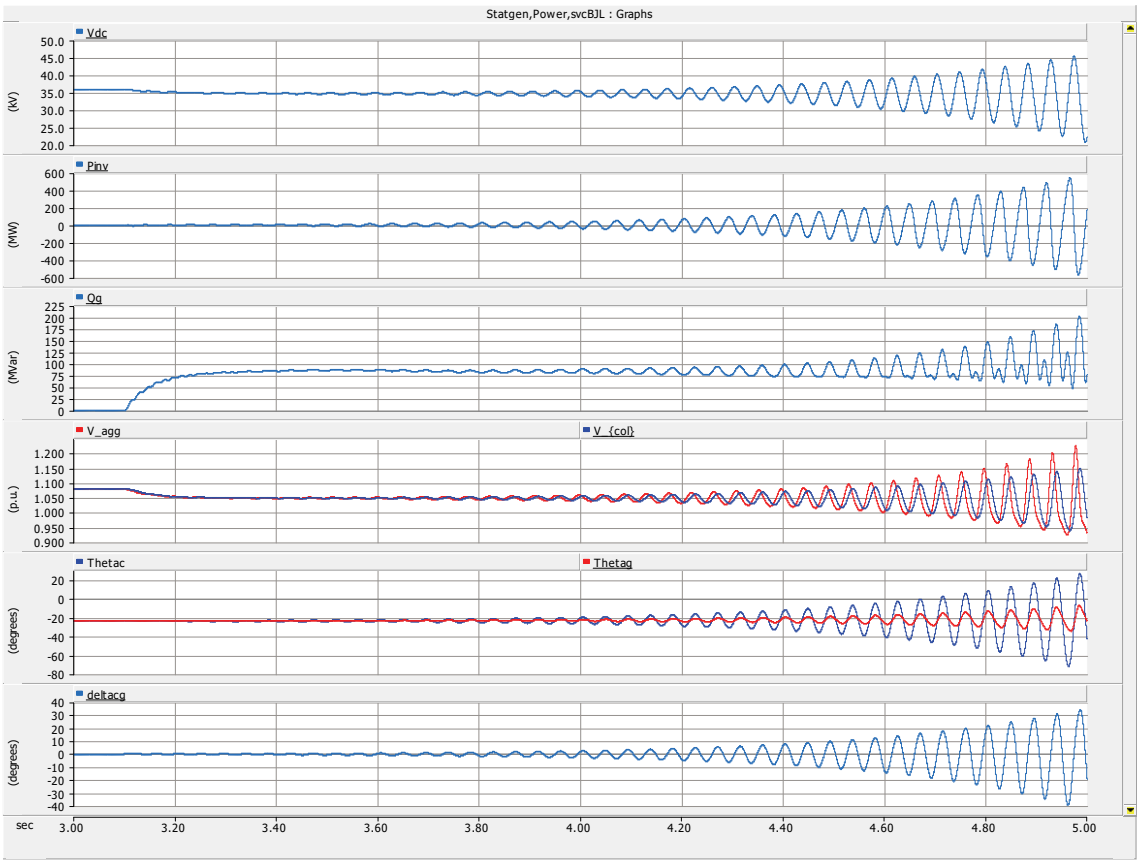

Fig. 64 Results when dc-capacitor is considered, in contrast with [22] and [23], which utilized $T_m = 0$. $K_{p\omega}=0$.

The angular velocities of the equivalents at Marabá and Serra de Mesa, ω_{mb} and ω_{sm}, respectively, are shown below in Fig. 65. Above, the total energy, E_{tot}, is shown. This total is calculated as the energy entering the converter minus the energy dissipated in the parallel resistor at dc-side. Continuing with the motor convention, negative energy means energy contribution to the grid. This is verified in a decreasing capacitor voltage, *Vdc*, shown in Fig. 64, when the total energy, E_{tot}, decreases and vice versa.

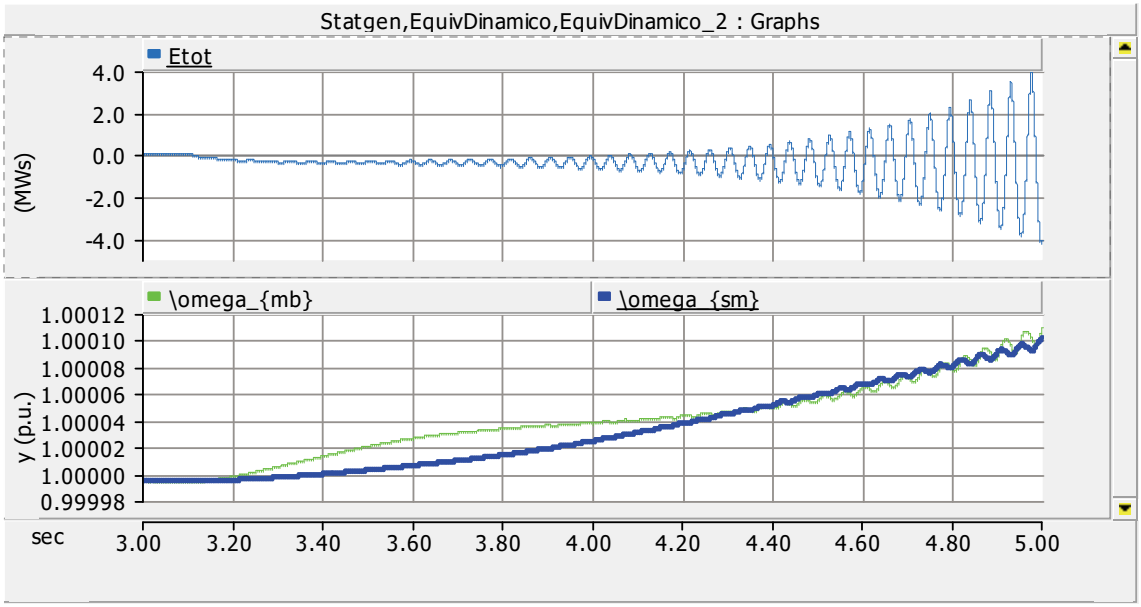

Fig. 65 At t=5s occurs a short-circuit in the grid. Etot = Einv – Erdc. $K_{p\omega}$=0.

The same results are shown for $K_{p\omega}$ = 0.009 in Fig. 66 and Fig. 67. For this proportional gain, the system is stable and fairly damped. At t = 30 s, a damped system frequency resonance can be observed as caused by the application of the POD signal, P_{ref}, and an oscillation of 0.3 Hz caused by the equivalents of Paulo Afonso e Serra de Mesa. After application of the POD signal, the 0.3 Hz oscillation is damped quickly and the 0.6 Hz oscillation of Marabá becomes visible. This one fades away as well.

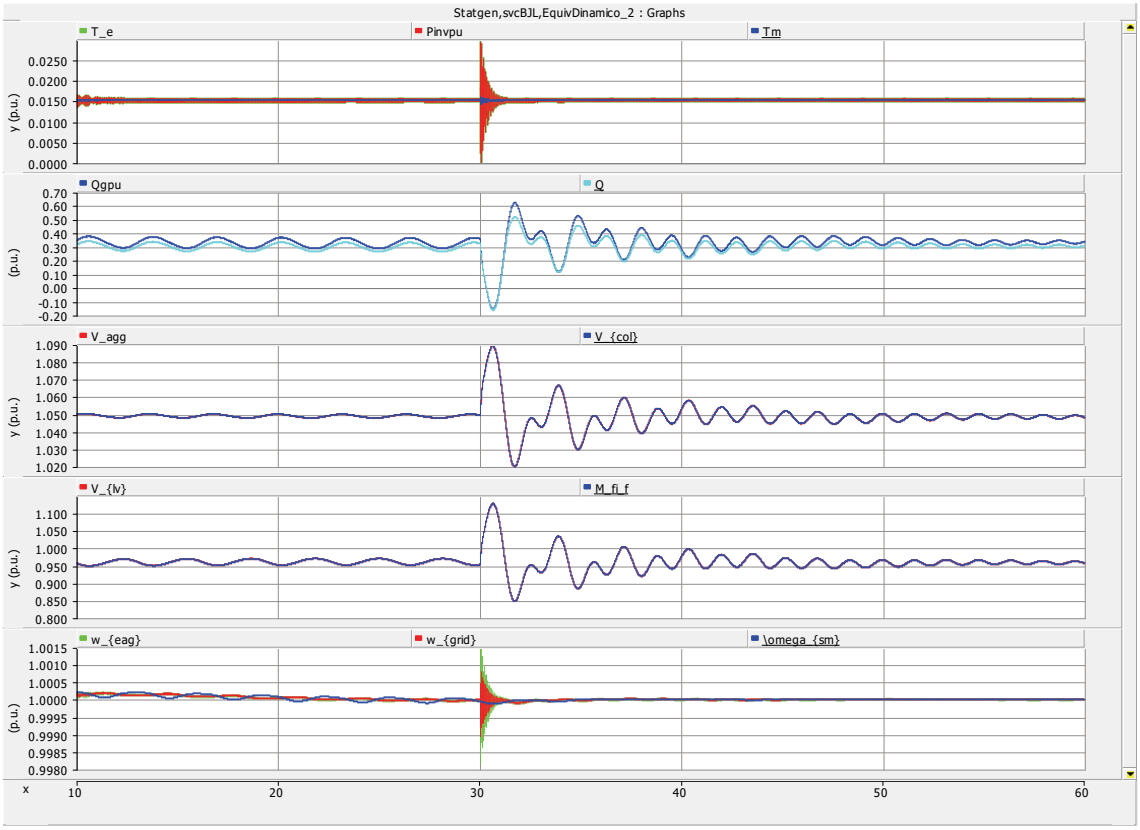

Fig. 66 J = 2H = 50 ms and $K_{p\omega}$=0.009, system stable in contrast with Fig. 63.

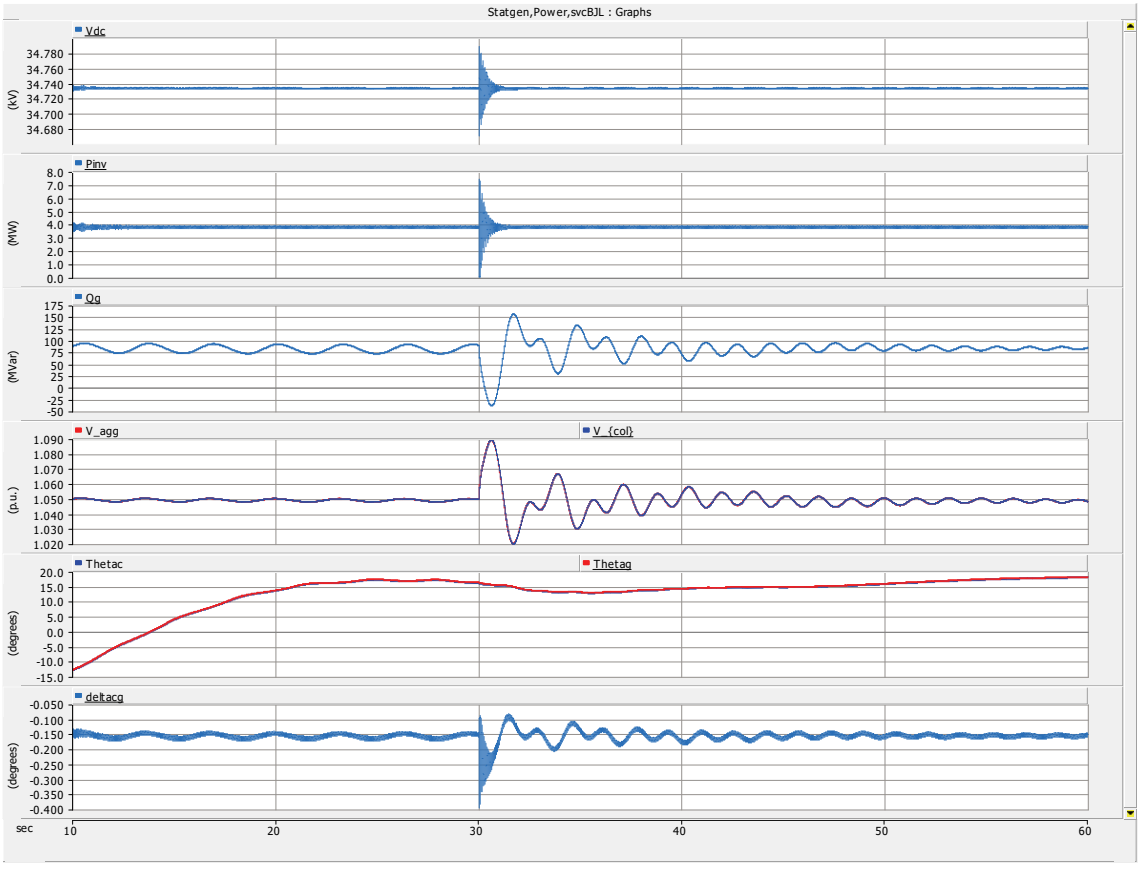

Fig. 67 J = 2H = 50 ms and $K_{p\omega}$=0.009, system stable in contrast with Fig. 64.

The effectiveness of the POD signal can even better been observed directly at the angular velocities of the dynamic equivalents as shown in Fig. 68. Clearly, the equivalents of Paulo Afonso and Serra de Mesa are oscillating one against the other. The equivalents of Marabá and Lajeado are oscillating against the system and thus three oscillating modes for four dynamic equivalents are identified.

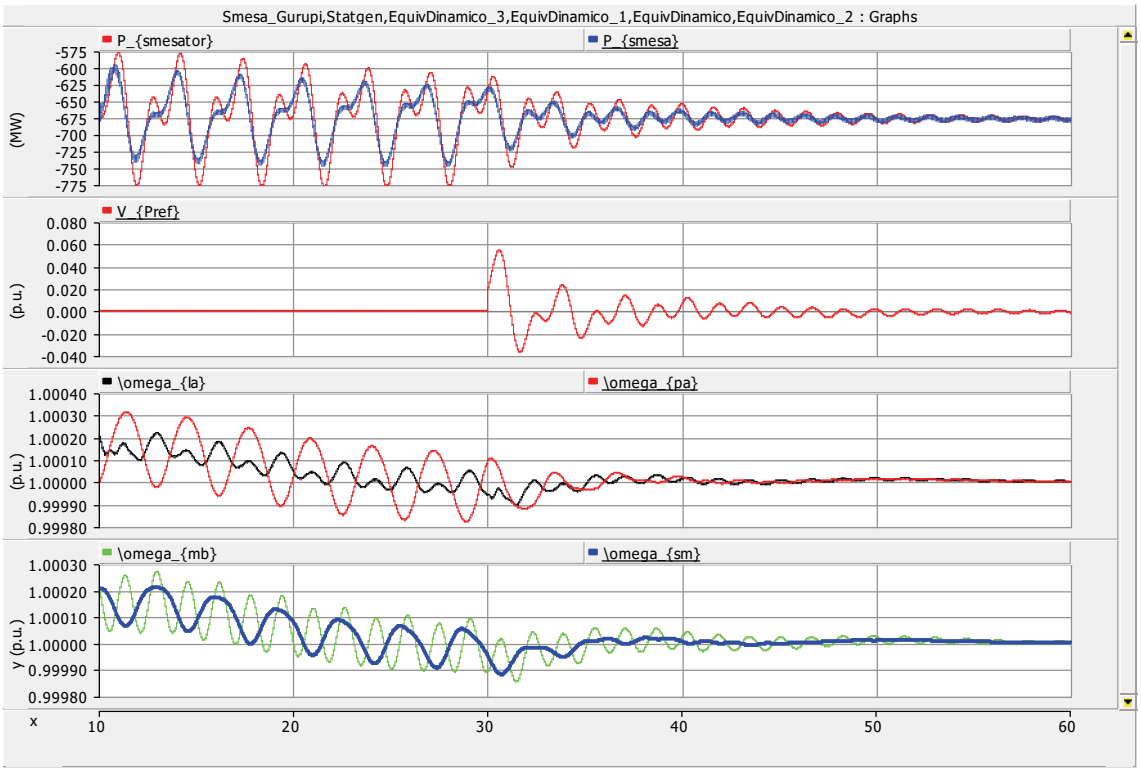

Fig. 68 Total active power flowing North (negative), P_{smesa}, measured at Serra de Mesa, the filtered active power, P_{smesator} (see Fig. 61), POD-signal, V_{Pref} (see Fig. 62), angular velocities, omega, of the 4 dynamic equivalents at Lajeado, {la}, Paulo Afonso, {pa}, Marabá, {mb} and Serra de Mesa,{sm}. $K_{p\omega}$=0.009.

While the virtual inertia was limited to $2H$ = 50 ms, based on the equivalent energy contained at the capacitor, no great contribution can be expected as shown in Fig. 69. Nevertheless, the oscillation with frequency of 22 Hz is practically damped in one second and no system frequency resonance is initiated.

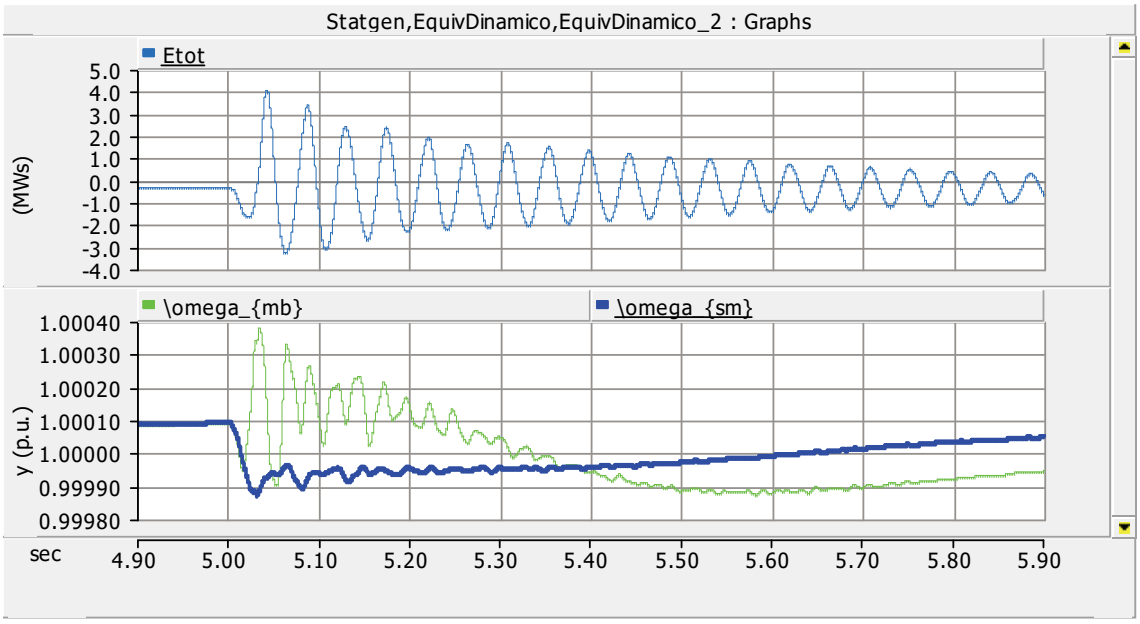

Fig. 69 $K_{p\omega}$=0.009, system stable in contrast with Fig. 65. Small energy contribution at short-circuit occurrence with 2H = 50 ms.

That the virtual inertia J of the synchronverter is not limited given by the equivalence of the energy contained in a capacitor and the kinetic energy is shown in the next simulations. Reminding that the results on the bus of Bom Jesus de Lapa are more severe than when modeling transmission lines based on geometric data, which includes the damping of travelling waves on a distance of around 1,000 km, an inertia $2H$ of 1 s was chosen. This inertia is 20 times bigger than the electrical energy inertia contained on the dc-capacitor.

Firstly, the proposed proportional gain, $K_{p\omega}$ is made zero again. For being slightly unstable, as predicted by the linear model, the oscillation can be observed in Fig. 70. The oscillation frequency is the square root of 20 times smaller as observed for $2H$ = 50 ms. Whereas the system is slightly unstable, the capacitor voltage did not drop at any time below half the reference value.

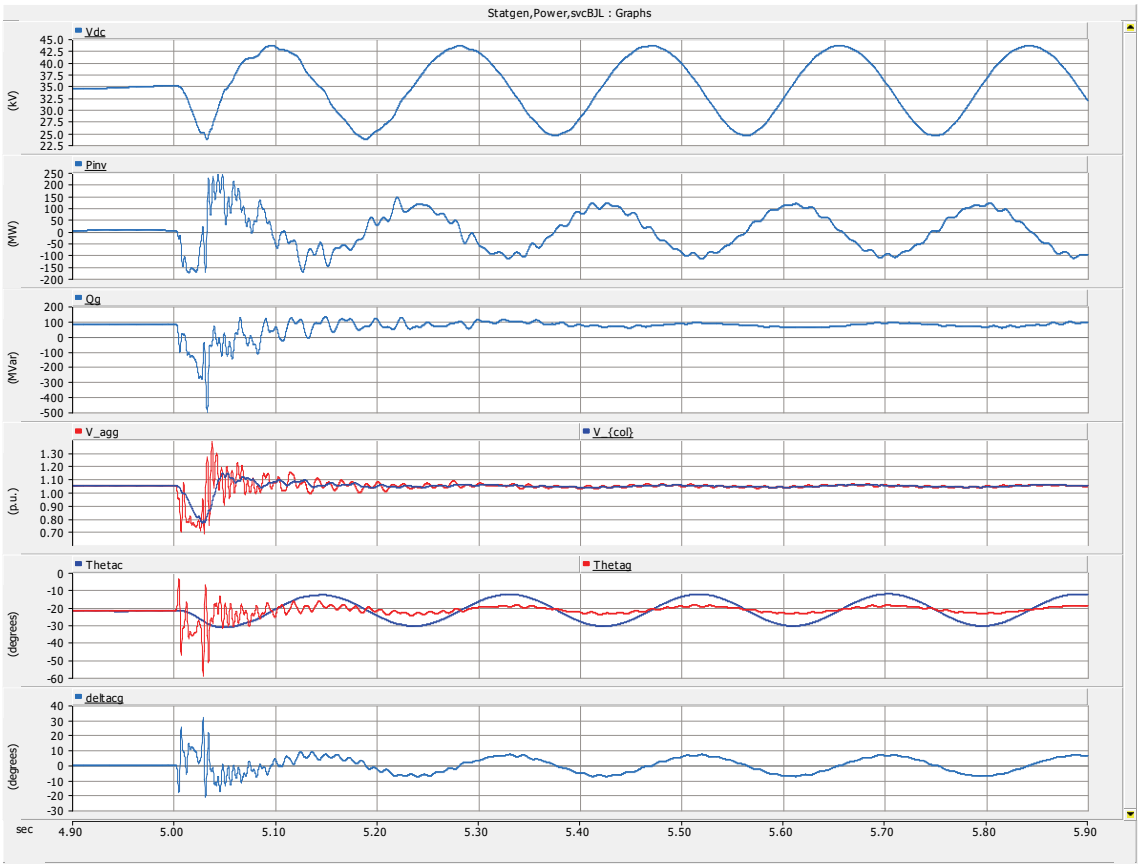

Fig. 70 J = 2H = 1 s and $K_{p\omega}$=0. Capacitor voltage remains above half the reference value even with a virtual inertia 20 times bigger than the electric energy contained on the dc-capacitor.

While the slightly unstable system continued for 60 seconds, and so the internal angular velocity, ω, of the STATCOM continued to oscillate at a little less than 5 Hz, interference with the dynamic equivalent at Lajeado could be observed. This is shown in Fig. 71.

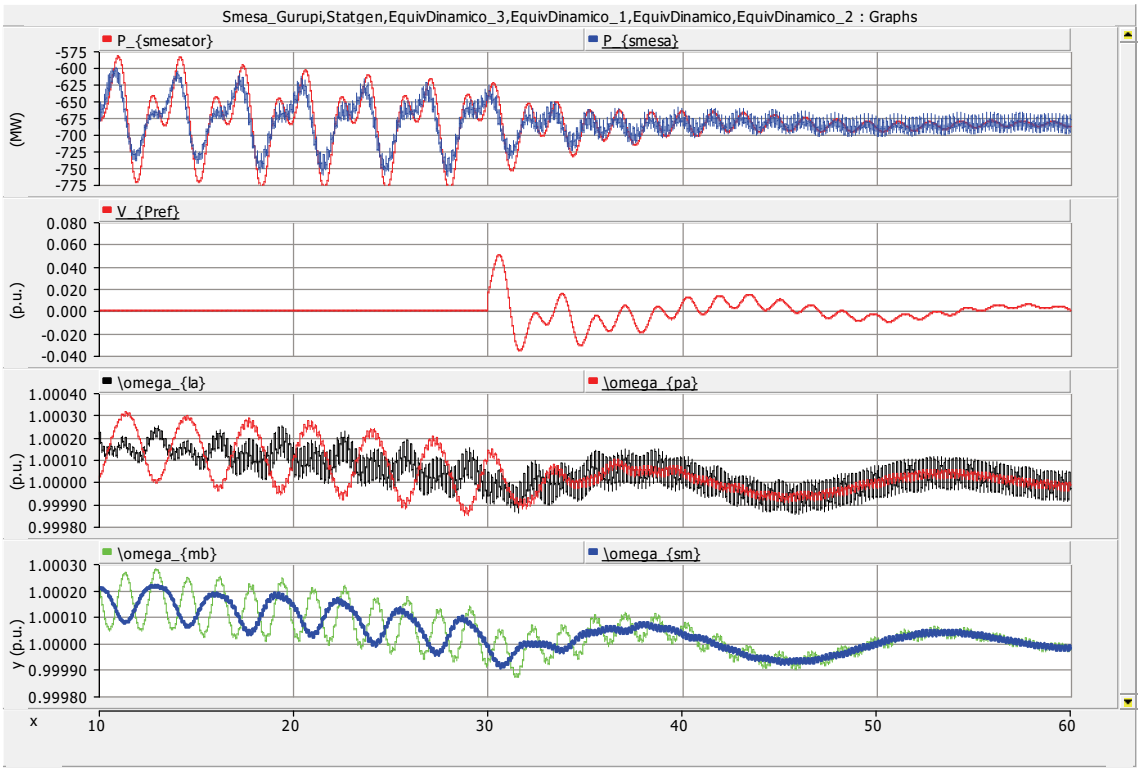

Fig. 71 The instability of the virtual inertia with a natural frequency of a little less than 5 Hz starts even to impact the dynamic equivalent of Lajeado with natural frequency of around 2 Hz.

Comparing Fig. 69, for the energy contribution with $2H$ = 50 ms, with Fig. 72, where $2H$ = 1 s, for the first 30 ms right after short-circuit a more than double contribution can be observed.

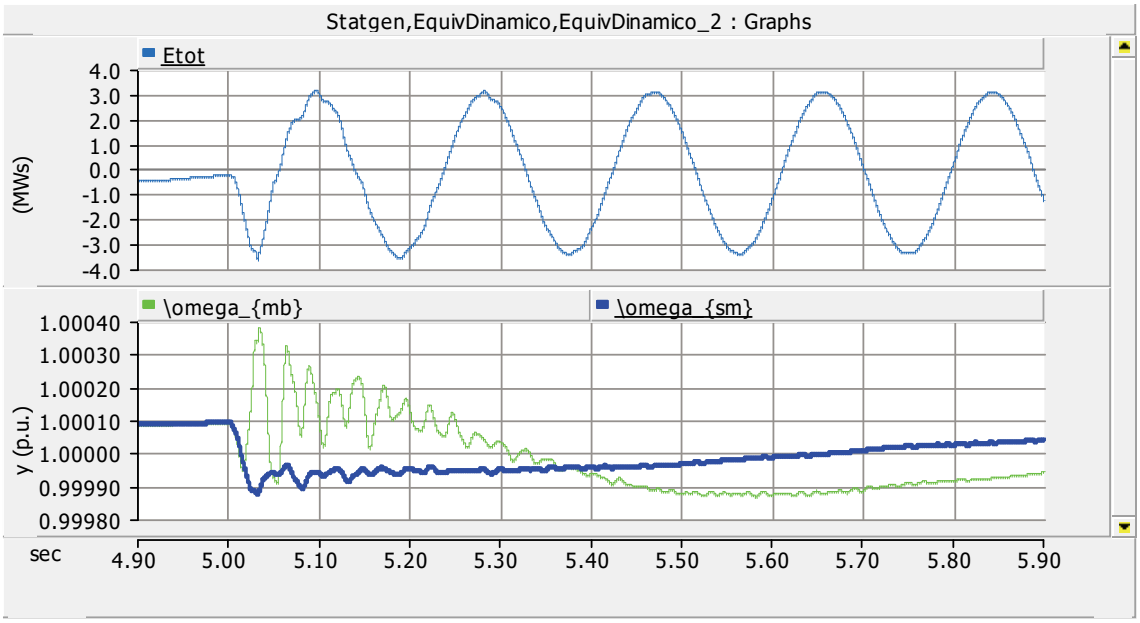

Fig. 72 J = 2H = 1 s and $K_{p\omega}$=0. More energy contribution at short-circuit occurrence than for 2H = 50 ms as shown in Fig. 69.

The results of the linear model as presented in item 4.1, gave the following results for $K_{p\omega}$ for a stable system: 0.000107 < $K_{p\omega}$ < 0.0122. This is for the case, the controlled bus is infinite. This is not true in this simulation case and since *X/R* of the short-circuit impedance is smaller than *X/R* of transformer and L filter with small resistance, the following results were performed with J = 1 s and $K_{p\omega}$ = 0.012, expecting to still find a stable system. The results are shown in Fig. 73 and Fig. 74. The system frequency resonance is still fairly damped, as can be observed.

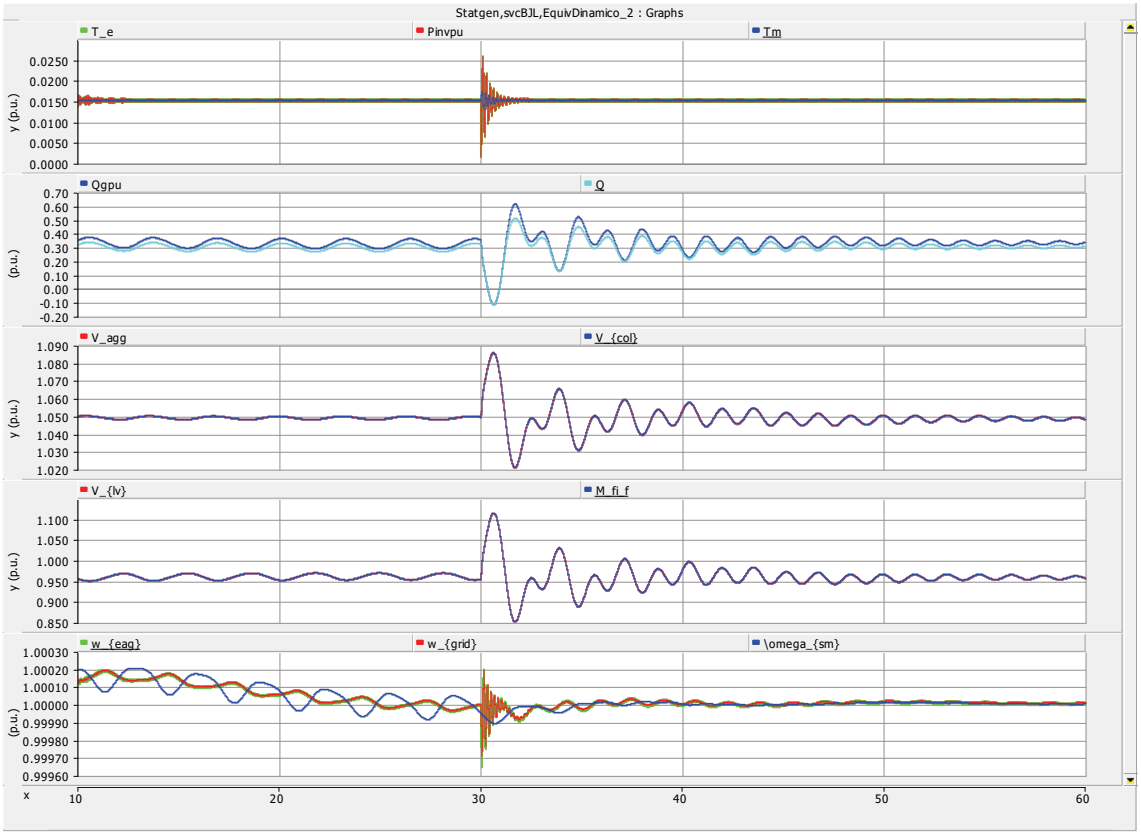

Fig. 73 J = 1 s and $K_{p\omega}$ = 0.012. To compare with Fig. 66.

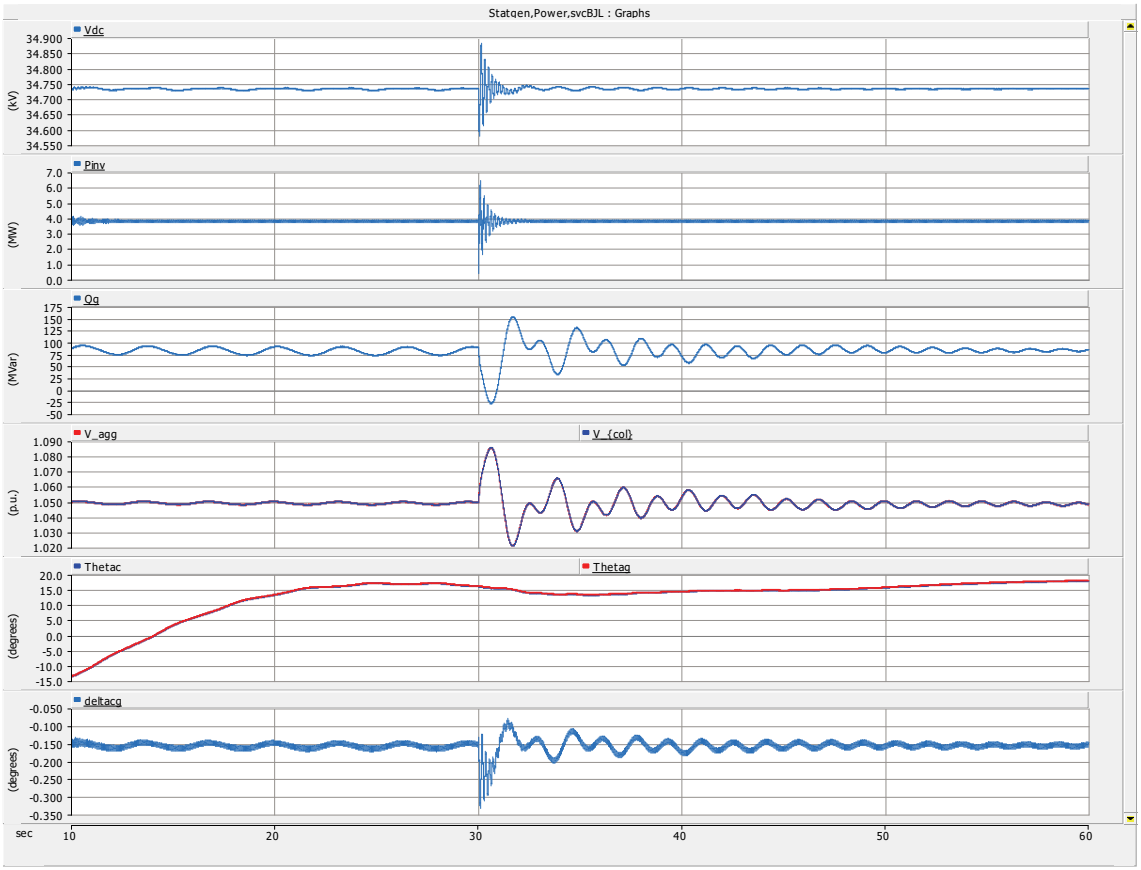

Fig. 74 J = 1 s and $K_{p\omega}$ = 0.012. To compare with Fig. 67.

With the virtual inertia of the STATCOM damped by the proposed proportional gain, the angular velocity of the equivalent at Lajeado is not affected anymore by the STATCOM. This can be seen in Fig. 75.

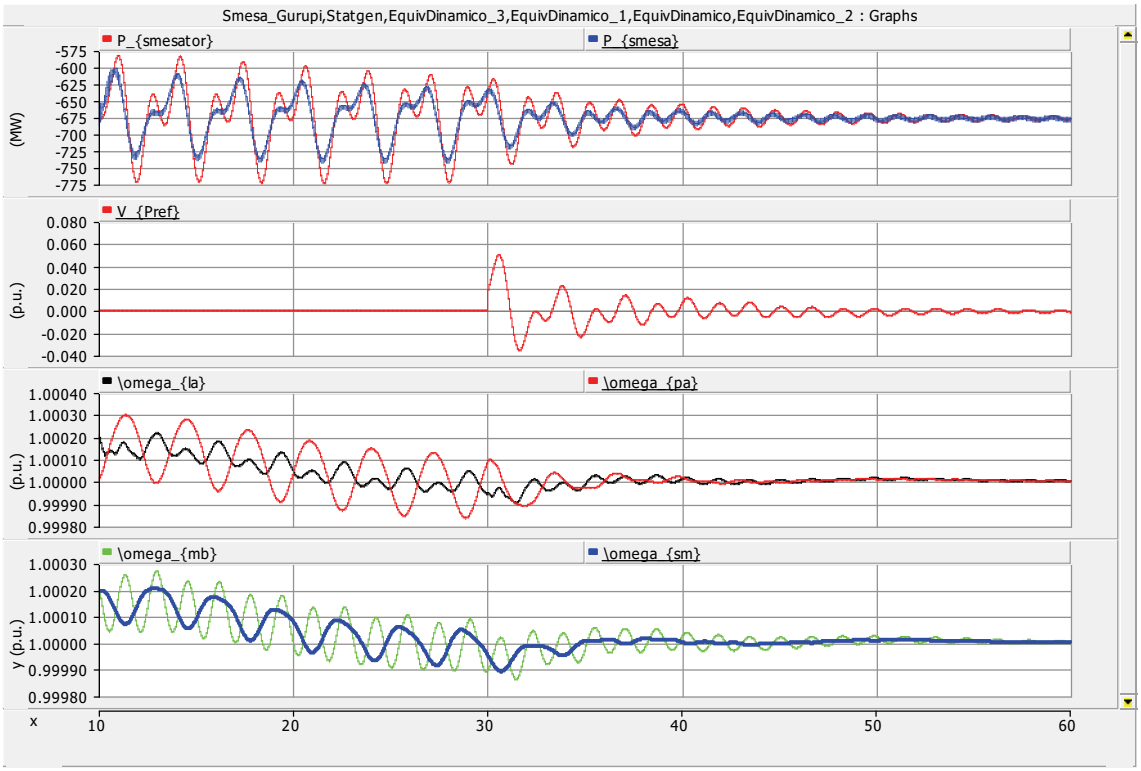

Fig. 75 J = 1 s and $K_{p\omega}$ = 0.012. No interference with the dynamic equivalent of Lajeado.

In Fig. 76 the energy contribution can be clearly observed for the first 30 ms after short-circuit to be similar as the undamped case as presented in Fig. 72. Further, as a difference is that with the proportional gain the STATCOM is significantly damped already for the first second after short-circuit. Thus, with a proportional gain $K_{p\omega}$ the self oscillation can be fairly damped, while the energy contribution at the first moments after a big perturbation is not affected significantly.

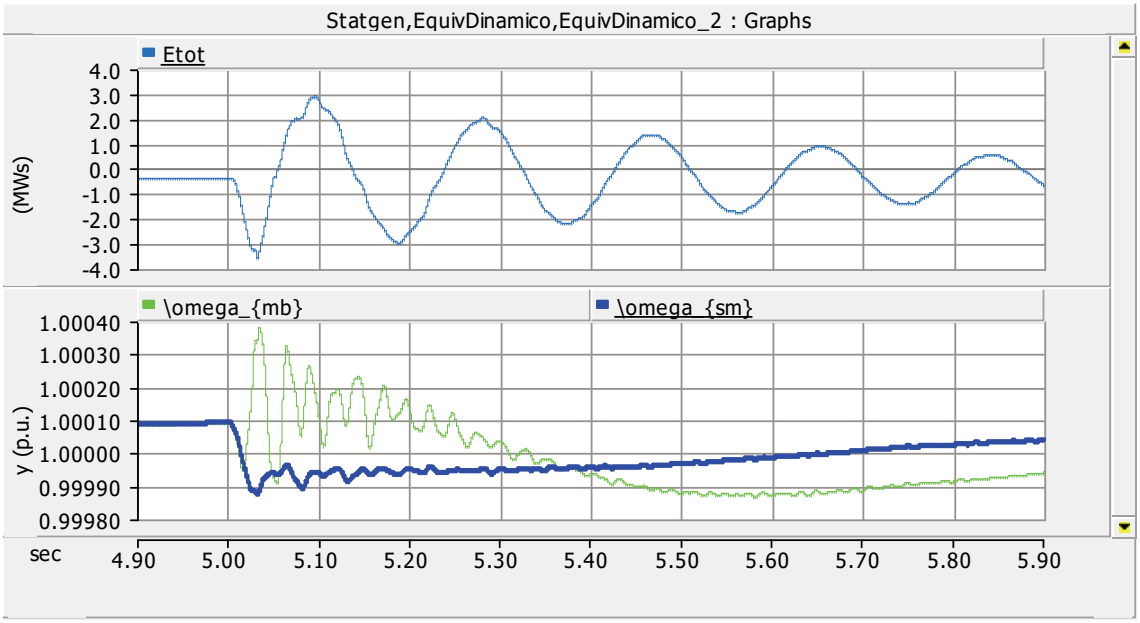

Fig. 76 J = 1 s and $K_{p\omega}$ = 0.012. At the instant of the short-circuit, the synchronverter contributes more to the frequency than in the case with inertia 20 times smaller, as can be seen in Fig. 69.

5 Conclusions and suggestions

Ongoing research in the world concerning the integration of distributed energy sources and Microgrids with the power system shows that two main streams of solutions can be detected. Although, nearly all the state-of-the-art research related to the integration of these sources include the adoption of inertia contribution, with or without swing equations to abandon the classic PLL, one is searching the solution in current controllers, while the other focuses on voltage controllers.

Besides the great advantage of a voltage controller can form its own grid, also the integration with the existent power system seems more natural, since still the major part of this system is fed by voltage sources, namely synchronous generators. The creator of the name synchronverter is leading the philosophy that all connected converters should be equipped with this simple controller. Even a ventilator of a personal computer should temporarily contribute to oppose to system frequency deviations. At last, when the controller mimics a real synchronous generator, existent stability programs and knowledge can be used directly for converters.

In this thesis the viability of the synchronverter concept applied to STATCOM was verified in the frequency and time domain. For the study in the frequency domain, three new transfer functions were developed besides the already published transfer function for the relation between small deviations of the load angle and active power, considering system frequency resonance. These relations seem of significant importance for the controller project of converters operating in high *X/R* grids. With these functions, feedback loops for active and reactive power were closed, considering the proposal to apply a proportional gain for non-generating converters operating as a synchronverter, compensating the lack of the active power droop loop.

In the time domain a comparison has been made with an already published controller without swing equation and electrical torque feedback at one side and the thesis proposal. For high *X/R* grids the electrical torque feedback with swing equation has shown to be superior, since the stability margin for the classic controller becomes negative for higher *X/R* grids. The controller gain is limited by the system frequency resonance for both solutions, though, less limiting for a synchronverter solution with proportional gain parallel to the virtual inertia.

At last, an improvement was shown for the converter response in relation to earlier studies [22][23] with the synchronverter controller applied to STATCOM with electromechanical mode damping. Although the proposed proportional gain did not show any effect on the actual electromechanical mode damping, it was capable to damp significantly all its own variables and thus the ones in the close neighborhood.

SUGGESTIONS

- Close the active loop controller for STATCOM without electric torque feedback and swing equation as well, and perform parameter variation analysis to find stability boundaries.
- Test in the frequency domain model other proposals than the proportional gain for torque difference to angular velocity, like transient active droop and proportional gain for virtual flux and their combination.
- Verify the effect of various filters on the measured signals in the frequency model.
- Analyze the stabilities margins for virtual resistance application.

References

[1] J. Hu, J. Zhu, D. G. Dorrell and J. M. Guerrero, "Virtual Flux Droop Method - A New Control Strategy of Inverters in Microgrids," *IEEE Transactions on Power Electronics,* vol. 29, pp. 4704-4711, Sept 2014.

[2] Q. C. Zhong and T. Hornik, "Cascaded Current-Voltage Control to Improve the Power Quality for a Grid-Connected Inverter With a Local Load," *IEEE Transactions on Industrial Electronics,* vol. 60, pp. 1344-1355, April 2013.

[3] Q. Shafiee, J. M. Guerrero and J. C. Vasquez, "Distributed Secondary Control for Islanded Microgrids-A Novel Approach," *IEEE Transactions on Power Electronics,* vol. 29, pp. 1018-1031, Feb 2014.

[4] M. A. Abusara, J. M. Guerrero and S. M. Sharkh, "Line-Interactive UPS for Microgrids," *IEEE Transactions on Industrial Electronics,* vol. 61, pp. 1292-1300, March 2014.

[5] C. H. E. N. Zhiyong, C. H. E. N. Yandong, J. M. GUERRERO, H. KUANG, Y. HUANG, Z. H. O. U. Leming and L. U. O. An, "Generalized coupling resonance modeling, analysis, and active damping of multi-parallel inverters in microgrid operating in grid-connected mode," *Journal of Modern Power Systems and Clean Energy,* vol. 4, pp. 63-75, Jan 2016.

[6] D. Remon, A. M. Cantarellas, J. D. Nieto, W. Zhang and P. Rodriguez, "Aggregated model of a distributed PV plant using the synchronous power controller," in *2015 IEEE 24th International Symposium on Industrial Electronics (ISIE)*, 2015.

[7] Y. Zhang, A. Allen and B. M. Hodge, "Impact of distribution-connected large-scale wind turbines on transmission system stability during large disturbances," in *2014 IEEE PES General Meeting | Conference Exposition*, 2014.

[8] A. Tzavellas, P. Nguyen, P. Ribeiro and W. Kling, "A game theory approach for coordinating multiple virtual synchronous generators," in *2013 IEEE Grenoble Conference*, 2013.

[9] M. P. N. van Wesenbeeck, S. W. H. de Haan, P. Varela and K. Visscher, "Grid tied converter with virtual kinetic storage," in *2009 IEEE Bucharest PowerTech*, 2009.

[10] Q. C. Zhong, P. L. Nguyen, Z. Ma and W. Sheng, "Self-Synchronized Synchronverters: Inverters Without a Dedicated Synchronization Unit," *IEEE Transactions on Power Electronics,* vol. 29, pp. 617-630, Feb 2014.

[11] C. Li, R. Burgos, I. Cvetkovic, D. Boroyevich, L. Mili and P. Rodriguez, "Analysis and design of virtual synchronous machine based STATCOM controller," in *2014 IEEE 15th Workshop on Control and Modeling for Power Electronics (COMPEL)*, 2014.

[12] P. Rodriguez, I. Candela, C. Citro, J. Rocabert and A. Luna, "Control of grid-connected power converters based on a virtual admittance control loop," in *2013 15th European Conference on Power Electronics and Applications (EPE)*, 2013.

[13] J. Driesen and K. Visscher, "Virtual synchronous generators," in *Power and Energy Society General Meeting - Conversion and Delivery of Electrical Energy in the 21st Century, 2008 IEEE*, 2008.

[14] Q. C. Zhong, "Harmonic Droop Controller to Reduce the Voltage Harmonics of Inverters," *IEEE Transactions on Industrial Electronics,* vol. 60, pp. 936-945,

March 2013.

[15] Q.-C. Zhong, "Robust Droop Controller for Accurate Proportional Load Sharing Among Inverters Operated in Parallel," *Industrial Electronics, IEEE Transactions on,* vol. 60, pp. 1281-1290, April 2013.

[16] G. C. Konstantopoulos, Q. C. Zhong, B. Ren and M. Krstic, "Bounded droop controller for accurate load sharing among paralleled inverters," in *2014 American Control Conference*, 2014.

[17] H. J. Avelar, W. A. Parreira, J. B. Vieira, L. C. G. de Freitas and E. A. A. Coelho, "A State Equation Model of a Single-Phase Grid-Connected Inverter Using a Droop Control Scheme With Extra Phase Shift Control Action," *IEEE Transactions on Industrial Electronics,* vol. 59, pp. 1527-1537, March 2012.

[18] C. Zhang, E. A. A. Coelho, J. M. Guerrero and J. C. Vasquez, "Modular Online Uninterruptible Power System Plug'nPlay Control and Stability Analysis," *IEEE Transactions on Industrial Electronics,* vol. 63, pp. 3765-3776, June 2016.

[19] C. hua Zhang, Q.-C. Zhong, J.-S. Meng, X. Chen, Q. Huang, S.-H. Chen and Z. peng Lv, "An improved synchronverter model and its dynamic behaviour comparison with synchronous generator," in *Renewable Power Generation Conference (RPG 2013), 2nd IET*, 2013.

[20] Q.-C. Zhong and D. Boroyevich, "A droop controller is intrinsically a phase-locked loop," in *Industrial Electronics Society, IECON 2013 - 39th Annual Conference of the IEEE*, 2013.

[21] Q.-C. Zhong and G. Weiss, "Synchronverters: Inverters That Mimic Synchronous Generators," *Industrial Electronics, IEEE Transactions on,* vol. 58, pp. 1259-1267, 2011.

[22] E. L. van Emmerik, B. W. França and M. Aredes, "A synchronverter to damp electromechanical oscillations in the Brazilian transmission grid," in *Industrial Electronics (ISIE), 2015 IEEE 24th International Symposium on*, 3-5 June 2015.

[23] E. L. van Emmerik, B. W. França, A. R. Castro, G. F. Gontijo, D. S. Oliveira and M. Aredes, "Synchronverter to damp multiple electromechanical oscillations," *Proceedings of the 8th Asia-Pacific Power and Energy Engineering Conference, Suzhou, China, April 15-17, 2016,* pp. 617-622, Mar 2016.

[24] P.-L. Nguyen, Q.-C. Zhong, F. Blaabjerg and J. M. Guerrero, "Synchronverter-based operation of STATCOM to Mimic Synchronous Condensers," in *Industrial Electronics and Applications (ICIEA), 2012 7th IEEE Conference on*, 2012.

[25] B. França, E. Emmerik, J. Caldeira e M. Aredes, "Sliding Droop Control For Distributed Generation In Microgrids," *Eletrônica de Potência,* vol. 22, pp. 429-439, 12 2017.

[26] "Proposed terms and definitions for flexible AC transmission system (FACTS)," *IEEE Transactions on Power Delivery,* vol. 12, pp. 1848-1853, Oct 1997.

[27] C. F. dos Santos, F. B. Grigoletto and M. Stefanello, "Power quality improvement in a grid connected voltage source inverter using the concept of virtual synchronous machine," in *2015 IEEE 13th Brazilian Power Electronics Conference and 1st Southern Power Electronics Conference (COBEP/SPEC)*, 2015.

[28] D. Remon, A. M. Cantarellas, E. Rakhshani, I. Candela and P. Rodriguez, "An active power self-synchronizing controller for grid-connected converters emulating inertia," in *Renewable Energy Research and Application (ICRERA), 2014*

International Conference on, 19-22 Oct. 2014.

[29] J. Alipoor, Y. Miura and T. Ise, "Distributed generation grid integration using virtual synchronous generator with adoptive virtual inertia," in *Energy Conversion Congress and Exposition (ECCE), 2013 IEEE*, 2013.

[30] J. Alipoor, Y. Miura and T. Ise, "Power System Stabilization Using Virtual Synchronous Generator With Alternating Moment of Inertia," *Emerging and Selected Topics in Power Electronics, IEEE Journal of,* vol. 3, pp. 451-458, June 2015.

[31] J. Wang, Y. Wang, Y. Gu, W. Li and X. He, "Synchronous frequency resonance of virtual synchronous generators and damping control," in *2015 9th International Conference on Power Electronics and ECCE Asia (ICPE-ECCE Asia)*, 2015.

[32] X. Haizhen, Z. Xing, L. Fang, M. Fubin, S. Rongliang and N. Hua, "An improved Virtual Synchronous Generator algorithm for system stability enhancement," in *2015 IEEE 2nd International Future Energy Electronics Conference (IFEEC)*, 2015.

[33] T. Shintai, Y. Miura and T. Ise, "Oscillation Damping of a Distributed Generator Using a Virtual Synchronous Generator," *IEEE Transactions on Power Delivery,* vol. 29, pp. 668-676, April 2014.

[34] J. Liu, Y. Miura and T. Ise, "Dynamic characteristics and stability comparisons between virtual synchronous generator and droop control in inverter-based distributed generators," in *2014 International Power Electronics Conference (IPEC-Hiroshima 2014 - ECCE ASIA)*, 2014.

[35] H.-P. Beck and R. Hesse, "Virtual synchronous machine," in *Electrical Power Quality and Utilisation, 2007. EPQU 2007. 9th International Conference on*, 2007.

[36] S. DÁrco, J. A. Suul and O. B. Fosso, "Small-signal modelling and parametric sensitivity of a Virtual Synchronous Machine," in *2014 Power Systems Computation Conference*, 2014.

[37] J. Zhu, J. M. Guerrero, W. Hung, C. D. Booth and G. P. Adam, "Generic inertia emulation controller for multi-terminal voltage-source-converter high voltage direct current systems," *IET Renewable Power Generation,* vol. 8, pp. 740-748, September 2014.

[38] J. Zhu, C. D. Booth, G. P. Adam and A. J. Roscoe, "Inertia emulation control of VSC-HVDC transmission system," in *2011 International Conference on Advanced Power System Automation and Protection*, 2011.

[39] P. Kundur, Power System Stability and Control, McGraw-Hill Professional, 1994.

[40] Q. C. Zhong e G. Weiss, “Static synchronous generators for distributed generation and renewable energy,” em *2009 IEEE/PES Power Systems Conference and Exposition*, 2009.

[41] "Static Synchronous Generators". Patent WO 2010/055322 A2, 2010.

[42] B. França, *Static Synchronous Generator with Sliding Droop Control for Distributed Generation in Microgrids*, Ph.D. thesis, COPPE/UFRJ, Rio de Janeiro, RJ, Brasil, 2016.

[43] L. G. B. Rolim, D. R. da CostaJr. and M. Aredes, "Analysis and Software Implementation of a Robust Synchronizing PLL Circuit Based on the pq Theory," *IEEE Transactions on Industrial Electronics,* vol. 53, pp. 1919-1926, Dec 2006.

[44] T. M. L. Assis and G. N. Taranto, "Increase of Transfer Limit in the Large Interconnected Brazlian System Constrained by Small-Signal Stability," in *CBA*,

2008.

[45] "Control of a Voltage Source Converter using Synchronous Machine Emulation". Patent WO 2010/022766, 2010.

[46] "Synchronous Power Controller for a generating System based on Static Power Converters". Patent WO 2012/117131 A1, 2012.

[47] "Virtual Controller of Electromechanical Characteristics for Static Power Converters". Patent WO 2012/117132 A1, 2012.

[48] "Virtual Admittance Controller based on Static Power Converters". Patent WO 2012/117133 A1, 2012.

[49] J. William D. Stevenson, Elementos de análise de sistemas de potência, 4a edição americana, 2a edição em português ed., Mc Graw-Hill, 1986.

[50] M. Beza and M. Bongiorno, "Power oscillation damping controller by static synchronous compensator with energy storage," in *2011 IEEE Energy Conversion Congress and Exposition*, 2011.

[51] H. Bevrani, M. Watanabe and Y. Mitani, "Oscillation Dynamics Analysis Based on Phasor Measurements," in *Power System Monitoring and Control*, Wiley-IEEE Press, 2014, pp. 288-.

[52] H. Ghasemi and C. Canizares, "Damping torque estimation and oscillatory stability margin prediction," in *2006 IEEE Power Engineering Society General Meeting*, 2006.

[53] H. Ghasemi and C. Canizares, "On-Line Damping Torque Estimation and Oscillatory Stability Margin Prediction," *Power Systems, IEEE Transactions on,* vol. 22, pp. 667-674, May 2007.

[54] G. Cao, Z. Y. Dong, Y. Wang, P. Zhang and Y. T. Oh, "VSC based STATCOM controller for damping multi-mode oscillations," in *2008 IEEE Power and Energy Society General Meeting - Conversion and Delivery of Electrical Energy in the 21st Century*, 2008.

[55] H. Akagi, Y. Kanazawa and A. Nabae, "Instantaneous Reactive Power Compensators Comprising Switching Devices without Energy Storage Components," *IEEE Transactions on Industry Applications,* Vols. IA-20, pp. 625-630, May 1984.

[56] E. H. Watanabe, R. M. Stephan and M. Aredes, "New concepts of instantaneous active and reactive powers in electrical systems with generic loads," *IEEE Transactions on Power Delivery,* vol. 8, pp. 697-703, Apr 1993.

[57] E. H. Watanabe, M. Aredes, J. L. Afonso, J. G. Pinto, L. F. C. Monteiro and H. Akagi, "Instantaneous p-q power theory for control of compensators in micro-grids," in *2010 International School on Nonsinusoidal Currents and Compensation*, 2010.

[58] B. Singh, R. Saha, A. Chandra e K. Al-Haddad, “Static synchronous compensators (STATCOM): a review,” *IET Power Electronics,* vol. 2, pp. 297-324, 7 2009.